

Peridynamic micromechanics of composites: a review

Valeriy A. Buryachenko

Micromechanics & Composites LLC, Cincinnati, Ohio 45202, USA

Abstract

A static peridynamic (proposed by Silling, see J. Mech. Phys. Solids 2000; 48:175–209) composite materials (CMs) of the random and periodic structures are considered. In the framework of the second background of micromechanics (also called computational analytical micromechanics, CAM), one proved that local micromechanics (LM) and peridynamic micromechanics (PM) are formally similar to each other for CM of both random and periodic structures. It allows straightforward generalization of LM methods to their PM counterparts. It turns out that a plurality of micromechanics phenomena [e.g. statistically homogeneous and inhomogeneous media, inhomogeneous loading (inhomogeneous body force is included), nonlinear and nonlocal constitutive laws of phases, and coupled physical phenomena] can be analyzed by one universal tool (called CAM), which is sufficiently flexible and based on physically clear hypotheses that can be modified and improved if necessary (up to abandonment of these hypotheses) in the framework of a unique scheme for analyses of a wide class of mentioned problems. The schemes of these approaches are considered in the current paper.

Keywords: Microstructures; inhomogeneous material; peridynamics; non-local methods; multiscale modeling

Table of Contents

| | |
|--|----|
| 1. Introduction..... | 2 |
| 2. Preliminaries..... | 11 |
| 2.1 Basic equations of peridynamics..... | 11 |
| 2.2 Statistical description of the composite microstructures..... | 15 |
| 2.3 Volumetric boundary conditions..... | 16 |
| 2.4 Periodic structures and volumetric periodic boundary conditions..... | 17 |
| 2.5 Some averages | 18 |
| 3. General integral equations (GIEs)..... | 19 |
| 3.1 Analytical and computational micromechanics. Linear GIEs in LM | 19 |
| 3.2 One and two inclusions in peridynamic macrodomain..... | 22 |
| 3.3 Nonlinear GIEs in peridynamic micromechanics..... | 26 |
| 3.4 Definition of effective elastic moduli..... | 28 |
| 4. Solution of general integral equations..... | 32 |
| 4.1 Closing assumptions..... | 32 |
| 4.2 Body forces with compact support..... | 34 |
| 4.3 Estimation of a set of surrogate operators..... | 36 |
| 4.4 Estimation of effective moduli..... | 40 |
| 4.5 Damage mechanics and microcracked media..... | 42 |
| 4.6 Schematic representation of nonlinear GIE implementation..... | 45 |
| 4.7 Nonlinear incremental Mori-Tanaka approach in PM..... | 49 |
| 5. Estimation of field fluctuations and effective energy-based criteria..... | 50 |

| | |
|---|----|
| 6. Fast Fourier transform methods in peridynamic micromechanics..... | 53 |
| 6.1 Fast Fourier transform..... | 53 |
| 6.2 Fast Fourier transform method in peridynamic micromechanics..... | 55 |
| 6.3 FFT of the nonlinear peridynamic equation..... | 58 |
| 7. Reduced order models in peridynamic micromechanics.... | 60 |
| 7.1 Clustering discretization method (CDM) in local micromechanics..... | 60 |
| 7.2 CDM in peridynamic micromechanics.. | 62 |
| 7.3 Data-driven modeling and machine learning based on CDM..... | 64 |
| 7.4 Proper Orthogonal Decomposition in PM..... | 65 |
| 8. Peridynamic micromechanics of laminated structure composites..... | 67 |
| 9. Conclusion..... | 69 |
| References..... | 71 |

1 Introduction

The prediction of the behavior of composite materials (CM) in terms of the mechanical properties of phases and their microstructure is a central problem of micromechanics. In turn, the stress field estimations in the constituents are based on a substitution into one or another micromechanical scheme of a solution (called basic problem) for one inclusion inside the infinite homogeneous matrix subjected to some homogeneous effective field. In the case of locally elastic properties of constituents, for both the ellipsoidal homogeneous inclusion and homogeneous effective field, this solution has an analytical representation in the form of Eshelby [131] tensor (see for references [276], [398]). Various numerical methods have been developed for the general inclusion shape. So, the finite element analysis (FEA) The truncation method is used to model the infinite medium using an increased size sample. Immediate considerations of the infinite medium were performed by either the boundary integral equation methods (see e.g., [217], Chapter 11 in [64]) or the volume integral equation ones (see for references, e.g., [47]). The general comprehensive reviews of the various methods of micromechanics were given in the books [47], [64], [116], [182], [261],[334].

Nonlocal mechanics was initiated in the 1960s by Kröner, Eringen, Kunin, Bažant and others (see for references [64]). Proposal of peridynamics by Silling [311] (see also [34], [114], [236], [272], [320], [312]), a nonlocal theory of solid mechanics initiated the explosive character of the progress in different physical phenomena based on replacing the classical local partial differential equation of the balance of linear momentum with the integral equation, which is free of any spatial derivatives of displacement. In nonlocal peridynamic theory, the equilibrium of a material point is provided by a sum of internal forces generated by surrounding points over a finite distance (called a horizon). In contrast, in the classical local theory, such interactions are only exerted by adjacent points through the contact forces. Generally, in peridynamics, the state-based approach permits the response of a material at a point to depend on the deformation of all bonds connected to the point within its finite radius horizon

([317], [312]) via a response function, which completely describes the interactions. It means that the forces between two peridynamic nodes depend also on deformations of other bonds surrounding these nodes within the horizons. The horizon can encompass discontinuities of different materials. The first formulation of peridynamics (so-called bond-based approach) is that the interactions only occur between pairs of points within a horizon. As is well known, a direct consequence of this assumption is that the Poisson's ratio for isotropic linear materials is fixed at $\nu = 1/4$ in three dimensions or $\nu = 1/3$ in two dimensions [311]. The major advantages of the state-based approach include a material response depending on collective quantities (like volume change or shear angle), which allows constitutive models from the local theory of solid mechanics to be incorporated directly within the peridynamic approach (called *correspondence model*; see [1], [317]) The state-based models can be subdivided into ordinary and non-ordinary PDs, in which the force is aligned and unaligned to the bond direction, respectively. The correspondence models that allow the reproduction of all the components of the classical continuum mechanics (CCM) elasticity tensor for a fully anisotropic material was developed in the framework of non-ordinary state-based PD (see for references and details [339]); these models suffer from instability issues and require additional stabilization techniques to obtain reasonable numerical results. The ordinary state-based model [299] overcomes these limitations, since it allows to accurately reproduce any component of the CCM elasticity tensor both in 2D and 3D cases.

The versatility and effectiveness of peridynamic models has been demonstrated in various practical applications, including damage accumulation, corrosion, the fracture and failure of composites of deterministic structure, crack instability, impact, the fracture of polycrystals, and nanofiber networks (see, e.g., [10], [11], [18], [84], [106], [169], [176], [206], [207], [236], [266], [289], [318], [399]).

For statistically homogeneous thermoperidynamic media subjected to homogeneous volumetric macro boundary loading, one proposed the background principles (see [50], [55]) in the framework of the bond-based approach considered. It was proven that the effective behavior of this media is governed by a local effective constitutive equation as in the conventional thermoelasticity theory [47]. The general result establishes the links between the effective properties (effective elastic moduli, effective thermal expansion) and the corresponding mechanical and transformation influence functions (do not miss the influence functions in peridynamics). It is obtained by the use of both the decomposition of local fields into the load and residual fields as well as extraction from the material properties a constituent of the matrix properties. The energetic definition of effective elastic moduli is obtained. A detected similarity of results for both the locally elastic and peridynamic composites is explained by the fundamental reasons because the methods used for obtaining the mentioned results widely exploit Hill's condition proved and the self-adjointness of the peridynamic operator. This similarity opens the opportunities for a straightforward generalization of their solutions for locally elastic CMs to the peridynamic ones (instead of the simplified methods such as, e.g. the mixture theory, see [10], [11], [12], Frank'et'2023, [163], [243], [356], [357], [369]).

Wide expansion of the methods of the LM (corresponding to classical continuum mechanics, CCM) into nonlocal phenomena (see [50], [55], [64]) was supported by a critical generalization of the LM. Namely, one [48], [49], [51], [53] proposed the general integral equation GIE of microinhomogeneous media forming the second background of micromechanics (also called computational analytical micromechanics, CAM). The first background of micromechanics is based on the so-called effective field hypothesis, EFH, proposed by Faraday, Poisson, Mossotti, Clausius, Lorenz, and Maxwell (1830-1880), see for Refs. [64]). The critical feature of the new GIEs is the absence of a direct dependence of GIE on both the Green function and the constitutive law (either local or nonlocal) without restrictions of the local micromechanics (such as, e.g., acceptance of the EFH and ellipsoidal symmetry of microtopology) that offers opportunities for a fundamental jump in multiscale and multiphysics research with drastically improved accuracy of local field estimations (even to the point of correction of a sign, see [64]). The basic hypotheses of locally elastic micromechanics (in the version of the second background of micromechanics, see [64] and [79], are generalized to their peridynamic counterparts in [61]. It should be mentioned the stochastic methods where the material property is modeled by a random variable, see for references [133], [134] (see also [84], [243], [324], [356], [357])). The solution of this stochastic equation describes the probability density function (PDF) of the state variable. However, the mentioned methods do not consider the standard engineering restriction such as nonoverlapping of randomly located inclusions; the estimations obtained by the mixture theory do not also depend on ratio of the horizon and inclusion size [84], [141], [243], [274], [356], [357]. Another limiting case associated with "randomly" inhomogeneous structure is the modeling of a critical stretch of each bond by the Weibull distribution function, see []

However, even for locally elastic CMs subjected to inhomogeneous loading, the effective deformations are described by a nonlocal (either the differential or integral) operator (see for references, e.g., [47], [64], [121], [314], [340]) relating a statistical average of fields in the point being considered with a statistical average of fields in the vicinity of this point. The situation becomes significantly more diversified if a few (or all) effects are simultaneously considered: statistically inhomogeneous media, inhomogeneous loading (inhomogeneous body force is included), nonlinear and nonlocal constitutive laws of phases, coupled physical phenomena, bounded microinhomogeneous domain. It turns out that this plurality of phenomena can be analyzed by one universal tool (called CAM), which is sufficiently flexible and based on physically clear hypotheses which can be modified and improved if necessary (up to abandonment these hypotheses) in the framework of a unique scheme for analyses of a wide class of mentioned problems. The nonlocal operators are also currently receiving much attention as homogenized surrogate models (for both overall fields and the field concentrator factors) that efficiently and accurately capture small-scale effects (and depend on ratios of both material (inclusion size and horizon) and field scales). The schemes of these approaches are considered in the current paper.

Although the effective properties of CM is the main goal of micromechanics, it is also

important to provide insight into the statistical distribution of local stresses in each phase. It is not a problem if a direct numerical simulation (DNS) for periodic structure CMs (see, e.g., [136], [242]) is available. However, consideration of random structure CMs with nonlinear constitutive behavior, including plasticity, damage, and creep, requires an acceptance of some additional assumptions. The popular hypothesis of the mean-field method takes into account only the average stresses in the phases $\langle \boldsymbol{\sigma} \rangle_i$ (see the notations in Section 2), which are used in most secant methods (see, e.g., [32], [329]). However, the second statistical moment of stress $\langle \boldsymbol{\sigma} \otimes \boldsymbol{\sigma} \rangle_i(\mathbf{x})$ is each phase $\mathbf{x} \in v_i \subset v^{(k)}$ ($k = 0, 1, \dots, N$) is directly used in the analyses of a wide class of nonlinear phenomena (strength, plasticity, and fracture) and some critical effects (e.g., dielectric breakdown, see [86], [295]). So, in the strength theory, the Tsai-Wu criterion has a tensor polynomial (see, e.g., [332]) failure surface depending on stresses. The onset of yielding in some cases of elastic-plastic materials has also a quadratic yield condition (see, e.g., [30]) generalizing some classical criteria, as, for example, the von Mises equivalent stress criterion. Stress potential in power-law creep is a nonlinear function of equivalent stresses (see, e.g., [47], [64], [282]). In linear fracture theory, the energy release rate for penny-shape crack has a quadratic dependence on the stress intensity factors (see [293]) which, in turn, are the linear functions of the stresses. One of the main achievements in local nonlinear micromechanics (see [282]) is a suitable approximation in the context of the variational principles permitting determining bounds for nonlinear composites, directly from the corresponding bounds for linear comparison composites with the same microstructures as the nonlinear composites. It was also concluded (see [326]) that the variational method can be interpreted as a secant method based on the estimations of the second moment of stresses.

Conceptually, more general nonlinear models were proposed in peridynamics. So, classical von Mises plasticity theory is generalized by Silling [317] by the introduction of a scale-valued yield surface as a nonlinear function of force state. In particular, the yield surface can be a quadratic function of the norm expressed through a dot product of the force state (analog of an equivalent Mises stress). In a peridynamic elastoplastic model proposed, a deformation state is decomposed to isotropic and deviatoric parts whereas a scale force state is decomposed on co-isotropic and co-deviatoric parts allowing the condition of plastic incompressibility to be enforced. Mitchell [252] developed this model by integrating the flow rule tracking along the lines of the classical theories of rate-independent J_2 plasticity. The author proposed a useful non-local yield criterion in terms of 3D force states equivalent to J_2 plasticity depending on the yield stress and horizon for the material. Madenci and Oterkus [237] presented constitutive relations for plastic deformation according to von Mises yield criteria with linear isotropic hardening. The expressions for the yield function and the rule of incremental plastic stretch are derived in terms of the horizon, shear modulus, force density, and hardening parameter of the medium. The yield surface is constructed using the relationship between the effective stress and equivalent plastic stretch. This model was later extended in [277] (see also [9]) where the von Mises yield criteria are exploited for a description of plastic yielding whereas the equivalent plastic stretch is utilized as an internal variable for the general form of the

mixture of isotropic and kinematic hardening. One [260] formulated two rate-independent yield functions equivalent to J_2 plasticity with associated flow rules using the force states and the strain energy density for 2D cases. One [279] proposed the elastoplastic law to describe isotropic, kinematic, and mixed hardening in 2D and 3D.

Another area of nonlinear phenomena is damage and failure where a bond is being “broken” or “intact” following certain failure criteria. Damage modeling initiated by the seminal work by Silling and Askari [316] (see also [236]) was determined by using critical stretch criteria of bonds. A critical stretch of inhomogeneous materials is described in [324] as a random variable that obeys the Weibull distribution. The potential role of employing a nonlinear peridynamic kernel in predicting the onset of fractures has been explored in [107] (see also [91], [92]). It was demonstrated that the presence of nonlinearity in the relative displacement can reproduce inherently the high potential energy peaks that indicate the formation of cracks. Another direction of damage modeling is associated with energy-based criteria such as, e.g., the critical bond strain energy density failure criteria [140], [209], [291], [327], [328], [341], [342], [370]. The last model was applied in energy-based peridynamic approach [265] (see also [215]) for fatigue cracking proposed. Here, the energy release rate for interaction between material points is expressed through the micropotentials of the interaction between these points. The definition of the critical energy release rate range and the energy-based peridynamic failure model for both phases crack initiation and crack growth phases are introduced. Pointwise energy-based bond breaking model states (see [172]) that a bond is broken and no longer carries load if the strain energy density at either of its endpoints exceeds some critical local strain energy density W_c when the point loses all of its bonds and is completely detached from the body.

Another area of the LM is periodic structure composites (see, e.g., [136], [151], [304], [400]). Traditionally, the methods used at the LM of CMs with either the random structure or periodic ones are essentially different. For periodic structure CMs, the term *asymptotic homogenization* (or two-scale expansion) apparently introduced by Babuska [15] analyzes the asymptotic behavior of the solution when the ratio of the representative size of microstructures (called a unit cell, UC) and the overall size of the structure is negligibly small (see e.g., [16], [136], [184]). Another version of the homogenization, so-called *computational homogenization* [325], determinations of macroscopic mechanical response (e.g., stress-driven by deformation) at the microscopic level are defined from the macroscopic variables (see e.g., [193], [251], [242], [331]). Applicability of methods of computational homogenization for either inelastic, nonlinear, or nonlocal problems can be performed in the framework of the same general scheme.

So, for peridynamic CMs with a periodic microstructure, Alali and Lipton [7] (see also [121], [123], [302]) constructed two-scale expansion for the solution (with neither numerical results nor a definition of the effective moduli) splitting into a microscopic component at the length scale of the inclusions, and a macroscopic component tracking the homogenized dynamics. The peridynamic generalization of the computational homogenization is initiated

by Madenci with coauthors [232] (see also [233], [110], [111], [207]) who suggested the peridynamic unit cell model (subjected to the classical periodic boundary conditions, PBC) for an estimation of the effective properties. The introduction of the volumetric periodic boundary conditions (VPBC) in [56], [57], [64] (see also [143], [144], [145], [166], [283], [360], [359], [361], [362]) permits generalizing of classical computational homogenization approaches. Another fundamental step in peridynamic computational homogenization is the estimation of effective moduli by the use of the averages of traction and displacements at the UC boundary [56], [57], [64] (this evaluation is most simple) rather than in a less general and more cumbersome method of exploiting the volume averages of the stresses and strains inside the UC volume [143], [144], [146], [166] (there are some difficulties in estimations of local strain fields in UC because the displacement field is not differentiable in UC).

The popular discretization methods for the solution of PD equations are the meshfree method with one-point Gaussian quadrature referring to it as “meshfree PD” [316] (see also the solutions for 1D case [36], [130], [127], [128], [317], [343], [345], 2D case [35], [164], [200], [296], [309], and 3D case [212], [216]), finite element methods (FEM, [37], [83], [229], [235], [333], [290], [328]), [354], and collocation methods ([227], [228], [392]). For temporal discretization, adaptive dynamic relaxation (ADR [190]) and velocity Verlet (VV [350]) methods are commonly used for solving quasi-static and dynamic problems, respectively, providing accurate and efficient solutions in peridynamics, see also [211]. These methods scale $O(N^2)$, where N is the total number of nodes in the discretization. PD has also been the basis of several advanced operator approaches sharing some similarities with the reproducing kernel particle method [24]. So, Madenci et al. [231] proposed the peridynamic differential operator (PDDO) which exploits Taylor series expansion (TSE) and PD function orthogonality. Subsequently, Madenci et al. [234] developed peridynamic least-squares minimization (PD-LSM) by replacing PD function orthogonality with the least squares method (LSM) through the final PD-LSM formulation. Later, Rabczuk and associates [114], [208], [209], and [285] proposed the peridynamic operator method (PDOM) which converts the local differentiation or its products into the nonlocal integral form. One key feature of this approach is that it does not require any special treatment in the presence of discontinuities or singularities.

In the LM, an alternative technique based on fast Fourier transforms (FFTs), or “FFT” methods for short, was proposed by Moulinec and Suquet [258], [259] a fast and efficient alternative to the FEM reducing a computational complexity from $O(N^2)$ to $O(N \log N)$. The first version of the FFT [258], [259] is based on the solution of an implicit periodic Lippmann–Schwinger (S-L) equation involving a convolution of the eigenstrain (called polarization) field with Green’s function of the elastic reference material. These convolutions in real space are transformed into products in the Fourier space where the implicit integral equation can be iteratively solved easily. It is possible then to classify FFT methods into three groups. The first group is called the Lippmann–Schwinger equation-based approaches, which include the polarization schemes, and the Krylov-based schemes (see [246], [246], [43], [44], [179], [349], [386]). The second group contains the so-called Fourier–Galerkin schemes

derived from the Galerkin approach, which is based on the weak formulation of the mechanical problem [97], [385]. The third group contains the schemes using the displacement field as the primary unknown variable instead of either the strain or polarization fields (see for details [225]). There are also a handful of reviews of the FFT methods focused on specific applications: e.g., the work [301] focuses on nonlinear homogenization, whereas the work [303] focuses on polycrystals. Nowadays, most FFT tools are open-source (see for references [226]) These algorithms are highly optimized in terms of computational complexity and memory and also take advantage of parallel programming where the FFT grid is distributed across processors.

A class of fast methods utilizing the structure of stiffness matrix is booming [215]. The natural convolutional structure of PD formulations is perfectly adapted to use Fourier transforms, as recently shown in [5] and [100] (see also [46], [124], [93], [222]). Bobaru and coauthors [171], [172] (see also [170], [175]) proposed a fast convolution-based method for peridynamic diffusion problems as well as for elasticity and fracture. The method applies to the class of constitutive models with specific convolutional structures and can benefit from the remarkable efficiency of the FFT method. A volume penalization technique for the nonlinear peridynamic model was proposed in [222] (see also [171], [172]) for eliminating the limitation of periodic solution and for non-periodic domains. However, to the best of the author’s knowledge, the FFT method was not applied to the computational homogenization problems of peridynamic CMs. The current study is dedicated to extending the FFT methods to the area of PM of CMs.

For the direct numerical simulation (DNS) of the periodic CMs, one of the concurrent homogenization schemes is FE^2 approach (see e.g., [147]) where the macroscale geometry is discretized with a FE mesh. Each integration point of the FEA is considered as RVE with its own FE mesh, i.e., the FE^2 approach solves two sets of FE meshes concurrently. Needless to say, the versatility of the FE^2 approach comes at a significant price: a very high computational burden, and a longer computational time.

Generally speaking, the reduced-order model (ROM) refers to any endeavor aimed at constructing a simplified model from a more complex one when the degrees of freedom (DoFs) of the ROM are several orders of magnitude lower than that of the DNS, which dramatically reduces the consumption of computing resources. The simplified ROM is capable of achieving a key balance between efficiency and accuracy, whereas the more complex case here is DNS. Transformation Field Analysis (TFA) proposed by Dvorak (see [117], [118]) considers the inelastic strain as an eigenstrain, presuming that the field of internal variables is a piecewise constant in each phase categorized by nonlinear behavior. Although TFA was not labeled as a ROM at that time, the TFA can, in a retrospective sense, be considered like an ignition spark for a wide class of ROMs [21], [33], [39], [80], [95], [96], [119], [159], [158], [196], [247], [248], [292], [335], and [379].

Clustering-based ROMs (CROMs) initiated by the self-consistent clustering analysis (SCA) by Liu *et al.* [218] (see also [203], [330], [390]) is a recent family of ROMs where

material points are categorized into one cluster Ω_i (for the k -means clustering, see [8], [81], [139], [221], [230], in the offline stage) if they have a similar response in the sense of strain concentration factors. The discretization process is used for the estimation of an interaction tensor, which is the influence of the stress in the J th cluster on the strain in the I th cluster. Originally, the iteration tensor was expressed in [218] by the use of the L-S equation. This method was generalized and used in FE-SCA type concurrent simulations for strain softening materials [219]; polycrystalline materials [183], [220], [380]; and woven composites [156], [157]. In a FEA-clustered version of SCA proposed in [85] and [262], the construction of the iteration matrix is fully done by FEA. Buryachenko [72] proved that TFA is, in fact, a background of clustering discretization methods (CDM); some exact representations for the relations of the effective field and material parameters are obtained. The adaptive clustering-based model proposed in [135] provides optimal refinement in regions where the corresponding fields present higher gradients (e.g., in the vicinity of a crack tip). The goal of the present publication is the generalization of basic concepts of clustering discretization methods of micromechanics of CMs with local nonlinear properties of phases to micromechanics of CMs with peridynamic properties of constituents.

Amongst the ROM techniques, Proper Orthogonal Decomposition (POD) is the most popular one owing to its simplicity and high efficiency; it has been successfully used in various fields, such as fluid mechanics, thermal science, material science, structural mechanics, and solid mechanics (see for refs. [22], [25], [88], [346]). The POD is a method to compute an orthogonal basis that provides a low-dimensional representation of a high-dimensional system state of the DNS. This yields an explicit POD reduced model that can be solved in place of the original DNS. Several fast algorithms based on POD for nonlocal problems have been proposed [227], [269], [355], [388], [391], [397]; in particular, the ROMs based on the weak form of nonlocal equations are constructed in [355], [388],[391]. A mesh-free collocation method based on a mixed reproducing kernel approximation with nodal interpolation property for solving PD equations was developed to explicitly obtain the projection of nonlocal boundary conditions [227].

It should be indicated that the hierarchical coarsening method proposed by Silling [313] (see also [142]) can be considered as a peridynamic version of the ROM. The key idea of the coarsening method is to analyze the behavior of high-fidelity models by the use of fewer degrees of freedom. The reduction in the model order is performed by substituting a high-fidelity model with a surrogate model with fewer degrees of freedom.

The most popular example for validating classical periodic homogenization in the LM and its extensions is the study of multilayered periodic CMs, see [82], [137], [184], [268], [273], [381]. In the case of invariance to parallel transfer along the layers in the LM, the equilibrium equation at the microlevel is reduced to a one-dimensional ordinary differential equation problem. However, for multilayered peridynamic media, Askari *et al.* [10] [12] (see also [150], [162], [163]) initiated a very attractive peridynamic model (directly exploiting a physical essence of peridynamic bonds), where the micromoduli of both fibers and matrix are

fitted to respective bulk elastic modulus in each direction. Madenci and Oterkus [236] (see also [18], [109], [165], [238], [239], [289], [363]) proposed the model based on the estimation of bond properties using an equivalency between the elastic energy density of the peridynamic theory and the classical local mechanics theory. The mentioned peridynamic models implicitly use the scaler separation hypothesis $l_\delta/2h \rightarrow 0$, and, because of this, the obtained estimations do not depend on the ratio of both the horizon l_δ and the thickness $2h$ of the layers. The current study is dedicated to the extension of the generalized Mori-Tanaka approach ([29], [256]) of peridynamic micromechanics of random structure CMs [62], [64] to the modeling of multilayered peridynamic media (without the scale separation hypothesis).

Peridynamic micromechanics is a new multidisciplinary area of research that combines peridynamics and micromechanics. To introduce readers to this new subject of PM, it is necessary to begin with the main notions, definitions, and classifications, which are presented with the understanding that any definition and classification scheme is neither comprehensive nor complete. It should also be mentioned that micromechanics and peridynamics areas have different histories. So, the history of micromechanics is richer than the history of peridynamics in the sense of both the duration (150 years longer) and publications (on $10^5 - 10^6$ papers more). The professional interests of the author are also overbalanced in micromechanics (at least in the sense of duration and publications). Because of this, the current review more likely reflects the point of view of the micromechanician. We focus on establishments of both the physical nature, the essence, similarity, and deep interconnection of different micromechanical models of PM rather than on analyses of particular numerical and experimental results, and the development of advanced numerical methods (existence and uniqueness of solution, their convergence, stability, and robustness) for both homogeneous media and CMs of deterministic structure (most likely this is the area of computational mathematics). However, for the presentation of PM as a unified theory, PM is described as the formalized schemes of blocked (or modular) structures so that the experts developing one block need not be experts in the underlying another block. The opportunity for the creation of this blocked structure of the PM is supported by a critical generalization of CAM, which is extremely flexible, robust, and general. This review has a dual goal. It can be used as guidance for practitioners in the selection of appropriate PM methods based on the characteristics and needs of the problem being considered. On the other side, it can be also exploited by developers in the choice of attack directions in broad prospective problems of the new field of peridynamic micromechanics.

The paper is organized as follows. In Section 2, a short introduction to the peridynamic theory adapted for a subsequent presentation is presented. Statistical description of the composite microstructures is described in accompanied by the volumetric homogeneous displacement loading conditions. Some field averages are considered. A history of the linear general integral equations (GIE) is shortly presented in Section 3. Nonlinear GIEs are proposed which contain either a statistical average field or the field produced in the infinite matrix by the body force with compact support. Solutions of the GIEs are presented in Section 4. Closing assumptions for solutions of two sorts of the GIEs mentioned are considered. By the use of

the body force with compact support as a training parameter, a set of surrogate effective operators are constructed. Effective moduli are obtained in the framework of some additional simplified hypotheses. Blocked (or modular) structures of the scheme implementation of non-linear GIEs are presented. Estimation of field fluctuations and effective energy-based criteria are considered in Section 5. Fast Fourier transform methods in peridynamic micromechanics are presented in Section 6. The clustering discretization method in peridynamic micromechanics is proposed in Section 7. Laminated structure peridynamic composites are modeled in Section 8. The conclusion is presented in Section 9.

2 Preliminaries.

2.1 Basic equations of peridynamics

One considers a linear elastic medium occupying an open simply connected bounded domain $w \subset \mathbb{R}^d$ with a smooth boundary Γ_0 and with an indicator function W and space dimensionality d ($d = 1, 2, 3$). The domain w with the boundary Γ^0 consists from a homogeneous matrix $v^{(0)}$ and a statistically homogeneous field $X = (v_i)$ of heterogeneity v_i with indicator functions, V_i and bounded by the closed smooth surfaces Γ_i ($i = 1, 2, \dots$). It is presumed that the heterogeneities can be grouped into phases $v^{(q)}$ ($q = 1, 2, \dots, N$) with identical mechanical and geometrical properties. The basic equations of local thermoelasticity of composites are considered

$$\nabla \cdot \boldsymbol{\sigma}(\mathbf{x}) = -\mathbf{b}(\mathbf{x}), \quad (2.1)$$

$$\boldsymbol{\sigma}(\mathbf{x}) = \mathbf{L}(\mathbf{x})\boldsymbol{\varepsilon}(\mathbf{x}) + \boldsymbol{\alpha}(\mathbf{x}), \quad \text{or} \quad \boldsymbol{\varepsilon}(\mathbf{x}) = \mathbf{M}(\mathbf{x})\boldsymbol{\sigma}(\mathbf{x}) + \boldsymbol{\beta}(\mathbf{x}), \quad (2.2)$$

$$\boldsymbol{\varepsilon}(\mathbf{x}) = [\nabla \otimes \mathbf{u} + (\nabla \otimes \mathbf{u})^\top]/2, \quad \nabla \times \boldsymbol{\varepsilon}(\mathbf{x}) \times \nabla = \mathbf{0}, \quad (2.3)$$

where \otimes and \times are the tensor and vector products, respectively, and $(\cdot)^\top$ denotes a matrix transposition. It is presumed that the body force density function $\mathbf{b}(\mathbf{x})$ is self-equilibrated and vanished outside some loading region B^b :

$$\int \mathbf{b}(\mathbf{x}) = \mathbf{0}, \quad \mathbf{b}(\mathbf{y}) = \mathbf{0}, \quad \mathbf{y} \notin B^b\{\mathbf{y} \mid |\mathbf{y}| < a^b\}. \quad (2.4)$$

$\mathbf{L}(\mathbf{x})$ and $\mathbf{M}(\mathbf{x}) \equiv \mathbf{L}(\mathbf{x})^{-1}$ are the known phase stiffness and compliance tensors. $\boldsymbol{\beta}(\mathbf{x})$ and $\boldsymbol{\alpha}(\mathbf{x}) = -\mathbf{L}(\mathbf{x})\boldsymbol{\beta}(\mathbf{x})$ are second-order tensors of local eigenstrains and eigenstresses. In particular, for isotropic phases, the local stiffness tensor $\mathbf{L}(\mathbf{x})$ is presented in terms of the local bulk $k(\mathbf{x})$ and shear $\mu(\mathbf{x})$ moduli and:

$$\mathbf{L}(\mathbf{x}) = (dk, 2\mu) \equiv dk(\mathbf{x})\mathbf{N}_1 + 2\mu(\mathbf{x})\mathbf{N}_2, \quad \boldsymbol{\beta}(\mathbf{x}) = \beta^t \theta \boldsymbol{\delta},$$

$\mathbf{N}_1 = \boldsymbol{\delta} \otimes \boldsymbol{\delta}/d$, $\mathbf{N}_2 = \mathbf{I} - \mathbf{N}_1$ ($d = 2$ or 3) whereas $\boldsymbol{\delta}$ and \mathbf{I} are the unit second-order and fourth-order tensors; $\theta = T - T_0$ denotes the temperature changes with respect to a reference temperature T_0 and β^t is a thermal expansion. For all material tensors \mathbf{g} (e.g., $\mathbf{L}, \mathbf{M}, \boldsymbol{\beta}, \boldsymbol{\alpha}$) the

notation $\mathbf{g}_1(\mathbf{x}) \equiv \mathbf{g}(\mathbf{x}) - \mathbf{g}^{(0)} = \mathbf{g}_1^{(m)}(\mathbf{x})$ ($\mathbf{x} \in v^{(m)}$, $m = 0, 1$) is exploited. The upper index $^{(m)}$ indicates the components, and the lower index i shows the individual heterogeneities; $v^{(0)} = w \setminus v$, $v \equiv \cup v_i$, $V(\mathbf{x}) = \sum V_i(\mathbf{x})$, and $V_i(\mathbf{x})$ are the indicator functions of v_i , equals 1 at $\mathbf{x} \in v_i$ and 0 otherwise, ($i = 1, 2, \dots$). Substitution of Eqs. (2.2) and (2.3) into Eq. (2.1) leads to a representation of the equilibrium equation (2.1) in the form

$${}^L\tilde{\mathcal{L}}(\mathbf{u})(\mathbf{x}) + \mathbf{b}(\mathbf{x}) = \mathbf{0}, \quad {}^L\tilde{\mathcal{L}}(\mathbf{u})(\mathbf{x}) := \nabla[\mathbf{L}\nabla\mathbf{u}(\mathbf{x}) + \boldsymbol{\alpha}(\mathbf{x})], \quad (2.5)$$

where ${}^L\tilde{\mathcal{L}}(\mathbf{u})(\mathbf{x})$ is an elliptic differential operator of the second order.

In this section, a summary of the linear peridynamic model introduced by Silling [311] (see also [35], [176], [201], [316]). An equilibrium equation is free of any derivatives of displacement (contrary to Eq. (2.5)) and presented in the following form

$$\tilde{\mathcal{L}}(\mathbf{u})(\mathbf{x}) + \mathbf{b}(\mathbf{x}) = \mathbf{0}, \quad \tilde{\mathcal{L}}(\mathbf{u})(\mathbf{x}) := \int \mathbf{f}(\mathbf{u}(\hat{\mathbf{x}}) - \mathbf{u}(\mathbf{x}), \hat{\mathbf{x}} - \mathbf{x}, \mathbf{x}) d\hat{\mathbf{x}}, \quad (2.6)$$

where \mathbf{f} is a *bond force density* whose value is the force vector that the point located at $\hat{\mathbf{x}}$ (in the reference configuration) exerts on the point located at \mathbf{x} (also in the reference configuration); the third argument \mathbf{x} of \mathbf{f} (2.6) can be dropped for the homogeneous media. Equations (2.5₁) and (2.6₁) have the same form for both local and peridynamic formulation with the different operators (2.5₂) and (2.6₂). Because of this, the superscripts ${}^L(\cdot)$ will correspond to the local case.

The relative position of two material points in the reference configuration $\boldsymbol{\xi} = \hat{\mathbf{x}} - \mathbf{x}$ and their relative displacement $\boldsymbol{\eta} = \mathbf{u}(\hat{\mathbf{x}}) - \mathbf{u}(\mathbf{x})$ are connected with the relative position vector between the two points in the deformed (or current) configuration $\boldsymbol{\eta} + \boldsymbol{\xi}$. Only points $\hat{\mathbf{x}}$ inside some neighborhood (horizon region) $\mathcal{H}_{\mathbf{x}}$ of \mathbf{x} interact with \mathbf{x} :

$$\mathbf{f}(\boldsymbol{\eta}, \boldsymbol{\xi}, \mathbf{x}) \equiv \mathbf{0} \quad \forall \hat{\mathbf{x}} \notin \mathcal{H}_{\mathbf{x}}. \quad (2.7)$$

The vector $\boldsymbol{\xi} = \hat{\mathbf{x}} - \mathbf{x}$ ($\hat{\mathbf{x}} \in \mathcal{H}_{\mathbf{x}}$) is called a *bond* to \mathbf{x} , and the collection of all bonds to \mathbf{x} form the horizon region $\mathcal{H}_{\mathbf{x}}$. Without a loss of generality, it is assumed that a shape of $\mathcal{H}_{\mathbf{x}}$ is spherical: $\mathcal{H}_{\mathbf{x}} = \{\hat{\mathbf{x}} : |\hat{\mathbf{x}} - \mathbf{x}| \leq l_{\delta}\}$ and a number l_{δ} , called the *horizon*, does not depend on \mathbf{x} . The properties of $\mathbf{f}(\boldsymbol{\eta}, \boldsymbol{\xi}, \mathbf{x})$ are considered in [311].

Peridynamic states introduced by Silling [317] (for a more detailed summary, see [321])) are the functions acting on bounds. There are scalar, vector, and modulus states producing the scalars, vectors, and 2nd order tensors, respectively. $\mathbf{T}[\mathbf{x}]\langle \boldsymbol{\xi} \rangle$ and $\mathbf{T}[\hat{\mathbf{x}}]\langle -\boldsymbol{\xi} \rangle$ are the *force vector states* at \mathbf{x} and $\hat{\mathbf{x}}$, which return the force densities associated with $\boldsymbol{\xi}$ and $-\boldsymbol{\xi}$, respectively. In the ordinary state-based peridynamics being considered, $\mathbf{T}[\mathbf{x}]\langle \boldsymbol{\xi} \rangle$ is parallel (in contrast with the non-ordinary model) to the deformation vector state and the equilibrium Eq. (2.6) is expressed through the force vector states as (see for details [317], [321])

$$\tilde{\mathcal{L}}(\mathbf{u})(\mathbf{x}) + \mathbf{b}(\mathbf{x}) = \mathbf{0}, \quad \tilde{\mathcal{L}}(\mathbf{u})(\mathbf{x}) := \int \{\mathbf{T}[\mathbf{x}]\langle \boldsymbol{\xi} \rangle - \mathbf{T}[\hat{\mathbf{x}}]\langle -\boldsymbol{\xi} \rangle\} d\hat{\mathbf{x}}. \quad (2.8)$$

A small displacement state \mathbf{u} when

$$\mathbf{l} := \sup_{|\xi| \leq l_\delta} |\boldsymbol{\eta}(\boldsymbol{\xi})| \ll l_\delta. \quad (2.9)$$

is considered. Force vector state

$$\underline{\mathbf{T}} = \underline{\mathbf{T}}^0 + \underline{\mathbb{K}} \bullet \underline{\mathbf{U}}. \quad (2.10)$$

is expressed through the *modulus state* $\underline{\mathbb{K}}$. Here, the operation of *dot product* \bullet of two vector states $\underline{\mathbf{A}}$, $\underline{\mathbf{B}}$ and a double state $\underline{\mathbb{D}}$ are introduced as

$$\begin{aligned} \underline{\mathbf{A}} \bullet \underline{\mathbf{B}} &= \langle \underline{\mathbf{A}}(\boldsymbol{\xi}) \cdot \underline{\mathbf{B}}(\boldsymbol{\xi}) \rangle^{\mathcal{H}_x} = \int_{\mathcal{H}_x} \underline{\mathbf{A}}(\boldsymbol{\xi}) \cdot \underline{\mathbf{B}}(\boldsymbol{\xi}) \, d\xi, \\ (\underline{\mathbb{D}} \bullet \underline{\mathbf{B}})_i(\boldsymbol{\xi}) &= \int_{\mathcal{H}_x} \underline{\mathbb{D}}_{ij}(\boldsymbol{\xi}, \boldsymbol{\zeta}) \cdot \underline{\mathbf{B}}_j(\boldsymbol{\zeta}) \, d\boldsymbol{\zeta}. \end{aligned} \quad (2.11)$$

Hereafter $\langle (\cdot) \rangle^{\mathcal{H}_x}(\mathbf{x})$ denotes the average over the horizon region \mathcal{H}_x with the center \mathbf{x} .

A linearized model for pure mechanical loading ($\boldsymbol{\beta} \equiv \mathbf{0}$) can be written from (2.8₂) as described by Silling [312]

$$\tilde{\mathcal{L}}(\mathbf{C}, \mathbf{u})(\mathbf{x}) + \mathbf{b}(\mathbf{x}) = \mathbf{0}, \quad (2.12)$$

$$\tilde{\mathcal{L}}(\mathbf{C}, \mathbf{u})(\mathbf{x}) : = \int_w \mathbf{C}(\mathbf{x}, \mathbf{q})(\mathbf{u}(\mathbf{q}) - \mathbf{u}(\mathbf{x})) \, dV_q, \quad (2.13)$$

where the integrand in Eq. (2.10) vanishing at $|\mathbf{x} - \mathbf{q}| \geq 2l_\delta$ may be non-null at $l_\delta < |\mathbf{x} - \mathbf{q}| < 2l_\delta$. The kernel with the following symmetries holds for any \mathbf{x} and \mathbf{q} :

$$\mathbf{C}^\top(\mathbf{x}, \mathbf{q}) = \mathbf{C}(\mathbf{q}, \mathbf{x}). \quad (2.14)$$

Thermoelastic cases ($\boldsymbol{\beta} \neq \mathbf{0}$) were considered in [236], [20], [189], [237].

For subsequent convenience, one introduces a vector-valued function $\tilde{\mathbf{f}} : \mathbb{R}^d \times \mathbb{R}^d \rightarrow \mathbb{R}^d$ by

$$\tilde{\mathbf{f}}(\mathbf{p}, \mathbf{q}) = \begin{cases} \mathbf{f}(\mathbf{u}(\mathbf{p}) - \mathbf{u}(\mathbf{q}), \mathbf{p} - \mathbf{q}, \mathbf{q}), & \text{if } \mathbf{p}, \mathbf{q} \in w, \\ \mathbf{0}, & \text{otherwise,} \end{cases} \quad (2.15)$$

which is presumed to be Riemann-integrable. Then, one can define the “peridynamic stress” $\boldsymbol{\sigma}(\mathbf{z})$ at the point \mathbf{z} as the total force that all material points $\hat{\mathbf{x}}$ to the right of \mathbf{z} exert on all material points to its left (see e.g., [64], [201], [322], [343]). For dD cases ($d = 1, 2, 3$)

$$\boldsymbol{\sigma}(\mathbf{x}) = \mathcal{L}^\sigma(\mathbf{u}), \quad (2.16)$$

$$\mathcal{L}^\sigma(\mathbf{u}) := \frac{1}{2} \int_S \int_0^\infty \int_0^\infty (y+z)^{d-1} \tilde{\mathbf{f}}(\mathbf{x} + y\mathbf{m}, \mathbf{x} - z\mathbf{m}) \otimes \mathbf{m} \, dz \, dy \, d\Omega_{\mathbf{m}}. \quad (2.17)$$

Here, S stands for the unit sphere, and $d\Omega_{\mathbf{m}}$ denotes a differential solid angle on S in the direction of any unite vector \mathbf{m} . It was proved [204] that the peridynamic stress is the same as the first Piola-Kirchhoff static Virial stress which offers a simple and clear expression for numerical calculations of peridynamic stress.

The equilibrium Eqs. (2.8), (2.21) and (2.16) of ordinary state-based PD are considered. When the interactions between material points are only pairwise, the equilibrium equations are reduced to the bond-based PD equations. One of the simplest nonlinear is the proportional microelastic material model [316]

$$\mathbf{f}^{\text{bond}}(\boldsymbol{\eta}, \boldsymbol{\xi}, \mathbf{x}) = f(|\boldsymbol{\eta} + \boldsymbol{\xi}|, \boldsymbol{\xi})\mathbf{e}, \quad f(|\boldsymbol{\eta} + \boldsymbol{\xi}|, \boldsymbol{\xi}) = c(\boldsymbol{\xi})s, \quad (2.18)$$

$$\mathbf{e} := \frac{\boldsymbol{\eta} + \boldsymbol{\xi}}{|\boldsymbol{\eta} + \boldsymbol{\xi}|}, \quad s := \frac{|\boldsymbol{\eta} + \boldsymbol{\xi}| - |\boldsymbol{\xi}|}{|\boldsymbol{\xi}|}, \quad (2.19)$$

where s denotes the bond stretch (also called bond strain) which is the relative change of the length of a bond, and c is referenced as the ‘‘bond constant’’. Although this model is linear in terms of the bond stretches, it is nonlinear in terms of displacements; thermoelastic cases ($\boldsymbol{\beta} \neq \mathbf{0}$) were considered in [20], [189], [236], [237]. A nonlinear model in terms of bond stretches (at $\boldsymbol{\beta} \equiv \mathbf{0}$)

$$f(|\boldsymbol{\eta} + \boldsymbol{\xi}|, \boldsymbol{\xi}) = c(\boldsymbol{\xi})[s + 3s^2/2 + s^3/2] \quad (2.20)$$

is considered in [172]. The potential role of employing a nonlinear peridynamic kernel in predicting the onset of fractures has been explored in [107] (see also [91], [92]).

A linearized version of the theory (for small displacement) for a microelastic homogeneous material (2.21) takes the form ($\forall \boldsymbol{\eta}, \boldsymbol{\xi}$)

$$\mathbf{f}^{\text{bond}}(\boldsymbol{\eta}, \boldsymbol{\xi}, \mathbf{x}) = \mathbf{f}_{\text{lin}}^{\text{bond}}(\boldsymbol{\eta}, \boldsymbol{\xi}, \mathbf{x}) = \mathbf{C}^{\text{bond}}(\boldsymbol{\xi}, \mathbf{x})\boldsymbol{\eta}, \quad (2.21)$$

Here, the material’s *micromodulus* function \mathbf{C} contains all constitutive information and its value is a second-order tensor given by

$$\mathbf{C}^{\text{bond}}(\boldsymbol{\xi}, \mathbf{x}) = \frac{\partial \mathbf{f}(\mathbf{0}, \boldsymbol{\xi}, \mathbf{x})}{\partial \boldsymbol{\eta}} \quad \forall \boldsymbol{\xi}. \quad (2.22)$$

Substitution of Eq. (2.21) into Eq. (2.6) leads to the equilibrium equation

$$\tilde{\mathcal{L}}(\mathbf{C}^{\text{bond}}, \mathbf{u})(\mathbf{x}) + \mathbf{b}(\mathbf{x}) = \mathbf{0}, \quad (2.23)$$

$$\tilde{\mathcal{L}}(\mathbf{C}^{\text{bond}}, \mathbf{u})(\mathbf{x}) := \int \mathbf{C}^{\text{bond}}(\mathbf{x}, \mathbf{q})(\mathbf{u}(\mathbf{q}) - \mathbf{u}(\mathbf{x})) dV_q. \quad (2.24)$$

For consistency with Newton’s third law, the micromodulus function \mathbf{C} for the homogeneous materials must be symmetric to its tensor structure as well as to arguments

$$\mathbf{C}^{\text{bond}}(\mathbf{x}, \mathbf{q}) = \mathbf{C}^{\text{bond}}(\mathbf{q}, \mathbf{x}) = (\mathbf{C}^{\text{bond}})^\top(\mathbf{x}, \mathbf{q}) \quad \forall \mathbf{x}, \mathbf{q}, \quad (2.25)$$

where the properties of \mathbf{C}^{bond} are discussed in detail in Silling [54] (see also [10, 33]). For example, for the micromodulus functions with the step-function and triangular profiles,

$$\mathbf{C}(\boldsymbol{\xi}) = \mathbf{C}V(\mathcal{H}_{\mathbf{x}}), \quad \mathbf{C}(\boldsymbol{\xi}) = \mathbf{C}(1 - |\boldsymbol{\xi}|/l_\delta)V(\mathcal{H}_{\mathbf{x}}), \quad (2.26)$$

respectively, where $V(\mathcal{H}_{\mathbf{x}})$ is the indicator function of $\mathcal{H}_{\mathbf{x}}$. The peridynamic solution of Eq. (2.23) with \mathbf{C} described by Eq. (2.26) is investigated in detail by both numerical and analytical methods in 1D (see [36], [249], [322], [343]), 2D (see [163], [164]), and 3D cases [250], [344].

For bond-based peridynamics, the stress representation (2.17) can be recast in terms of displacements

$$\begin{aligned} \mathcal{L}^\sigma(\mathbf{C}, \mathbf{u}) : &= \frac{1}{2} \int_S \int_0^\infty \int_0^\infty (y+z)^{d-1} \mathbf{C}^{\text{bond}}((y+z)\mathbf{m}, \mathbf{x} - z\mathbf{m}) \\ &\times [\mathbf{u}(\mathbf{x} + y\mathbf{m}) - \mathbf{u}(\mathbf{x} - z\mathbf{m})] \otimes \mathbf{m} dz dy d\Omega_{\mathbf{m}}. \end{aligned} \quad (2.27)$$

It is interesting that equilibrium Eqs. (2.22) and (2.23) formally coincide, although the kernels $\mathbf{C}(\mathbf{x}, \mathbf{q})$ (2.23) and $\mathbf{C}^{\text{bond}}(\mathbf{x}, \mathbf{q})$ (2.21) are conceptually different with different symmetry properties (2.15) and (2.25), respectively. Moreover, in the state-based version, the maximum interaction distance between the points is $2l_\delta$ whereas this distance in bond-based peridynamics coincides with the horizon l_δ . However, this similarity provides a possibility to reformulate the results obtained before for the linear bond-based peridynamic micromechanics (see for details [64] and [79]) to their counterparts for the linear ordinary state-based ones.

2.2 Statistical description of the composite microstructures

Two material length scales (see, e.g., [334]) are considered: the macroscopic scale L , characterizing the extent of w , and the microscopic scale a , related with the heterogeneities v_i . Moreover, one supposes that the applied field varies on a characteristic length scale Λ . The limit of our interests for both the material scales and field one are either

$$L \gg \Lambda \geq a \geq l_\delta \quad \text{or} \quad L \gg \Lambda \gg a \geq l_\delta, \quad (2.28)$$

where the inequalities (2.28₂) are called a scale separation hypothesis. All random quantities under discussion are described by statistically inhomogeneous random fields. Let us introduce a conditional probability density $\varphi(v_i, \mathbf{x}_i | v_1, \mathbf{x}_1, \dots, v_n, \mathbf{x}_n)$ for finding a heterogeneity of type i with the center \mathbf{x}_i in the domain v_i , given that the fixed heterogeneities v_1, \dots, v_n are centered at $\mathbf{x}_1, \dots, \mathbf{x}_n$. The notation $\varphi(v_i, \mathbf{x}_i | v_1, \mathbf{x}_1, \dots, v_n, \mathbf{x}_n)$ denotes the case $\mathbf{x}_i \neq \mathbf{x}_1, \dots, \mathbf{x}_n$. A random field being considered is called statistically homogeneous its multi-point statistical moments of any order are shift-invariant functions of spatial variables. Of course, $\varphi(v_i, \mathbf{x}_i | v_1, \mathbf{x}_1, \dots, v_n, \mathbf{x}_n) = 0$ (since heterogeneities cannot overlap) for

values of \mathbf{x}_i lying inside the some area $\cup v_{mi}^0$ ($m = 1, \dots, n$) called “excluded volumes”, where $v_{mi}^0 \supset v_m$ with indicator function V_{mi}^0 is the “excluded volumes” of \mathbf{x}_i with respect to v_m (it is usually assumed that $v_{mi}^0 \equiv v_m^0$), and $\varphi(v_i, \mathbf{x}_i; v_1, \mathbf{x}_1, \dots, v_n, \mathbf{x}_n) \rightarrow \varphi(v_i, \mathbf{x}_i)$ as $|\mathbf{x}_i - \mathbf{x}_m| \rightarrow \infty$, $m = 1, \dots, n$ (since no long-range order is assumed). $\varphi(v_i, \mathbf{x})$ is a number density, $n^{(k)} = n^{(k)}(\mathbf{x})$ of component $v_i \in v^{(k)}$ at the point \mathbf{x} and $c^{(k)} = c^{(k)}(\mathbf{x})$ is the concentration, i.e. volume fraction, of the component $v_i \in v^{(k)}$ at the point \mathbf{x} : $c^{(k)}(\mathbf{x}) = \langle V^{(k)} \rangle(\mathbf{x}) = \bar{v}_i n^{(k)}(\mathbf{x})$, $\bar{v}_i = \text{mes} v_i$ ($k = 1, 2, \dots, N$; $i = 1, 2, \dots$), $c^{(0)}(\mathbf{x}) = 1 - \langle V \rangle(\mathbf{x})$.

A very short description of the notations presented is immediately used in subsequent representations. For clear mathematical definitions of basic stochastic geometry conceptions (such as, e.g., random fields, probability space, probability density, statistically homogeneous and inhomogeneous fields, ergodicity, clustered media, etc.), the interested readers are referred to [89] applications to a wide class of micromechanical problems and continuum physics can be found, e.g., in [64], [240], [334].

2.3 Volumetric boundary conditions

Owing to nonlocality, the equilibrium equation (2.6) is combined with a “boundary” condition, used as a volumetric constraint in the so-called interaction domain w_Γ (in opposite to the local case where the boundary conditions are imposed directly at the bounding surface $\Gamma^{(0)}$, see for details [311], [188]; i.e., the nonlocal boundary w_Γ is a d -dimensional region unlike its $(d-1)$ -dimensional counterpart Γ^0 in local problems. The interaction domain w_Γ contains points \mathbf{y} not in w interacting with points $\mathbf{x} \in w$. The most popular shape for w_Γ with prescribed either the forces or displacements is a boundary layer of thickness given by $2l_c$ (see [229]): $w_\Gamma = \{w \oplus \mathcal{H}_0\} \setminus w$, where $w \oplus \mathcal{H}_0$ is the Minkowski sum $w (\mathcal{A} \oplus \mathcal{B} := \cup_{\mathbf{x} \in \mathcal{A}, \mathbf{y} \in \mathcal{B}} \{\mathbf{x} + \mathbf{y}\})$; then w is the internal region of \bar{w} (see [311]).

It is presumed that \bar{w} is considered as a cutting out of a macrodomain (containing a statistically large number of inclusion’s realization) from the random heterogeneous medium covering the entire space \mathbb{R}^d . Then, the Dirichlet, or Neumann volumetric boundary conditions (VBC, see [122], [244]) are called homogeneous volumetric loading conditions if there exist some symmetric constant tensors either $\boldsymbol{\varepsilon}^{w_\Gamma}$ or $\boldsymbol{\sigma}^{w_\Gamma}$ such that

$$\mathbf{u}(\mathbf{x}) = \mathbf{h}(\mathbf{y}) = \boldsymbol{\varepsilon}^{w_\Gamma} \mathbf{y}, \quad \forall \mathbf{y} \in w_{\Gamma u} = w_\Gamma, \quad (2.29)$$

$$\tilde{\mathcal{L}}(\mathbf{x}) = -\mathbf{g}(\mathbf{y}) = -\boldsymbol{\sigma}^{w_\Gamma} \mathbf{n}(\mathbf{y}), \quad \forall \mathbf{y} \in w_{\Gamma \sigma} = w_\Gamma, \quad (2.30)$$

respectively. There are no specific restrictions on the smoothness and shape of Γ_0 , which is defined only by the convenience of representation. It should be mentioned that in the LM, the analogs of the VBC (2.29) and (2.30) correspond to the analyses of the equations for either strain or stresses, respectively, which are formally similar to each other. However, in peridynamic micromechanics, a primary unknown variable is displacement (rather than stresses), and, because of this, the VBC (2.29) is assumed.

Seemingly to the volumetric boundary domain w_{Γ_i} , we introduce a volumetric interface boundary (called also interaction interface, see [306], [6]) $v_{\Gamma_i} = v_{\Gamma_i}^+ \cup v_{\Gamma_i}^-$ where $v_{\Gamma_i}^+$ and $v_{\Gamma_i}^-$ are the boundary layers (internal and external, respectively) divided by the geometric boundary Γ_i and have a thickness expressed through the horizon as $2l_\delta$. The geometrical boundaries of the boundary layers $v_{\Gamma_i}^+$ and $v_{\Gamma_i}^-$ are Γ_i^+ and Γ_i^- , respectively. For a general form of the inclusion v_i the external volumetric interface Γ_i^- can be expressed through the Minkowski sum $\Gamma_i^- = \{v_i \oplus 2\mathcal{H}_0\} \setminus v_i$, where $2\mathcal{H}_0 := \{\mathbf{x} \mid \mathbf{x}/2 \in \mathcal{H}_0\}$. A nonlocal closure of the inclusion $v_i^l := v_i \oplus 2\mathcal{H}_0$ (with an indicator function $V_i^l(\mathbf{x})$) is called an *extended inclusion* while $v^l := \cup v_i^l$ ($i = 1, 2, \dots$) (with the indicator function $V^l(\mathbf{x}) = \sum_i V_i^l(\mathbf{x})$) stands for the extended inclusion phase. In so doing $v^{l(0)} := w \setminus v^l \subset v^{(0)}$ is called a *truncated matrix*.

In the simplest case, a micromodulus of interaction interface of the inclusion v_i (see, e.g. [6], [7], [316]) is presented as an average value of the material properties at two material points connecting dissimilar materials ($V^{(0)}(\mathbf{x}) + V_i(\hat{\mathbf{x}}) = V^{(0)}(\hat{\mathbf{x}}) + V_i(\mathbf{x}) = 1$)

$$\mathbf{C}^i(\mathbf{x}, \hat{\mathbf{x}}) = [\mathbf{C}^{(0)}(\mathbf{x}, \hat{\mathbf{x}}) + \mathbf{C}_i(\mathbf{x}, \hat{\mathbf{x}})]/2 \quad (2.31)$$

although more sophisticated models of interaction interface properties (see, e.g., [35], [232], [198], see for references [26]), can be incorporated into the general subsequent representations. In particular, a variation of $\mathbf{C}^i(\mathbf{x}, \hat{\mathbf{x}})$ was presented in [232] and [283] in a spirit of the functionally graded materials theory described in, e.g. [47].

2.4 Periodic structures and volumetric periodic boundary conditions

For simplicity of notations for periodic media, we consider 2D cases $w = \cup \Omega_{ij}$ ($i, j = 0, \pm 1, \pm 2, \dots$) with the square unit cells Ω_{ij} and the centers of the unite cells $\mathbf{\Lambda} = \{\mathbf{x}_{ij}\}$. Let a representative unit cell Ω_{00} with the corner points \mathbf{x}_{kl}^c ($k, l = \pm 1$) has the boundary $\Gamma^0 = \cup \Gamma_{ij}^0$ where the boundary partition $\mathbf{x}_{ij}^0 \in \Gamma_{ij}^0$ separates the UCs Ω_{00} and Ω_{ij} ($i = 0, \pm 1, j = \pm(1 - |i|)$, see Fig. 19.2 in [64]). A representative volume element (or the unit cell, UC) Ω_{00} is deformed in a repetitive way as its neighbors. The position vectors $\mathbf{x}_{ij}^0 \in \Gamma_{ij}^0$ or $\mathbf{x}_{kl}^0 \in \Gamma_{kl}^0$ are presented by the corner points \mathbf{x}_{mn}^c ($i = 0, \pm 1, j = \pm(1 - |i|), k = -i, l = -j, m, n = \pm 1$); e.g., $\mathbf{x}_{ij}^0 = \mathbf{x}_{kl}^c + \mathbf{x}_{1,-1}^c - \mathbf{x}_{-1,-1}^c$ for the $i = 1, j = 0$. N field points \mathbf{x}_i ($i = 1, \dots, N$) in the central cube $\Omega_{00} = \{[-l^\Omega, l^\Omega]^d\}$ are periodically reflected as \mathbf{x}_i^α into the neighboring cubes Ω_α , where $\alpha = (\alpha_1, \dots, \alpha_d) \in Z^+$, and $\alpha_i = 0, \pm 1$ ($i = 1, \dots, d$). If the source point $\mathbf{x}_p + \boldsymbol{\xi} \in \Omega_\alpha$ ($\boldsymbol{\xi} \in \mathcal{H}_p$) then the peridynamic counterpart of the local PBC called new *volumetric periodic boundary conditions* (VPBC, see [56], [64]) represent periodic displacements and antiperiodic tractions

$$\mathbf{u}(\mathbf{x}_p + \boldsymbol{\xi}) = \mathbf{u}(\mathbf{x}_p + \boldsymbol{\xi} - 2\boldsymbol{\alpha}^l) + 2\varepsilon^{w\Gamma} \boldsymbol{\alpha}^l, \quad (2.32)$$

$$\mathbf{t}(\mathbf{x}_\alpha^0) = -\mathbf{t}(\mathbf{x}_\gamma^0), \quad (2.33)$$

respectively, where $\boldsymbol{\gamma} = -\boldsymbol{\alpha}$ and \mathbf{x}_α^0 are defined analogously to \mathbf{x}_{ij}^0 . The VPBC (2.32) and (2.33) were used in computational homogenization theory for CMs with both the bond-based [56], [64] and non-ordinary state-based [143] peridynamic properties of constituents.

2.5 Some averages

In the case of statistically homogeneous random functions $\mathbf{f}(\mathbf{x})$, the ergodicity condition is assumed when the spatial average estimated over one sufficiently large sample and statistical mean coincide for both the whole volume w and the individual constituent $v^{(k)}$ ($k = 0, 1, \dots, N$):

$$\langle \mathbf{f} \rangle = \{\mathbf{f}\} \equiv \lim_{w \uparrow \mathbb{R}^d} |w|^{-1} \int_w \mathbf{f}(\mathbf{x})(\mathbf{x}) d\mathbf{x}, \quad (2.34)$$

$$\langle \mathbf{f} \rangle^{(k)} = \{\mathbf{f}\}^{(k)} \equiv \lim_{w \uparrow \mathbb{R}^d} |w|^{-1} \int_w \mathbf{f}(\mathbf{x})(\mathbf{x}) V^{(k)} d\mathbf{x}, \quad (2.35)$$

where $|w| = \text{mes } w$. Under the Gauss theorem, the volume averages by integrals over the corresponding boundary are expressed. In particular, for the homogeneous boundary conditions either (2.29) or (2.30) the mean value $\{\boldsymbol{\varepsilon}\}$ or $\{\boldsymbol{\sigma}\}$ of $\boldsymbol{\varepsilon}$ or $\boldsymbol{\sigma}$ coincide with $\boldsymbol{\varepsilon}^{w\Gamma}$ and $\boldsymbol{\sigma}^{w\Gamma}$ (see, e.g. [64]).

The volume averages of the strains and stresses inside the extended inclusion v_i^l can be presented by the averages over the external inclusion boundary Γ_i^- by the use of Gauss's theorem

$$\langle \boldsymbol{\varepsilon} V^l \rangle = \boldsymbol{\varepsilon}^{l(1)} = \boldsymbol{\varepsilon}^{l\omega(1)} := \frac{1}{\bar{w}} \sum_i \int_{\Gamma_i^-} \mathbf{u}(\mathbf{s}) \overset{\mathcal{S}}{\otimes} \mathbf{n}(\mathbf{s}) d\mathbf{s}, \quad (2.36)$$

$$\langle \boldsymbol{\sigma} V^l \rangle = \boldsymbol{\sigma}^{l(1)} = \boldsymbol{\sigma}^{l\omega(1)} := \frac{1}{\bar{w}} \sum_i \int_{\Gamma_i^-} \mathbf{t}(\mathbf{s}) \overset{\mathcal{S}}{\otimes} \mathbf{s} d\mathbf{s}. \quad (2.37)$$

The absence of numerical differentiation defines an advantage of the surface average (2.36) with respect to the volume average. The surface average of stresses (2.37) has the well-known advantage of the reduction of dimension by one that can be crucial for the analyst. In Eqs. (2.36) and (2.37) the averages over the modified phases (e.g., the extended inclusions or truncated matrix) are used

$$\langle \mathbf{f} \rangle^{l(k)} = \{\mathbf{f}\}^{l(k)} \equiv \lim_{w \uparrow \mathbb{R}^d} |w|^{-1} \int_w \mathbf{f}(\mathbf{x})(\mathbf{x}) V^{l(k)} d\mathbf{x}, \quad (2.38)$$

instead of the averages (2.34₂) exploited in local micromechanics.

It should be mentioned that all averages(2.32)-(2.38) and the equality

$$\{\mathbf{g}\} = c^{(0)} \{\mathbf{g}\}^{(0)} + c^{(1)} \{\mathbf{g}\}^{(1)}, \quad (2.39)$$

(e.g., $\mathbf{g} = \boldsymbol{\varepsilon}, \boldsymbol{\sigma}, \boldsymbol{\tau}, \boldsymbol{\eta}$), is fulfilled only for statistically homogeneous media subjected to the homogeneous boundary conditions. If any of these conditions are broken, then it is necessary to consider two sorts of conditional averages (see for details [47], [64]). At first, $\langle \mathbf{g} \rangle^{(q)}(\mathbf{x})$ can be found as $\langle \mathbf{g} \rangle^{(q)}(\mathbf{x}) = \langle V^{(q)} \rangle^{-1}(\mathbf{x}) \langle \mathbf{g} V^{(q)} \rangle(\mathbf{x})$. Usually, it is simpler to estimate the conditional averages of these tensors in the concrete point with the micro-coordinate \mathbf{z} of the fixed inclusion $\mathbf{z} \in v_q$: $\langle \mathbf{g} | v_q, \mathbf{x}_q \rangle(\mathbf{x}, \mathbf{z}) \equiv \langle \mathbf{g} \rangle_q(\mathbf{x}, \mathbf{z})$. Then a relation between the mentioned averages takes place $[\mathbf{x} = (x_1, \dots, x_d)^\top]$:

$$c^{l(q)}(\mathbf{x}) \langle \mathbf{g} \rangle^{l(q)}(\mathbf{x}) = \int_{v_q^{l1}(\mathbf{x})} n^{l(q)}(\mathbf{y}) \langle \mathbf{g} | v_q, \mathbf{y} \rangle(\mathbf{x}, \mathbf{y} - \mathbf{x}) d\mathbf{y}. \quad (2.40)$$

where $v_q^1(\mathbf{x})$ is construct as a limit $v_{kq}^{l0} \rightarrow v_q^1(\mathbf{x})$ if a fixed ellipsoid v_k is shrinking to the point \mathbf{x} ; in a similar manner $v_{kq}^{l0} \rightarrow v_q^{l1}(\mathbf{x})$ is constructed for the peridynamic case.

3 General integral equations (GIEs)

3.1 Analytical and computational micromechanics. Linear GIEs in LM

In this subsection, a colored history of the GIEs in LM is presented.

The first background of local micromechanics was begun by Poisson and Faraday (in the electricity and magnetism context), Mossotti and Clausius (in the dielectric context), Lorenz (in the refractivity context), and Maxwell (in the conductivity context), see for references [47], [64]. They considered the different physical phenomena with an identical background concept (so-called effective field hypothesis, EFH, **H1a**) as a local homogeneous field acting on the inclusions and differing from the applied (at the infinity) macroscopic one, e.g.,

$$\bar{\boldsymbol{\varepsilon}}_i(\mathbf{x}) = \text{const}, \quad \bar{\boldsymbol{\varepsilon}}(\mathbf{x}) \neq \boldsymbol{\varepsilon}^{w\Gamma} \quad (\mathbf{x} \in v_i). \quad (3.1)$$

The concept of the EFH (even if this term is not mentioned) in combination with subsequent assumptions totally predominates (and creates the fundamental limitations) in all four groups of *analytical micromechanics* (classification by Willis [353]) of *random* random structure matrix CMs in physics and mechanics of heterogeneous media:

$$\begin{array}{ll} \underline{\text{Gr1}} \text{ model methods,} & \underline{\text{Gr2}} \text{ perturbation methods,} \\ \underline{\text{Gr3}} \text{ variational methods,} & \underline{\text{Gr4}} \text{ self – consistent methods} \end{array} \quad (3.2)$$

of truncation of a hierarchy among which there are no rigorous boundaries (see for references and details [47], [64], [116], [182], [334]). The destiny of *analytical micromechanics* is providing the required estimations by more cheap, fast, robust, and flexible methods (although it takes additional intellectual complexity to the implementations) than direct numerical simulation (DNS).

In contrast, *computational micromechanics* for CM of *deterministic* structures is based on DNS which can be found by different numerical methods. Computational micromechanics can be classified into three broad categories (blocks):

$$\begin{array}{ccc} \text{Block 1) Asymptotic} & \text{Block 2) Computational,} & \text{Block 3) Finite set of} \\ \text{homogenization,} & \text{homogenization,} & \text{inclusions.} \end{array} \quad (3.3)$$

Blocks 1 and 2 are applied to periodic structure composites (see Introduction). Block 3 corresponds to one and the finite set of inclusions for either the finite size sample or the infinite matrix with a finite set of inclusions (in such a case, the problem can be solved by either the volume integral equation methods or boundary integral equation one, see for references, e.g. [64]). Thus, a fundamental difference between computational micromechanics and analytical one is the use (or not use) of DNS (see Fig. 1); i.e. this difference has no connection with the difference between the meaning of words analytical and computational.

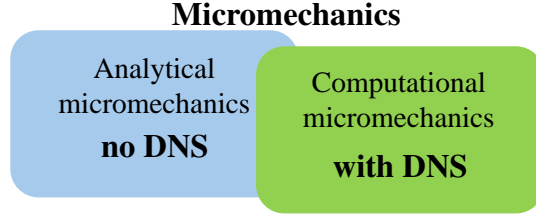


Fig. 1: The scheme of Micromechanics

A central ingredient of analytical micromechanics is the GIE which is the exact integral equation connecting the random fields at the point being considered and the surrounding points. The different GIEs ordered in increasing generality (see for details [53] are reproduced [64])

$$\boldsymbol{\varepsilon}(\mathbf{x}) = \boldsymbol{\varepsilon}^{w\Gamma} + \int \mathbf{U}(\mathbf{x} - \mathbf{y}) {}^L\boldsymbol{\tau}(\mathbf{y}) d\mathbf{y}, \quad {}^L\boldsymbol{\tau}(\mathbf{y}) := {}^L\mathbf{L}_1(\mathbf{y})\boldsymbol{\varepsilon}(\mathbf{y}) \quad (3.4)$$

$$\boldsymbol{\varepsilon}(\mathbf{x}) = \langle \boldsymbol{\varepsilon} \rangle + \int \mathbf{U}(\mathbf{x} - \mathbf{y}) [{}^L\boldsymbol{\tau}(\mathbf{y}) - \langle {}^L\boldsymbol{\tau} \rangle] d\mathbf{y}, \quad (3.5)$$

$$\boldsymbol{\varepsilon}(\mathbf{x}) = \langle \boldsymbol{\varepsilon} \rangle(\mathbf{x}) + \int \mathbf{U}(\mathbf{x} - \mathbf{y}) [{}^L\boldsymbol{\tau}(\mathbf{y}) - \overline{{}^L\boldsymbol{\tau}}(\mathbf{y})] d\mathbf{y}, \quad (3.6)$$

$$\boldsymbol{\varepsilon}(\mathbf{x}) = \langle \boldsymbol{\varepsilon} \rangle(\mathbf{x}) + \int [\mathbf{U}(\mathbf{x} - \mathbf{y}) {}^L\boldsymbol{\tau}(\mathbf{y}) - \underline{\mathbf{U}}(\mathbf{x} - \mathbf{y}) {}^L\boldsymbol{\tau}(\mathbf{y})] d\mathbf{y}, \quad (3.7)$$

where ${}^L\boldsymbol{\tau}(\mathbf{y})$ is the stress polarisation tensor, $\langle (\cdot) \rangle$ and $\langle (\cdot) \rangle(\mathbf{x})$ are the statistical averages introduced in Subsection 2.2. Hereafter, one introduces the infinite body Green's function $\mathbf{G}^{(0)}$ of the Navier equation with homogeneous elastic modulus tensor ${}^L\mathbf{L}^{(0)}$ defined by $\nabla \left\{ {}^L\mathbf{L}^{(0)} [\nabla \otimes \mathbf{G}^{(0)}(\mathbf{x})] \right\} = -\boldsymbol{\delta}\boldsymbol{\delta}(\mathbf{x})$, of order $O(\int |\mathbf{x}|^{1-d} d|\mathbf{x}|)$ as $|\mathbf{x}| \rightarrow \infty$ and vanishing at infinity ($|\mathbf{x}| \rightarrow \infty$). The Green's tensors for the strains is used $\mathbf{U}(\mathbf{x}) = \nabla \nabla \mathbf{G}^{(0)}(\mathbf{x})$.

In Eq. (3.4) the perturbations produced by the surrounding particles (see Eqs. (3.4)) are presented by a direct superposition scheme of summations of these perturbations that leads to the integral, which is not absolutely convergent at infinity. The idea of the so-called method of renormalization (with the introduction of the term $\langle \mathcal{L}^\tau \rangle$ (3.5)) goes back to Lord Rayleigh (1892) [287] who was the first to encounter the mentioned difficulty when considering effective conductivity of periodic system containing a square array of cylinders or cubic lattice of spheres. At last, almost in 90 years after Lord Rayleigh [287], the correctness of GIE (3.5) was independently proved by several authors Shermergor [310], Khoroshun [187], and O'Brian [267]. Equations (3.5) and (3.6) were generalized to either statistically homogeneous or statistically inhomogeneous (so-called graded), respectively, structures of CMs [47]. However, Buryachenko [48] proved that the EFH (3.5) is intrinsically incorporated into the famous term $\langle \mathcal{L}^\tau \rangle$ (3.5) proposed by Lord Rayleigh [287] and, thus, the solution of Eqs. (3.5) and (3.6) without EFH (3.1) is impossible. But no give up! The mentioned impossibility indicates the necessity of corrections of Eqs. (3.5) and (3.6). Indeed, let us move the angle bracket of statistical average “ \langle ” from the old position $\bar{\cdot}$ (3.6) to a new one $\langle \cdot \rangle$ (3.7). This trivial action symbolizes the born of the second background of micromechanics (called also computational analytical micromechanics, see [65], CAM, see rigorous proof in [64]) which is the most fundamental step in analytical micromechanics (see Fig. 1) for the last 130 years after Lord Rayleigh [287].

Let the inclusions v_1, \dots, v_n be fixed and two sorts of effective fields are defined for the strain field $\bar{\varepsilon}_i(\mathbf{x})$, $\tilde{\varepsilon}_{1,\dots,n}(\mathbf{x})$ (a case of the stress field is considered similarly) by the use of the rearrangement of Eq. (3.7) in the following manner (an analogous particular case of these manipulation approaches for linear elasticity problem is given in [48]):

$$\varepsilon(\mathbf{x}) = \bar{\varepsilon}_i(\mathbf{x}) + \mathcal{L}_i^{\varepsilon\tau}(\mathbf{x} - \mathbf{x}_i, L\tau), \quad (3.8)$$

$$\mathcal{L}_i^{\varepsilon\tau}(\mathbf{x} - \mathbf{x}_i, \tau) := \varepsilon(\mathbf{x}) - \bar{\varepsilon}_i(\mathbf{x}) = \int \mathbf{U}(\mathbf{x} - \mathbf{y}) L\tau(\mathbf{y}) V_i(\mathbf{y}) d\mathbf{y}, \quad (3.9)$$

$$\bar{\varepsilon}_i(\mathbf{x}) = \tilde{\varepsilon}_{1,\dots,n}(\mathbf{x}) + \sum_{j \neq i}^n \mathcal{L}_j^\tau(\mathbf{x} - \mathbf{x}_j, L\tau), \quad (3.10)$$

$$\begin{aligned} \tilde{\varepsilon}_{1,\dots,n}(\mathbf{x}) &= \langle \varepsilon \rangle(\mathbf{x}) + \int [\mathcal{L}_k^{\varepsilon L\tau}(\mathbf{x} - \mathbf{x}_k, \tau) V^\delta(\mathbf{x}_k |; v_1, \mathbf{x}_1; \dots; v_n, \mathbf{x}_n) \\ &\quad - \langle \mathcal{L}_k^{\varepsilon\tau}(\mathbf{x} - \mathbf{x}_k, L\tau) \rangle(\mathbf{x}_k)] d\mathbf{x}_k, \end{aligned} \quad (3.11)$$

for $\mathbf{x} \in v_i$, $i = 1, 2, \dots, n$. Here the perturbators $\mathcal{L}_i^{\varepsilon\tau}(\mathbf{x} - \mathbf{x}_i, L\tau)$ ($\mathbf{x} \in \mathbb{R}^d$) (3.9₁) are introduced. They describes perturbation produced by the inclusion v_i ; in particular, $\mathcal{L}_i^{\varepsilon\tau}(\mathbf{x} - \mathbf{x}_i, L\tau)$ can be expressed through the Green function (3.11₂). $V^\delta(\mathbf{x}_k |; v_1, \mathbf{x}_1; \dots; v_n, \mathbf{x}_n) = \sum_m \delta(\mathbf{x}_k - \mathbf{x}_m) - \sum_{i=1}^n \delta(\mathbf{x}_k - \mathbf{x}_i)$ is a random delta function of heterogeneity centers \mathbf{x}_m ($m = 1, 2, \dots$) under the condition that $\mathbf{x}_k \neq \mathbf{x}_i$, $\mathbf{x}_i \neq \mathbf{x}_j$ if $i \neq j$ ($i, j = 1, \dots, n$). The definitions of the effective fields $\bar{\varepsilon}_i(\mathbf{x})$ and $\tilde{\varepsilon}_{1,2,\dots,n}(\mathbf{x})$ as well as their statistical averages $\langle \bar{\varepsilon}_i \rangle(\mathbf{x})$ and $\langle \tilde{\varepsilon}_{1,2,\dots,n} \rangle(\mathbf{x})$ are nothing more than a notation convenience for different terms of the infinite systems (3.8)-(3.11).

Then, considering some conditional statistical averages of the general integral equations (3.8)-(3.11) yields an infinite system of *integral equations* ($n = 1, 2, \dots$) for the effective fields proposed in [53], [64])

$$\begin{aligned} \langle \bar{\varepsilon} \mid v_1, \mathbf{x}_1; \dots; v_n, \mathbf{x}_n \rangle(\mathbf{x}) - \sum_{i \neq k}^n \langle \mathcal{L}_i^{\varepsilon\varepsilon}(\mathbf{x} - \mathbf{x}_i, \bar{\varepsilon}) \mid v_1, \mathbf{x}_1; \dots; v_n, \mathbf{x}_n \rangle_i = \langle \varepsilon \rangle(\mathbf{x}) \\ + \int \{ \langle \mathcal{L}_j^{\varepsilon\varepsilon}(\mathbf{x} - \mathbf{x}_j, \bar{\varepsilon}) \mid v_1, \mathbf{x}_1; \dots; v_n, \mathbf{x}_n \rangle_j \varphi(v_j, \mathbf{x}_j \mid v_1, \mathbf{x}_1, \dots, v_n, \mathbf{x}_n) \\ - \langle \mathcal{L}_j^{\varepsilon\varepsilon}(\mathbf{x} - \mathbf{x}_j, \bar{\varepsilon}) \rangle(\mathbf{x}_j) \} d\mathbf{x}_j, \end{aligned} \quad (3.12)$$

where a new perturbator $\mathcal{L}_i^{\varepsilon\varepsilon}(\mathbf{x} - \mathbf{x}_i, \bar{\varepsilon})$ is in fact a solution of Eq. (3.10₁). Since $\mathbf{x} \in v_1, \dots, v_n$ in the n -th line of the system can take the values inside the inclusions v_1, \dots, v_n , the n -th line contains n equations. Statistical averaging $\langle (\cdot) \rangle_i$ stands for the averaging over all surrounding heterogeneities at the fixed v_i , while the average $\langle (\cdot) \rangle(\mathbf{x}_j)$ implies the averaging over all possible location of v_i with possible dependence of this average on the macro-coordinate \mathbf{x}_j as for FGMs.

Comment 3.1. The perturbator $\mathcal{L}_i^{\varepsilon\varepsilon}(\mathbf{x} - \mathbf{x}_i, \bar{\varepsilon})$ is not necessarily expressed through the Green function (3.9₂). So, although the perturbator $\mathcal{L}_i^{\varepsilon\varepsilon}(\mathbf{x} - \mathbf{x}_i, \bar{\varepsilon})$ was estimated by the volume integral equation method (see Subsection 9.5.2 in [64]) and by the interface integral technique (see Section 11.3 in [64]), it was also estimated by the FEA (see Subsection 9.5.1 in [64]); i.e., the perturbator $\mathcal{L}_i^{\varepsilon\varepsilon}(\mathbf{x} - \mathbf{x}_i, \bar{\varepsilon})$ can be evaluated by any available numerical method. Furthermore, Eq. (3.14) has a few features. First of all, Eq. (3.13) was obtained without using (explicit or implicit) of the EFH (3.1). Equation (3.14) has no Green function (as Eqs. (3.5) and (3.6)), and, moreover, there is no constitutive law in Eq. (3.13).

Comment 3.2. Equations (3.13) were generalized for other problems of local micromechanics: thermoelasticity, coupled problems, and wave propagation (see Section 15.6 in [64]). Equations (3.13) were also generalized to CMs with strongly nonlocal (strain type and displacement type, peridynamics) and weakly nonlocal (strain-gradient and stress-gradient) properties of phases (see Chapter 14 in [64]). However, a fundamental restriction of all mentioned GIEs (and their generalizations) is their linearity to a primary unknown variable. To the best of the author's knowledge, nonlinear versions of the GIE (for both LM and PM) directly (or implicitly) depending on nonlinear constitutive phase properties are absent. In the next section, the nonlinear GIEs are proposed.

3.2 One and two inclusions in peridynamic macrodomain

Let us consider the governing equation for an infinite \mathbb{R}^d ($d = 1, 2, 3$) homogeneous linear bond-based peridynamic medium (2.23), (2.25)

$$\tilde{\mathcal{L}}^{(0)}(\mathbf{C}^{\text{bond}(0)} \mathbf{u}^{b(0)})(\mathbf{x}) + \mathbf{b}(\mathbf{x}) = \mathbf{0} \quad (3.13)$$

with the micromodulus $\mathbf{C}^{\text{bond}(0)}$. The self-equilibrated body force density $\mathbf{b}(\mathbf{x})$ produces a displacement

$$\mathbf{u}^{b(0)}(\mathbf{x}) \equiv -(\tilde{\mathcal{L}}^{(0)})^{-1}\mathbf{b}. \quad (3.14)$$

The indicator function $W^{\bar{w}}$ of the nonlocal closure $\bar{w} = w \cup w_\Gamma$ is split as

$$W^{\bar{w}}(\mathbf{x}) = W(\mathbf{x}) + W^{w_\Gamma}(\mathbf{x}). \quad (3.15)$$

Equations (3.13) are solved by iteration method

$$\sum_q \hat{\mathbb{K}}_{pq}^{(0)} \mathbf{u}_q^{b(0)[n+1]} = -\hat{\mathbf{b}}_p^{[n]}, \quad \hat{\mathbb{K}}_{pq}^{(0)} = \mathbb{K}_{pq}^{(0)} W(\mathbf{x}_q), \quad (3.16)$$

$$\begin{aligned} \mathbb{K}_{pq}^{(0)} &= \mathbf{C}^{\text{bond}(0)}(\mathbf{x}_p, \mathbf{x}_q) \bar{V}_{pq} - \delta_{pq} \sum_{r \in \mathcal{H}_p} \mathbf{C}^{\text{bond}(0)}(\mathbf{x}_p, \mathbf{x}_r) \bar{V}_{pr}, \\ -\hat{\mathbf{b}}_p^{[n]} &= -\mathbf{b}_p - \sum_{r \in \mathcal{H}_p} \mathbf{C}^{\text{bond}(0)}(\mathbf{x}_p, \mathbf{x}_r) \mathbf{u}_r^{b(0)[n]} \bar{V}_{pr} + W^{w_\Gamma}(\mathbf{x}_p), \end{aligned} \quad (3.17)$$

where a mid-point-type integration scheme is used with subscripts denoting the node number $\mathbf{u}_p = \mathbf{u}(\mathbf{x}_p)$, $\mathbf{b}_p = \mathbf{b}(\mathbf{x}_p)$. For every interaction between the nodes q and p , only the volume fraction \bar{V}_{pq} of the volume \bar{V}_q of node q inside the cut-off distance l_δ of node p is counted. Estimation of the partial volumes \bar{V}_{pq} (partial volume algorithm) for $d = 1, 2, 3$ was proposed in [275] (see also [161], [307], [298])

An initial approximation $\mathbf{u}^{b(0)[0]}$ is chosen as a locally elastic solution of Eq. (2.5)

$$\mathbf{u}_p^{b(0)[0]} = L\mathbf{u}_p = \int L\mathbf{G}(\mathbf{x}_p - \mathbf{y})\mathbf{b}(\mathbf{y}) d\mathbf{y}. \quad (3.18)$$

$L\mathbf{G}(\mathbf{x}_p - \mathbf{y})$ is the infinite body Green's function (of order $O(\int |\mathbf{x}|^{1-d} d|\mathbf{x}|)$ as $|\mathbf{x}| \rightarrow \infty$) of the Navier equation (2.5) with homogeneous elastic modulus tensor $\mathbf{L}^{(0)}$, defined by

$$\mathbf{L}^{(0)} = \frac{1}{2} \int_{\mathcal{H}_x} \boldsymbol{\xi} \mathbf{C}^{\text{bond}(0)}(\boldsymbol{\xi}, \mathbf{x}) \boldsymbol{\xi} d\mathbf{y}. \quad (3.19)$$

Solution (3.16) was obtained for the linear bond-based media (2.23) and (2.25). However, the same scheme is applicable for nonlinear peridynamic media

$$\sum_q \mathbf{f}^{(0)}(\boldsymbol{\eta}_{pq}^{b(0)[n+1]}, \boldsymbol{\xi}_{pq}) \bar{V}_{pq} = -\tilde{\mathbf{b}}_p^{[n]}, \quad (3.20)$$

$$-\tilde{\mathbf{b}}_p^{[n]} = -\mathbf{b}_p - \sum_{r \in \mathcal{H}_p} \mathbf{f}^{(0)}(\boldsymbol{\eta}_{pr}^{b(0)[n]}, \boldsymbol{\xi}_{pr}) \bar{V}_{pr} + W^{w_\Gamma}(\mathbf{x}_p), \quad (3.21)$$

where for each n Eq. (3.20) can be solved by either the iteration or quadrature method (see, e.g., [236]).

Let us consider a macrodomain w with one inclusion v_i subjected to the prescribed effective field loading $\bar{\boldsymbol{\varepsilon}}(\mathbf{x})$. Then, Eq. (2.6) for a general peridynamic operator $\tilde{\mathcal{L}}$ can be presented as

$$\tilde{\mathcal{L}}(\mathbf{u})(\mathbf{x}) = \tilde{\mathcal{L}}^{(0)}(\bar{\boldsymbol{\varepsilon}})(\mathbf{x}), \quad (3.22)$$

where $\tilde{\mathcal{L}}^{(0)}(\bar{\boldsymbol{\varepsilon}})(\mathbf{x})$ is a fictitious body force generated by the effective field $\bar{\boldsymbol{\varepsilon}}(\mathbf{x})$. In particular, for the homogeneous $\bar{\boldsymbol{\varepsilon}} = \boldsymbol{\varepsilon}^{w\Gamma}$, $\tilde{\mathcal{L}}^{(0)}(\bar{\boldsymbol{\varepsilon}})(\mathbf{x}) = \tilde{\mathcal{L}}^{(0)}(\boldsymbol{\varepsilon}^{w\Gamma})(\mathbf{x})$. The right-hand sides of Eqs. (3.14) and (3.22) are defined by the operators $\tilde{\mathcal{L}}^{(0)}$ and $(\tilde{\mathcal{L}}^{(0)})^{-1}$, respectively, which are inverse to each other. The main advantage of the decompositions (3.22) (see also p. 774 in [64]) is elimination in (3.22) of the nonlocal volumetric boundary conditions (2.29) and (2.30) prescribed over a nonzero volume. In nonlocal theories, the boundaries are fuzzy, so that prescribed displacement or load conditions have to be imposed in finite volumetric regions w_Γ rather than on boundary surfaces Γ^0 . Such extension of classical boundary conditions is not clearly defined (see [34], Chapter 14). In our case of Eq. (3.22), difficulty in imposing properly the boundary conditions with *surface effect* (see for references and details, e.g. [297], [382]) are avoided.

Seemingly to Eq. (3.20), we can assume that the solution of Eq. (3.22) is found for both the macrodomain w and infinite medium \mathbb{R}^d . Construction of the solution of Eqs. (3.20) and (3.22) in a general case is beyond the scope of the current presentation; in particular, in some cases (e.g. in either the plasticity model, cohesive crack model, or the phase-field model, see, e.g., [19], [105], [254]) such a solution can be obtained for the respective increments. Hereafter for the contraction a solution of Eq. (3.22) for nonlinear elastic case the *perturbators* and field concentrations are defined in the reduced form

$$\boldsymbol{\vartheta}(\mathbf{z}) - \bar{\boldsymbol{\vartheta}}(\mathbf{z}) = \mathcal{L}_i^{\theta\zeta}(\mathbf{z}, \bar{\boldsymbol{\zeta}}), \quad \boldsymbol{\vartheta}(\mathbf{z}) = \mathcal{A}_i^{\theta\zeta}(\bar{\boldsymbol{\zeta}})(\mathbf{z}), \quad (3.23)$$

where the duplet substitutions

$$(\mathbf{u}, \boldsymbol{\eta}) \leftrightarrow \boldsymbol{\vartheta}, \quad (\mathbf{u}, \boldsymbol{\varepsilon}) \leftrightarrow \boldsymbol{\zeta}, \quad [\mathbf{x}, (\hat{\mathbf{x}}, \mathbf{x})] \leftrightarrow \mathbf{z} \quad (3.24)$$

are introduced. Strictly speaking, the perturbators $\mathcal{L}_i^{\theta\theta}(\mathbf{z}, \theta)$ are just the notations of some problem that is destined to be solved in the equation $\theta - \bar{\theta} = \mathcal{L}_i^{\theta\theta}(\mathbf{z}, \theta)$ while the perturbators $\mathcal{L}_i^{\theta\zeta}(\mathbf{z}, \bar{\boldsymbol{\zeta}})$ are the solutions of this problem. The elements of the doublet $\boldsymbol{\vartheta}$ correspond to the variables in the left-hand side of the Eq. (3.23); the elements of the doublet $\boldsymbol{\zeta}$ correspond to the effective fields on the right-hand sides of the definitions, whereas the elements \mathbf{x} and $(\hat{\mathbf{x}}, \mathbf{x})$ of the doublet \mathbf{z} corresponds to the parameters \mathbf{u} and $\boldsymbol{\eta}$, respectively. The superindices $\theta\zeta$ of the perturbators $\mathcal{L}^{\theta\zeta}$ correspond to the variables in the left-hand side $\boldsymbol{\vartheta}$ and right-hand side $\boldsymbol{\zeta}$, respectively.

Let us consider two inclusions v_i and v_j placed in an infinite homogeneous matrix and subjected to the inhomogeneous field $\tilde{\boldsymbol{\zeta}}_{i,j}(\mathbf{x})$ ($\mathbf{u}, \boldsymbol{\eta} = \boldsymbol{\vartheta}$; $\mathbf{u}, \boldsymbol{\varepsilon} = \boldsymbol{\zeta}$; $[\mathbf{x}, (\hat{\mathbf{x}}, \mathbf{x})] = \mathbf{z}$; $\mathbf{x} \in \mathbb{R}^d$).

For $\mathbf{x} \in v_i$, Eqs. (3.23) can be recast in the form

$$\boldsymbol{\vartheta}(\mathbf{z}) = \bar{\boldsymbol{\vartheta}}_i(\mathbf{z}) + \mathcal{L}_i^{\theta\zeta}(\mathbf{z} - \mathbf{x}_i, \tilde{\boldsymbol{\zeta}}_{i,j}), \quad (3.25)$$

$$\bar{\boldsymbol{\vartheta}}_i(\mathbf{z}) = \tilde{\boldsymbol{\vartheta}}_{i,j}(\mathbf{z}) + \mathcal{L}_j^{\theta\zeta}(\mathbf{z}, \tilde{\boldsymbol{\zeta}}_{i,j}). \quad (3.26)$$

We can transform Eqs. (3.25) and (3.26) into the following ones ($\mathbf{z} \in v_i^l$)

$$\boldsymbol{\vartheta}(\mathbf{z}) - \tilde{\boldsymbol{\vartheta}}_{i,j}(\mathbf{z}) - \mathcal{L}_i^{\theta\zeta}(\mathbf{z} - \mathbf{x}_i, \tilde{\boldsymbol{\zeta}}_{i,j}) := \mathcal{L}_{i,j}^{\theta\zeta}(\mathbf{z}, \tilde{\boldsymbol{\zeta}}_{i,j}) \quad (3.27)$$

defining the perturbator $\mathcal{L}_{i,j}^{\theta\zeta}(\mathbf{z}, \tilde{\boldsymbol{\zeta}}_{i,j})$ which can be found by any numerical method analogously to the operator $\mathcal{L}_i^{\theta\zeta}(\mathbf{z} - \mathbf{x}_i, \bar{\boldsymbol{\zeta}}_i)$ (3.23). It should be mentioned that the operators $\mathcal{L}_i^{\theta\zeta}(\mathbf{z} - \mathbf{x}_i, \tilde{\boldsymbol{\zeta}}_{i,j})$ and $\mathcal{L}_{i,j}^{\theta\zeta}(\mathbf{z}, \tilde{\boldsymbol{\zeta}}_{i,j})$ (3.27) act on the effective fields $\tilde{\boldsymbol{\zeta}}_{i,j}(\mathbf{x})$ at $\mathbf{x} \in v_i$ and $\mathbf{x} \in v_i, v_j$, respectively, and the kernel of the operator $\mathcal{L}_{i,j}^{\theta\zeta}$ can be decomposed ($K = I, J$):

$$\mathcal{L}_{i,j}^{\theta\zeta}(\mathbf{z}, \mathbf{y}) = \mathcal{L}_{i,j}^{I\theta\zeta}(\mathbf{z}, \mathbf{y}) + \mathcal{L}_{i,j}^{J\theta\zeta}(\mathbf{z}, \mathbf{y}), \quad \mathcal{L}_{i,j}^{K\theta\zeta}(\mathbf{z}, \mathbf{y}) = \mathcal{L}_{i,j}^{\theta\zeta}(\mathbf{z}, \mathbf{y})V_k(\mathbf{y}), \quad (3.28)$$

where one follows Mura's tensor indicial notation (see for details [64]); i.e. repeated lowercase indices are summed up from 1 to d , while uppercase indices always take on the same numbers as the corresponding lowercase ones but are not summed up. Hence, the double superindices $\theta\zeta$ is used analogously to the double superindices uu and $u\varepsilon$ in Eqs. (3.23).

The fields inside the extended heterogeneity $\mathbf{z} \in v_i^l$ can be estimated from Eq. (3.27)

$$\boldsymbol{\vartheta}(\mathbf{z}) - \mathcal{A}_i^{\theta\zeta}(\tilde{\boldsymbol{\zeta}}_{i,j})(\mathbf{z}) = \mathcal{A}_{i,j}^{\theta\zeta}(\tilde{\boldsymbol{\zeta}}_{i,j})(\mathbf{z}), \quad (3.29)$$

where the concentration operators are defined through the corresponding perturbators seemingly to Eqs. (3.23). The tensors $\mathcal{A}_{i,j}^{\theta\zeta}(\tilde{\boldsymbol{\vartheta}}_{i,j}(\mathbf{z}))$ define the perturbation of the field $\boldsymbol{\vartheta}(\mathbf{z})$ introduced by the placement of the inclusion v_j interacting with the inclusion v_i . The tensors $\mathcal{A}_{i,j}^{\theta\zeta\infty}(\tilde{\boldsymbol{\vartheta}}_{i,j})(\mathbf{z})$ describe another perturbation of the field $\boldsymbol{\vartheta}(\mathbf{z})$ at $\mathbf{z} \in v_i^l$ produced by the inclusion v_j interacting only with the external loading $\tilde{\boldsymbol{\vartheta}}_{i,j}(\mathbf{y})$ ($\mathbf{y} \in v_j$) but not with the inclusion v_i .

Similarly, the effective field perturbators $\mathcal{J}_{i,j}^{\theta\zeta}$ and $\mathcal{J}_{i,j}^{\theta\zeta\infty}$ can be defined; they describe the perturbation of the effective field $\bar{\boldsymbol{\vartheta}}_i(\mathbf{z}) - \tilde{\boldsymbol{\vartheta}}_{i,j}(\mathbf{z})$ introduced by both the heterogeneity v_j (interacting with v_i) and the fictitious inclusion with the response operator $\mathcal{L}^{(0)}$ and eigenfield $\boldsymbol{\beta}_1^{\text{fict}}(\mathbf{y})$ corresponding to the field in the remote inclusion v_j (without interaction with v_i) ($\mathbf{y} \in v_j$, $\mathbf{x} \in v_i$, $\mathbf{z} \in \mathbb{R}^d$)

$$\bar{\boldsymbol{\vartheta}}_i(\mathbf{z}) - \tilde{\boldsymbol{\vartheta}}_{i,j}(\mathbf{z}) = \mathcal{J}_{i,j}^{\theta\zeta}(\tilde{\boldsymbol{\zeta}}_{i,j})(\mathbf{z}) \quad (3.30)$$

$$\bar{\boldsymbol{\vartheta}}_i(\mathbf{z}) - \tilde{\boldsymbol{\vartheta}}_{i,j}(\mathbf{z}) = \mathcal{J}_{i,j}^{\theta\zeta\infty}(\tilde{\boldsymbol{\zeta}}_{i,j})(\mathbf{z}), \quad (3.31)$$

(see for details [64]).

Comment 3.3. Estimation of the perturbator $\mathcal{L}_i^{\theta\zeta}(\mathbf{z}, \bar{\zeta})$ (3.29) is, in fact, a basic problem of micromechanics (see Introduction) for one inclusion inside the infinite homogeneous matrix. In the PM, estimation of the perturbator $\mathcal{L}_i^{\theta\zeta}(\mathbf{z}, \bar{\zeta})$ (3.29) was considered by four different methods (see [64], [60]) for the linear body-force medium with the same horizon l_δ in both the inclusion and matrix. The generalization to the linear state-based model as well as to the multiphysics coupled problem (see the LM applications in [53]) are straightforward. The popular discretization methods for the solution of PD equations (see for references [100], [101], [212]) are the meshfree method with one-point Gaussian quadrature referring to it as “meshfree PD” [316] (see also the solutions for 1D case [36], [127], [128], [130], [317], [343], [345] and 2D case [35], [164], [200], [296]), finite element methods (FEM, [83], [229], [290], [327], [328], [333]), [354], quadrature and collocation approaches ([305], [394], [395]), and the boundary element method [210]. Adaptive algorithm (see, e.g., [35], [36], [61]) using a multi-grid approach with fine grid spacing only in critical regions is designed in multi-adaptive approach ([271]) to dynamically switch both the discretization scheme and the grid spacing of the regions.

Comment 3.4. The significantly less trivial phenomenon is another limiting case of CCM-PD coupling, where usually small areas of a domain \mathbb{R}^d , which might be affected by the presence of discontinuities are described with a PD model, whereas the remaining parts of the system are described through a more efficient CCM model. The goal of Local-to-Nonlocal (LtN) coupling (see [27], [270], [383], [384], [389]) is to alleviate the computational burden by combining the computational efficiency of PDEs with the accuracy of nonlocal models under the assumption that the location of nonlocal effects can be preliminary prescribed (it looks like a localized plasticity model in the vicinity of inclusions in the LM of CMs, see pp. 556-565 [64]). The reader can use a comprehensive review [102] as a guide for selecting the most appropriate method for the problem at hand. It would be interesting to estimate $\mathcal{L}_i^{\theta\zeta}(\mathbf{z}, \bar{\zeta})$ for the different nonlocal models in the phases (up to the vanishing length scale $l_\delta/a \rightarrow 0$).

3.3 Nonlinear general integral equations in peridynamic micromechanics

For the loading by the body force with a compact support $\mathbf{b}(\mathbf{x})$ (2.4), the direct summations of all surrounding perturbators $\mathcal{L}_j^{\theta\zeta}(\mathbf{z}, \bar{\zeta})$ (3.23) exerting on the fixed inclusion v_i is described by the GIE ($\mathbf{z} \in v_i$) (see for details [78])

$$\langle \vartheta \rangle_i(\mathbf{z}) = \vartheta^{b(0)}(\mathbf{z}) + \int \mathcal{L}_j^{\theta\zeta}(\mathbf{z} - \mathbf{x}_j, \bar{\zeta}) \varphi(v_j, \mathbf{x}_j | v_1, \mathbf{x}_1) d\mathbf{x}_j. \quad (3.32)$$

with the deterministic fields $\vartheta^{b(0)}(\mathbf{z})$ produced by the body force $\mathbf{b}(\mathbf{x})$ in the infinite homogeneous matrix. For a particular linear locally elastic case and acceptance of the EFH **H1a**) (3.1), Eq. (3.32) is reduced to the equation proposed in [115] as an intermediate step for

obtaining GIE (3.5). A centering of Eqs. (3.32) is considered which performs a subtraction from both sides of Eq. (4.25) of their statistical averages. It leads to the GIE

$$\begin{aligned} \langle \boldsymbol{\vartheta} \rangle_i(\mathbf{z}) &= \langle \boldsymbol{\vartheta} \rangle(\mathbf{z}) + \int [\mathcal{L}_j^{\theta\zeta}(\mathbf{z} - \mathbf{x}_j, \bar{\boldsymbol{\zeta}}) \varphi(v_j, \mathbf{x}_j | v_i, \mathbf{x}_i) \\ &\quad - \langle \mathcal{L}_j^{\theta\zeta}(\mathbf{z} - \mathbf{x}_j, \bar{\boldsymbol{\zeta}}) \rangle(\mathbf{x}_j)] d\mathbf{x}_j, \end{aligned} \quad (3.33)$$

which is more general and valid for any inhomogeneous $\langle \boldsymbol{\vartheta} \rangle(\mathbf{z})$ while Eqs. (3.32) are only correct for the the body force $\mathbf{b}(\mathbf{x})$ with a compact support. Owing to the centering of Eq. (3.32), Eq. (3.33) contains the renormalizing term $\langle \mathcal{L}_j^{\theta\zeta}(\mathbf{z} - \mathbf{x}_j, \bar{\boldsymbol{\zeta}}) \rangle(\mathbf{x}_j)$ providing an absolute convergence of the integrals involved in Eqs. (3.33).

From Eq. (3.32), the representations for the effective fields can obtained as a revision of Eqs. (3.11). In slightly modified version, the statistical averages $\langle \bar{\mathbf{u}} | v_1, \mathbf{x}_1; \dots; v_n, \mathbf{x}_n \rangle(\mathbf{x})$ and $\langle \bar{\boldsymbol{\varepsilon}} | v_1, \mathbf{x}_1; \dots; v_n, \mathbf{x}_n \rangle(\mathbf{x})$ of the effective fields (3.23) for the fixed inclusions v_1, \dots, v_n are expressed by the following GIEs ($\mathbf{x} \in v_k$, $k = 1, 2, \dots, n$)

$$\begin{aligned} \langle \bar{\boldsymbol{\vartheta}} \mid v_1, \mathbf{x}_1; \dots; v_n, \mathbf{x}_n \rangle(\mathbf{z}) &- \sum_{i \neq k}^n \mathcal{L}_i^{\theta\zeta}(\mathbf{z}, \bar{\boldsymbol{\zeta}}) | v_1, \mathbf{x}_1; \dots; v_n, \mathbf{x}_n \rangle_i \\ &= \langle \boldsymbol{\vartheta} \rangle(\mathbf{z}) + \int \{ \mathcal{L}_j^{\theta\zeta}(\mathbf{z} - \mathbf{x}_j, \bar{\boldsymbol{\zeta}}) | v_1, \mathbf{x}_1; \dots; v_n, \mathbf{x}_n \rangle_j \\ &\quad \times \varphi(v_j, \mathbf{x}_j | v_1, \mathbf{x}_1, \dots, v_n, \mathbf{x}_n) - \langle \mathcal{L}_j^{\theta\zeta}(\mathbf{z} - \mathbf{x}_j, \bar{\boldsymbol{\zeta}}) \rangle(\mathbf{x}_j) \} d\mathbf{x}_j. \end{aligned} \quad (3.34)$$

Seemingly, from the GIE (3.35) for the body force loading with a compact support $\mathbf{b}(\mathbf{x})$, the representations for the effective field ($\mathbf{x} \in v_k$, $k = 1, \dots, n$) can be obtained

$$\begin{aligned} \langle \bar{\boldsymbol{\vartheta}} \mid v_1, \mathbf{x}_1; \dots; v_n, \mathbf{x}_n \rangle(\mathbf{z}) &- \sum_{i \neq k}^n \mathcal{L}_i^{\theta\zeta}(\mathbf{z}, \bar{\boldsymbol{\zeta}}) | v_1, \mathbf{x}_1; \dots; v_n, \mathbf{x}_n \rangle_i = \boldsymbol{\vartheta}^{b(0)}(\mathbf{z}) \\ &+ \int \mathcal{L}_j^{\theta\zeta}(\mathbf{z} - \mathbf{x}_j, \bar{\boldsymbol{\zeta}}) | v_1, \mathbf{x}_1; \dots; v_n, \mathbf{x}_n \rangle_j \varphi(v_j, \mathbf{x}_j | v_1, \mathbf{x}_1, \dots, v_n, \mathbf{x}_n) d\mathbf{x}_j. \end{aligned} \quad (3.35)$$

In Eqs. (3.34) and (3.35) the conditional perturbator $\langle \mathcal{L}_j^{\theta\zeta}(\mathbf{z}, \bar{\boldsymbol{\zeta}}) | v_i, \mathbf{x}_i \rangle_j$ can be expressed through the explicit perturbator for two interacting heterogeneities subjected to the field $\tilde{\boldsymbol{\zeta}}_{i,j}$

$$\begin{aligned} \langle \bar{\boldsymbol{\vartheta}}_i \rangle(\mathbf{z}) &= \langle \boldsymbol{\vartheta} \rangle(\mathbf{z}) + \int \{ \mathcal{J}_{i,j}^{\theta\zeta}(\langle \tilde{\boldsymbol{\zeta}}_{i,j} \rangle)(\mathbf{z}) \varphi(v_j, \mathbf{x}_j | v_i, \mathbf{x}_i) - \mathcal{J}_{i,j}^{\theta\zeta\infty}(\langle \tilde{\boldsymbol{\zeta}}_{i,j} \rangle)(\mathbf{z}) \} d\mathbf{x}_j, \\ \langle \bar{\boldsymbol{\vartheta}}_i \rangle(\mathbf{z}) &= \boldsymbol{\vartheta}^{b(0)}(\mathbf{z}) + \int \mathcal{J}_{i,j}^{\theta\zeta}(\langle \tilde{\boldsymbol{\zeta}}_{i,j} \rangle)(\mathbf{z}) \varphi(v_j, \mathbf{x}_j | v_i, \mathbf{x}_i) d\mathbf{x}_j, \end{aligned} \quad (3.36)$$

Equations (3.36) are constructed by the use of some building blocks described by the numerical solutions for both one and two inclusions inside the infinite homogeneous matrix

subjected to the effective field loading. The equation (3.36) is *exact* and involves two sorts of statistically averaged effective fields $\langle \bar{\zeta}_i \rangle(\mathbf{x})$ and $\langle \tilde{\zeta}_{i,j} \rangle(\mathbf{x})$, which can be found by the use of the closing assumption considered in the next section.

Comment 3.5. As in Comment 3.1, Eqs. (3.34) and (3.35) were obtained without using (explicit or implicit) of the EFH (3.1). Equations (3.34) and (3.35) have no Green function (as Eqs. (3.5) and (3.6)). The most intriguing feature of Eqs. (3.34) and (3.35) is the absence of a constitutive law in these equations. As can be seen, Eq. (3.34) completely coincides with the corresponding equations (3.13) for the locally elastic CMs (see [53]). It means that the same equation can be exploited for both the peridynamic CMs and locally elastic CMs. The GIEs (3.34) and (3.35) proposed are adapted to the straightforward generalizations of corresponding methods of local thermoelastic micromechanics (see, e.g., [47], [51], [53]). Equation (3.33) was obtained before for the particular linear peridynamic models (bond-based [55] and state-based [69]), which are peridynamic counterparts of the linear GIE (3.13) in the LM. Equation (3.32) was also proposed before for the linear bond-based model (see [73]). However, Eqs. (3.32) and (3.33) are now proposed for CM (statistically homogeneous and inhomogeneous structures) with the phases described by any peridynamic model (e.g., bond-based and state-based, linear and nonlinear, ordinary and non-ordinary) with nonlinear elastic constitutive law. I.e. we have a rare case when the methods developed in PM initiate the new methods of LM unknown before (such as nonlinear GIEs). Of course, nothing in Eqs. (3.32)-(3.36) is analytical, but these Eqs. (3.32)-(3.36) belong to the class of *Analytical Micromechanics* simply because DNS are not used (see Fig. 1) in Eqs. (3.32)-(3.36).

Comment 3.6. It should be mentioned that in nonlinear LM of random structure CMs, there are two directions of research. The first direction is based on the estimation of the second statistical moment of stress $\langle \sigma \otimes \sigma \rangle_i(\mathbf{x})$ in each phase $\mathbf{x} \in v_i \subset v^{(k)}$ ($k = 0, 1, \dots, n$) (see for details Section 5). The nonlinear variational approach [282] makes effective use of the various estimates available for linear composites, allowing the determination of corresponding estimates for nonlinear composites. However, the linear GIE (3.5) is a starting point in both directions. The author finds it difficult to predict the consequences of the replacement of background (replacement of the linear GIE (3.5) by nonlinear one (3.7)) in totally dominated general tools of nonlinear LM (PM is an additional story). It is only a banal absence of resources; it deserves further investigation.

3.4 Definition of effective elastic moduli

Peridynamic counterpart of the tensorial decomposition (${}^L\mathbf{L}(\mathbf{x}) = {}^L\mathbf{L}^{(0)} + {}^L\mathbf{L}_1(\mathbf{x})$) for linear local elasticity

$$\boldsymbol{\sigma}(\mathbf{x}) = {}^L\mathbf{L}^{(0)}\boldsymbol{\varepsilon}(\mathbf{x}) + {}^L\boldsymbol{\tau}(\mathbf{x}), \quad {}^L\boldsymbol{\tau}(\mathbf{x}) := \boldsymbol{\sigma}(\mathbf{x}) - {}^L\mathbf{L}^{(0)}(\mathbf{x})\boldsymbol{\varepsilon}(\mathbf{x}) \quad (3.37)$$

can be presented in the next form for the operator (2.16), (2.17)

$$\mathcal{L}^\sigma(\mathbf{u})(\mathbf{x}) = \mathcal{L}^{\sigma(0)}(\mathbf{u})(\mathbf{x}) + \mathcal{L}_1^\sigma(\mathbf{u})(\mathbf{x}), \quad (3.38)$$

were $\mathcal{L}^{\sigma(0)}$ denotes an action of the operator \mathcal{L}^σ on the medium with the material properties of the matrix defined by $\mathbf{f}^{(0)}$ [for example, for the bond force (2.21), $\mathbf{C}^{\text{bond}}(\boldsymbol{\xi}, \mathbf{x}) \equiv \mathbf{C}^{\text{bond}(0)}(\boldsymbol{\xi})$] and the displacement fields $\mathbf{u}(\mathbf{y})$ of the real CM. The jump operator $\mathcal{L}_1^\sigma(\mathbf{u}^l)(\mathbf{x})$ defined by Eq. (3.38) is called the *local stress polarization tensor* [compare with Eq. (3.37)] and represented as

$$\boldsymbol{\tau}(\mathbf{x}) = \mathcal{L}_1^\sigma(\mathbf{u})(\mathbf{x}) = \frac{1}{2} \int_S \int_0^\infty \int_0^\infty (y+z)^{d-1} \tilde{\mathbf{f}}_1(\mathbf{x} + y\mathbf{m}, \mathbf{x} - z\mathbf{m}) \otimes \mathbf{m} dz dy d\Omega_{\mathbf{m}}, \quad (3.39)$$

where

$$\tilde{\mathbf{f}}_1(\mathbf{p}, \mathbf{q}) := \tilde{\mathbf{f}}(\mathbf{p}, \mathbf{q}) - \tilde{\mathbf{f}}^{(0)}(\mathbf{p}, \mathbf{q}). \quad (3.40)$$

Although ${}^L\boldsymbol{\tau}(\mathbf{x})$ (3.37₂) and $\boldsymbol{\tau}(\mathbf{x})$ (3.39) are determined for linear local and nonlinear (in general) peridynamic media, respectively, a common feature of $\boldsymbol{\tau}(\mathbf{x})$ (3.39) and ${}^L\boldsymbol{\tau}(\mathbf{x})$ (3.37₂) is that both these tensors vanish inside the truncated matrix ($\mathbf{x} \in v^{l(0)} := w \setminus v^l$, $v^l := v \oplus 2\mathcal{H}_0$) and expressed through the jumps of material properties of both the inclusions and matrix (described by the operators and tensors, respectively); for the locally elastic problem $v^{l(0)} \equiv v^{(0)}$ and $\mathcal{H}_0 = \emptyset$.

Subsequent relations are presented for linear properties of the matrix, e.g., (2.5) and (2.21), and statistically homogeneous media subjected to the homogeneous volumetric boundary conditions (2.29) and (2.30). The volume averages are performed for Eqs. (3.37) and (3.38)

$$\langle \boldsymbol{\sigma} \rangle = {}^L\mathbf{L}^{(0)} \langle \boldsymbol{\varepsilon} \rangle + \langle {}^L\boldsymbol{\tau} \rangle, \quad \langle {}^L\mathbf{L}^{(0)} \boldsymbol{\varepsilon} \rangle = {}^L\mathbf{L}^{(0)} \langle \boldsymbol{\varepsilon} \rangle, \quad (3.41)$$

$$\langle \mathcal{L}^\sigma(\mathbf{u}) \rangle(\mathbf{x}) = \langle \mathcal{L}^{\sigma(0)}(\mathbf{u}) \rangle(\mathbf{x}) + \langle \mathcal{L}_1^\sigma(\mathbf{u}) \rangle(\mathbf{x}), \quad (3.42)$$

respectively. For statistically homogeneous media, a peridynamic analog of the locally elastic counterpart (3.41₂) is presented as

$$\begin{aligned} \langle \mathcal{L}^{\sigma(0)}(\mathbf{u}) \rangle(\mathbf{x}) &= \frac{1}{2} \langle \int_S \int_0^\infty \int_0^\infty (y+z)^{d-1} \tilde{\mathbf{f}}^{(0)}(\mathbf{x} + y\mathbf{m}, \mathbf{x} - z\mathbf{m}) \otimes \mathbf{m} dz dy d\Omega_{\mathbf{m}} \rangle \\ &= \frac{1}{2} \int_S \int_0^\infty \int_0^\infty (y+z)^{d-1} \mathbf{f}^{(0)}(\langle \mathbf{u} \rangle(\mathbf{x} + y\mathbf{m}) - \langle \mathbf{u} \rangle(\mathbf{x} - z\mathbf{m})) \\ &\quad + (y+z)\mathbf{m} \otimes \mathbf{m} dz dy d\Omega_{\mathbf{m}} = \mathbf{L}^{(0)} \langle \boldsymbol{\varepsilon} \rangle. \end{aligned} \quad (3.43)$$

Here, the equality (3.43₂) was obtained due to the linearity of $\mathbf{f}^{(0)}$ from the random variable \mathbf{u} while all remaining functions (such as, e.g., $\mathbf{C}^{(0)}(\mathbf{x}, \hat{\mathbf{x}})$, and the integration limits) are deterministic at the fixed \mathbf{x} and $\hat{\mathbf{x}}$. Because of this, analogously to the averaged Eqs. (3.41₂), a deterministic function describing the matrix properties (e.g., $\mathbf{C}^{(0)}(\mathbf{x}, \hat{\mathbf{x}})$) can be carried out (along with the corresponding integral operations) from the averaging operation $\langle \cdot \rangle$ at each \mathbf{x} and $\hat{\mathbf{x}}$. In its turn, the equality (3.43₃), in fact, defines the modulus $\mathbf{L}^{(0)}$ through the equality (see (2.17), $\mathbf{u} = \boldsymbol{\xi}$, $\boldsymbol{\xi} = (y+z)\mathbf{m}$)

$$\mathbf{L}^{(0)} = \mathcal{L}^{\sigma(0)}(\mathbf{C}^{(0)}, \mathbf{u}), \quad (3.44)$$

which can be also equivalently expressed through the energetic definition

$$\mathbf{L}^{(0)} = \frac{1}{2} \underline{\mathbf{X}} \langle \boldsymbol{\xi} \rangle \bullet \underline{\mathbb{K}}^{(0)} \bullet \underline{\mathbf{X}} \langle \boldsymbol{\xi} \rangle, \quad (\underline{\mathbf{X}} \langle \boldsymbol{\xi} \rangle = \boldsymbol{\xi}). \quad (3.45)$$

No assumption about $\mathbf{C}^{(0)}$ (e.g., either the spherical shape of $\mathcal{H}_{\mathbf{x}}$ or isotropy of $\mathbf{C}^{(0)}$) was used at the derivatives of Eqs. (3.44) and (3.45). The energetic definition of $\mathbf{L}^{(0)}$ has been used in [103] and [104] to establish a consistent micro-macro moduli correspondence between material parameters of anisotropic peridynamics $\mathbf{C}^{(0)}$ and classical continuum mechanics $\mathbf{L}^{(0)}$.

Hence, the representation (3.43) leads to the simplification of the averaged Eq. (3.42) (compare with Eq. (3.41₁)):

$$\langle \boldsymbol{\sigma} \rangle = \mathbf{L}^{(0)} \langle \boldsymbol{\varepsilon} \rangle + \langle \boldsymbol{\tau} \rangle^l, \quad (3.46)$$

that yields the representation for the effective elastic modulus similar to their locally elastic counterpart

$$\mathbf{L}^* = \mathbf{L}^{(0)} + \mathbf{R}^*, \quad \langle \boldsymbol{\tau} \rangle^l = \mathbf{R}^* \langle \boldsymbol{\varepsilon} \rangle. \quad (3.47)$$

Energetic definitions

$$\mathbf{L}^* = \frac{1}{2} \left\langle \int_{\mathcal{H}_{\mathbf{x}}} \mathbf{A}_u^{*\eta \top}(\boldsymbol{\xi}) \mathbf{C}(\boldsymbol{\xi}, \mathbf{x}) \mathbf{A}_u^{*\eta}(\boldsymbol{\xi}) d\mathbf{y} \right\rangle, \quad (3.48)$$

$$\mathbf{L}^* = \langle \mathbf{A}_\varepsilon^{*\top} \mathcal{L}^\sigma(\mathbf{A}_u^*) \rangle, \quad \boldsymbol{\varepsilon}(\mathbf{x}) := \mathbf{A}_\varepsilon^*(\mathbf{x}) \langle \boldsymbol{\varepsilon} \rangle. \quad (3.49)$$

were proposed in [55] for $\mathbf{A}_u^{*\eta}(\boldsymbol{\xi}) := \mathbf{A}_u^*(\mathbf{y}) - \mathbf{A}_u^*(\mathbf{x})$, $\mathbf{u}(\mathbf{x}) := \mathbf{A}_u^*(\mathbf{x}) \langle \boldsymbol{\varepsilon} \rangle$ by the use of self-adjointness of the operator $\tilde{\mathcal{L}}$ (2.13) (see [4]) and generalized Hill's equality, respectively.

It should be mentioned that the volume average $\langle \boldsymbol{\tau} \rangle_i^l$ (3.46) of the local polarization tensor $\boldsymbol{\tau}$ (3.39) is accomplished over the extended inclusion phase v^l . Then, the volume average of the peridynamic analog of decomposition (3.37₂) can be expressed in the form

$$\begin{aligned} \langle \boldsymbol{\tau} \rangle_i^l &= \langle \boldsymbol{\sigma} \rangle_i^l - \frac{1}{2} \left\langle \int_S \int_0^\infty \int_0^\infty (y+z)^{(d-1)} \left\{ \mathbf{C}^{(0)}(\mathbf{x} + y\mathbf{m}, \mathbf{x} - z\mathbf{m}) \right. \right. \\ &\quad \left. \left. \times [\mathbf{u}(\mathbf{x} + y\mathbf{m}) - \mathbf{u}(\mathbf{x} - z\mathbf{m})] \right\} \otimes \mathbf{m} dz dy d\Omega_{\mathbf{m}} \right\rangle_i^l = \langle \boldsymbol{\sigma} \rangle_i^l - \mathbf{L}^{(0)} \langle \boldsymbol{\varepsilon} \rangle_i^l, \end{aligned} \quad (3.50)$$

where the second equality (3.50₂) is obtained simply (3.43). $\langle \boldsymbol{\tau} \rangle_i^l$ can be also expressed through the surface integrals (2.34) and (2.35) by the use of identical equality

$$\langle \boldsymbol{\tau} \rangle_i^l = \langle \boldsymbol{\tau} \rangle_i^{l\omega} := \langle \mathbf{t}(\mathbf{s}) \overset{\mathcal{S}}{\otimes} \mathbf{s} \rangle_i^{l\omega} - \mathbf{L}^{(0)} \langle \mathbf{u}(\mathbf{s}) \overset{\mathcal{S}}{\otimes} \mathbf{n}(\mathbf{s}) \rangle_i^{l\omega}, \quad (3.51)$$

which was considered before in [61] at the eigenstress $\boldsymbol{\alpha} \equiv \mathbf{0}$ for the bond-based case [with $v^l := v \oplus \mathcal{H}_0$ instead of $v^l := v \oplus 2\mathcal{H}_0$ as in Eq. (3.51)] and for linear state-based case [69], [70] (for $\boldsymbol{\alpha} \neq \mathbf{0}$ and both the linear matrix and linear inclusions) as well as for the locally

elastic case (at $v^l = v$) [59]. The representation $\langle \boldsymbol{\tau} \rangle_i^{l\omega}$ (3.51₂) can be also expressed through the displacement field

$$\langle \boldsymbol{\tau} \rangle_i^{l\omega} := \langle [\mathcal{L}^\sigma(\mathbf{u})(\mathbf{s}) \otimes \mathbf{n}(\mathbf{s})] \otimes \overset{\mathcal{S}}{\mathbf{s}} \rangle_i^{l\omega} - \mathbf{L}^{(0)} \langle \mathbf{u}(\mathbf{s}) \otimes \overset{\mathcal{S}}{\mathbf{n}}(\mathbf{s}) \rangle_i^{l\omega}. \quad (3.52)$$

The representations (3.46)-(3.52) were obtained for statistically homogeneous media with the averaging $\langle (\cdot) \rangle$ by the use of substitutions of $\langle \mathbf{u} \rangle(\mathbf{x})$ into the integrals in Eqs. (3.43) and (3.50). This scheme is also applicable to periodic structure CMs. Indeed, let us \mathbf{x}_α are the centers of the cells Ω_α . At the parallel transition of the grid \mathbf{x}_α over the vector $\boldsymbol{\chi}$ (with uniform random distribution on Ω_{00}) the corresponding material tensors $\mathbf{C}(\mathbf{x}, \boldsymbol{\chi})$, and the solution $\mathbf{u}(\mathbf{x}, \boldsymbol{\chi})$ will also change. Thus, for each $\boldsymbol{\chi} \in \Omega_{00}$ the solution $\mathbf{u}(\mathbf{x}, \boldsymbol{\chi})$ can be obtained that makes it possible to define an effective (or macroscopic) displacement

$$\langle \mathbf{u} \rangle^\Omega(\mathbf{x}) = \frac{1}{|\Omega_{00}|} \int_{\Omega_{00}} \mathbf{u}(\mathbf{x}, \boldsymbol{\chi}) d\boldsymbol{\chi}, \quad \mathbf{x} \in w. \quad (3.53)$$

obtained by averaging over the number of the displacement realizations $\mathbf{u}(\mathbf{x}, \boldsymbol{\chi})$ produced by a parallel transform of $\mathbf{L}(\mathbf{x}, \boldsymbol{\chi})$ rather than by averaging of one realization $\mathbf{u}(\mathbf{x})$ over the moving-window Ω_{00} . Substitution of Eq. (3.51) into Eqs. (3.43) and (3.46) leads to conclusion that (3.42)-(3.52) are also proved for the periodic media with the averaging $\langle (\cdot) \rangle^\Omega$ and, therefore, the operation $\langle (\cdot) \rangle$ in Eqs. (3.42)-(3.52) can be replaced by $\langle\langle (\cdot) \rangle\rangle$, where

$$\langle\langle (\cdot) \rangle\rangle = \langle (\cdot) \rangle \quad \text{or} \quad \langle\langle (\cdot) \rangle\rangle = \langle (\cdot) \rangle^\Omega \quad (3.54)$$

for either the statistically homogeneous or periodic structures, respectively.

The limit of vanishing length scale (scale separation hypothesis)

$$l_\delta/a \rightarrow 0 \quad (3.55)$$

reduces Eqs. (3.46), (3.47) and (3.50) to the locally elastic counterparts ($\mathbf{s} \in \partial v_i$)

$$\langle\langle \boldsymbol{\sigma} \rangle\rangle = {}^L\mathbf{L}^{(0)} \langle\langle \boldsymbol{\varepsilon} \rangle\rangle + \langle\langle {}^L\boldsymbol{\tau} \rangle\rangle, \quad \mathbf{L}^* = {}^L\mathbf{L}^{(0)} + {}^L\mathbf{R}^*, \quad \langle\langle {}^L\boldsymbol{\tau} \rangle\rangle = {}^L\mathbf{R}^* \langle\langle \boldsymbol{\varepsilon} \rangle\rangle, \quad (3.56)$$

$$\langle\langle {}^L\boldsymbol{\tau} \rangle\rangle_i = \langle\langle {}^L\boldsymbol{\tau}^s \rangle\rangle_i^\omega, \quad {}^L\boldsymbol{\tau}^s(\mathbf{s}) := \mathbf{t}(\mathbf{s}) \otimes \overset{\mathcal{S}}{\mathbf{s}} - {}^L\mathbf{L}^{(0)} \mathbf{u}(\mathbf{s}) \otimes \overset{\mathcal{S}}{\mathbf{n}}(\mathbf{s}). \quad (3.57)$$

Equation (3.57) implies a summation over all inclusions $v_i \subset \Omega_{00}$ in the case of periodic structure CMs. Although in an analogy with $\langle\langle {}^L\boldsymbol{\tau}^s \rangle\rangle_i^\omega$ (3.57), $\langle\langle \boldsymbol{\tau} \rangle\rangle_i^{l\omega}$ (3.51) is called average local interface field, we keep in mind that the local interface polarization tensor (as in Eq. (3.57₂)) can not be defined in the PM. Indeed, a similarity between $\langle\langle {}^L\boldsymbol{\tau}^s \rangle\rangle_i^\omega$ (3.57) and $\langle\langle \boldsymbol{\tau} \rangle\rangle_i^{l\omega}$ (3.46) which is more manifested than similarity between ${}^L\mathbf{R}^*$ (3.56) and \mathbf{R}^* (3.47). In both cases $\langle\langle {}^L\boldsymbol{\tau}^s \rangle\rangle_i^\omega$ (3.56) and $\langle\langle \boldsymbol{\tau} \rangle\rangle_i^{l\omega}$ (3.47) we need to estimate the surface averages of formally the same function $\mathbf{t}(\mathbf{s}) \otimes \overset{\mathcal{S}}{\mathbf{s}} - \mathbf{L}^{(0)}[\mathbf{u}(\mathbf{s}) \otimes \overset{\mathcal{S}}{\mathbf{n}}(\mathbf{s})]$ over the surfaces, Γ_i and Γ_i^- , respectively, though the local modulus $\mathbf{L}^{(0)}$ (determined by Eq. (3.47)) is not defined at the external interface $\mathbf{s} \in \Gamma_i^-$, and, moreover, the interface traction $\mathbf{t}(\mathbf{s})$ and displacement $\mathbf{u}(\mathbf{s})$ are appeared in Eq. (3.51) after the statistical average operation (3.50) rather than before as in Eq. (3.57₂).

4 Solution of nonlinear GIEs

4.1 Closing assumptions

The so-called effective field hypothesis, the the main approximate hypothesis of many micromechanical methods, is formulated by Eq. (3.1) (see for details [47]). For the closing of Eq. (3.23), the following hypothesis is applied:

Hypothesis H2a). *Each pair of inclusions v_i and v_j is subjected to the inhomogeneous field $\tilde{\zeta}_{i,j}(\mathbf{x})$, and statistical average $\langle \tilde{\zeta}_{i,j} \rangle(\mathbf{x})$ is defined by the formula ($\zeta = \mathbf{u}, \varepsilon$)*

$$\langle \tilde{\zeta}_{i,j} \rangle(\mathbf{x}) = \langle \bar{\zeta}_k \rangle(\mathbf{x}) \quad (4.1)$$

at $\mathbf{x} \in v_k$, $k = i, j$.

The hypothesis **H2a**, rewritten in terms of the fields $\varepsilon(\mathbf{x})$, ($\mathbf{x} \in v_i$), is a standard closing assumption (see for details, e.g., [47], [182], [353]) degenerating to the “quasicrystalline” approximation by Lax [199], which ignores the binary interaction of heterogeneities and presumes homogeneity of the effective fields:

Hypothesis H2b, “quasi-crystalline” approximation. *It is supposed that the mean value of the effective field at a point $\mathbf{x} \in v_i$ does not depend on the field inside other heterogeneities $v_j \neq v_i$, $\mathbf{x} \in v_k$, ($k = i, j$):*

$$\langle \bar{\zeta} | v_i, \mathbf{x}_i; v_j, \rangle(\mathbf{x}) = \langle \bar{\zeta}_k \rangle(\mathbf{x}) \quad (4.2)$$

$$\langle \bar{\zeta}_k \rangle(\mathbf{x}) \equiv \text{const.} \quad (4.3)$$

Acceptance of hypothesis **H2a** closes the systems (3.33) and (3.32) in the following forms,

$$\begin{aligned} \langle \bar{\vartheta}_i \rangle(\mathbf{z}) &= \langle \vartheta \rangle(\mathbf{z}) + \int \{ [\mathcal{J}_{i,j}^{I\theta\zeta}(\mathbf{z}, \langle \bar{\zeta}_i \rangle) + \mathcal{J}_{i,j}^{J\theta\zeta}(\mathbf{z}, \langle \bar{\zeta}_j \rangle)] \\ &\quad \times \varphi(v_j, \mathbf{x}_j; v_i, \mathbf{x}_i) - \mathcal{J}_{i,j}^{\theta\zeta\infty}(\mathbf{z}, \langle \bar{\zeta}_j \rangle) \} d\mathbf{x}_j, \end{aligned} \quad (4.4)$$

$$\langle \bar{\vartheta}_i \rangle(\mathbf{z}) = \vartheta^{b(0)}(\mathbf{z}) + \int [\mathcal{J}_{i,j}^{I\theta\zeta}(\mathbf{z}, \langle \bar{\zeta}_i \rangle) + \mathcal{J}_{i,j}^{J\theta\zeta}(\mathbf{z}, \langle \bar{\zeta}_j \rangle)] \varphi(v_j, \mathbf{x}_j; v_i, \mathbf{x}_i) d\mathbf{x}_j, \quad (4.5)$$

were a decomposition $\mathcal{J}_{i,j}^{\theta\zeta} = \mathcal{J}_{i,j}^{I\theta\zeta} + \mathcal{J}_{i,j}^{J\theta\zeta}$ was introduced analogously to Eq. (3.28).

It is interesting that the integrands of Eqs. (2.82) and (4.5) are formally similar to each other. So, the force vector states $\mathbf{T}[\mathbf{x}]\langle \xi \rangle$ and $\mathbf{T}[\hat{\mathbf{x}}]\langle -\xi \rangle$ are “attached” to the horizon regions $\mathcal{H}_{\mathbf{x}}$ and $\mathcal{H}_{\hat{\mathbf{x}}}$ with the centers \mathbf{x} and $\hat{\mathbf{x}}$, respectively, whereas $\mathcal{J}_{i,j}^{I\theta\zeta}(\mathbf{z}, \langle \bar{\zeta}_i \rangle)$ and $\mathcal{J}_{i,j}^{J\theta\zeta}(\mathbf{z}, \langle \bar{\zeta}_j \rangle)$ are “attached” to the inclusions v_i and v_j with the centers \mathbf{x}_i and \mathbf{x}_j , respectively. The force vector states depend on the displacement fields (in the form of the prescribed operator) in the horizon regions $\mathcal{H}_{\mathbf{x}}$ and $\mathcal{H}_{\hat{\mathbf{x}}}$, whereas the perturbators (4.5) depend on the effective field $\bar{\zeta}_i$ and $\bar{\zeta}_j$ (with priory unknown operator form) in the inclusions v_i and v_j , respectively.

An integral Eqs. (4.4) and (4.5) can be solved by the iteration method of the recursion formula

$$\begin{aligned} \langle \bar{\boldsymbol{\vartheta}}_i^{[n+1]} \rangle(\mathbf{z}) &= \langle \boldsymbol{\vartheta} \rangle(\mathbf{z}) + \int \{ [\mathcal{J}_{i,j}^{I\theta\zeta}(\langle \bar{\boldsymbol{\zeta}}_i^{[n]} \rangle)(\mathbf{z}) + \mathcal{J}_{i,j}^{J\theta\zeta}(\langle \bar{\boldsymbol{\zeta}}_j^{[n]} \rangle)(\mathbf{z})] \\ &\quad \times \varphi(v_j, \mathbf{x}_j | v_i, \mathbf{x}_i) - \mathcal{J}_{i,j}^{\theta\zeta\infty}(\langle \bar{\boldsymbol{\zeta}}_j^{[n]} \rangle)(\mathbf{z}) \} d\mathbf{x}_j, \end{aligned} \quad (4.6)$$

$$\langle \boldsymbol{\vartheta}^{[n+1]} \rangle_i(\mathbf{z}) = \mathcal{A}_i^{\theta\zeta}(\langle \bar{\boldsymbol{\zeta}}_i^{[n+1]} \rangle)(\mathbf{z}), \quad (4.7)$$

$$\bar{v}_i \langle \boldsymbol{\tau}^{[n+1]} \rangle_i(\mathbf{x}) = \mathcal{R}_i(\langle \bar{\boldsymbol{\zeta}}_i^{[n+1]} \rangle)(\mathbf{x}), \quad (4.8)$$

and

$$\begin{aligned} \langle \bar{\boldsymbol{\vartheta}}_i^{[n+1]} \rangle(\mathbf{z}) &= \boldsymbol{\vartheta}^{b(0)}(\mathbf{z}) + \int [\mathcal{J}_{i,j}^{I\theta\zeta}(\langle \bar{\boldsymbol{\zeta}}_i^{[n]} \rangle)(\mathbf{z}) + \mathcal{J}_{i,j}^{J\theta\zeta}(\langle \bar{\boldsymbol{\zeta}}_j^{[n]} \rangle)(\mathbf{z})] \\ &\quad \times \varphi(v_j, \mathbf{x}_j | v_i, \mathbf{x}_i) d\mathbf{x}_j, \end{aligned} \quad (4.9)$$

$$\langle \boldsymbol{\vartheta}^{[n+1]} \rangle_i(\mathbf{z}) = \mathcal{A}_i^{\theta\zeta}(\langle \bar{\boldsymbol{\zeta}}_i^{[n+1]} \rangle)(\mathbf{z}), \quad (4.10)$$

$$\bar{v}_i \langle \boldsymbol{\tau}^{[n+1]} \rangle_i(\mathbf{x}) = \mathcal{R}_i(\langle \bar{\boldsymbol{\zeta}}_i^{[n+1]} \rangle)(\mathbf{x}), \quad (4.11)$$

respectively, with an initial approximation in the form of explicite solution obtained from Eqs. (4.3) and (4.4) in the framework of the EFH **H1a** (3.1) (see for details [64]).

Equations (4.4) and (4.5) can be simplified in the framework of Hypothesis **Hb2**, see Eqs. (4.2) and (4.3) which are also used in the LM (see [47]). However, it is possible a straightforward generalization of “quasicrystalline” approximation by Lax, see (4.2), when the assumption (4.2) and (4.2) are relaxed: $\langle \bar{\boldsymbol{\zeta}}_k \rangle(\mathbf{z}) \not\equiv \text{const}$ at $\mathbf{z} \in v_k^l$, ($k = i, j$; a case of the local elasticity was considered in [48], [49]) that is equivalent to the equality

$$\langle \mathcal{L}_j^{\theta\zeta}(\mathbf{z}, \bar{\boldsymbol{\zeta}}_j) | v_i, \mathbf{x}_i \rangle = \langle \mathcal{L}_j^{\theta\zeta}(\mathbf{z}, \bar{\boldsymbol{\zeta}}_j) \rangle. \quad (4.12)$$

It greatly simplifies the problems (4.5) and (4.6) where in such a case $\mathcal{J}_{i,j}^{\theta\zeta} = \mathcal{J}_{i,j}^{\theta\zeta\infty}$ ($\mathbf{x} \in v_i$) reducing these equations to

$$\langle \bar{\boldsymbol{\vartheta}}_i^{[n+1]} \rangle(\mathbf{z}) = \langle \boldsymbol{\vartheta} \rangle(\mathbf{z}) + \int \mathcal{J}_{i,j}^{\theta\zeta\infty}(\langle \bar{\boldsymbol{\zeta}}_j^{[n]} \rangle)(\mathbf{z}) [\varphi(v_j, \mathbf{x}_j | v_i, \mathbf{x}_i) - n^{(j)}(\mathbf{x}_j)] d\mathbf{x}_j, \quad (4.13)$$

$$\langle \bar{\boldsymbol{\vartheta}}_i^{[n+1]} \rangle(\mathbf{z}) = \boldsymbol{\vartheta}^{b(0)}(\mathbf{z}) + \int \mathcal{J}_{i,j}^{\theta\zeta\infty}(\langle \bar{\boldsymbol{\zeta}}_j^{[n]} \rangle)(\mathbf{z}) \varphi(v_j, \mathbf{x}_j | v_i, \mathbf{x}_i) d\mathbf{x}_j, \quad (4.14)$$

respectively. The second background of LM proposed in [48], [49] in the form of Eq. (4.13) permits to abandonment of the basic concepts of micromechanics: the hypothesis of “ellipsoidal symmetry”, and the effective field hypothesis (EFH **H1a** considered in the next Section 5.2). Some new effects were discovered that were impossible in the the framework of the classical (the first) background of micromechanics.

Equations (4.9) and (4.10) are obtained for general nonlinear cases of either the state-based (2.8) or bond-based (e.g. (2.15)) PM. Equations (4.13) and (4.14) are reduced to the corresponding equations obtained before for either linear bond-based (2.10) PM [61], [62] or linear state-based PM (2.13) and (2.14) [69].

4.2 Body forces with compact support

The scheme (4.9) forms the Neumann series for the solution ($\mathbf{x} \in v_i^l$)

$$\langle \bar{\mathbf{u}} \rangle_i(\mathbf{x}) := \langle \lim_{n \rightarrow \infty} \bar{\mathbf{u}}^{[n+1]} \rangle_i(\mathbf{x}) = \widehat{\mathbf{D}}_i^{ub}(\mathbf{b}, \mathbf{x}), \quad (4.15)$$

which yields the representation for the statistical average of displacements inside the fixed extended inclusion ($\mathbf{x} \in v_i^l$) (conditional average)

$$\langle \mathbf{u} \rangle_i(\mathbf{x}) = \widehat{\mathbf{D}}_i^{ub}(\mathbf{b}, \mathbf{x}) + \mathcal{L}_i^{uu}(\mathbf{x} - \mathbf{x}_i, \widehat{\mathbf{D}}_i^{ub}(\mathbf{b}, \mathbf{x})). \quad (4.16)$$

It should be mentioned that the tensor $\widehat{\mathbf{D}}_q^{ub}(\mathbf{b}, \mathbf{y})$ (4.15) is an inhomogeneous function of coordinates of the moving inclusion $\mathbf{y} \in v_q^l$. Moreover, the tensors $\widehat{\mathbf{D}}_q^{ub}(\mathbf{b}, \mathbf{y})$ (4.15) depend on all intersecting inclusions (at least at $|\mathbf{x}_q| \leq a^\delta + l_\delta$).

Equation (4.16) allows us to estimate a statistical average of the displacement field in the macropoint \mathbf{X}

$$\langle \mathbf{u} \rangle(\mathbf{X}) := c^{l(0)} \langle \mathbf{u} \rangle^{l(0)}(\mathbf{X}) + c^{l(1)} \langle \mathbf{u} \rangle^{l(1)}(\mathbf{X}) \quad (4.17)$$

expressed through the statistical averages of displacements in the point \mathbf{X} in the matrix $\langle \mathbf{u} \rangle^{l(0)}(\mathbf{X})$ and inclusions $\langle \mathbf{u} \rangle^{l(1)}(\mathbf{X})$. Indeed, at first we built some auxiliary set $v_i^1(\mathbf{X})$ with the indicator function $V_i^1(\mathbf{X})$ and the boundary $\partial v_i^1(\mathbf{X})$ formed by the centers of translated ellipsoids $v_q(\mathbf{0})$ around the fixed point \mathbf{X} . $v_i^1(\mathbf{X})$ is constructed as a limit $v_{ki}^0 \rightarrow v_q^1(\mathbf{X})$ if a fixed ellipsoid v_k is shrinking to the point \mathbf{X} . Then $\langle \mathbf{u} \rangle^{l(1)}(\mathbf{X})$ can be estimated as ($\mathbf{y} \in v_q^l$)

$$c^{l(1)} \langle \mathbf{u} \rangle^{l(1)}(\mathbf{X}) = c^{l(1)} \mathbf{u}^{b(0)}(\mathbf{X}) + \int_{v_i^1(\mathbf{X})} n^{(1)}(\mathbf{x}_q) \mathcal{L}_q^{uu}(\mathbf{X} - \mathbf{x}_q, \mathcal{D}_q^u(\mathbf{b}, \mathbf{y})) d\mathbf{x}_q, \quad (4.18)$$

and, therefore, the statistical average of displacements (4.17) is expressed through the body force density ($\mathbf{y} \in v_q^l$)

$$\begin{aligned} \langle \mathbf{u} \rangle(\mathbf{X}) &= \mathbf{u}^{b(0)}(\mathbf{X}) + c^{(0)} \int \mathcal{L}_q^{uu}(\mathbf{X} - \mathbf{x}_q, \mathcal{D}_q^{ub}(\mathbf{b}, \mathbf{y})) \varphi(v_q, \mathbf{x}_q; \mathbf{X}) d\mathbf{x}_q \\ &+ \int_{v_i^1(\mathbf{X})} n^{(1)}(\mathbf{x}_q) \mathcal{L}_q^{uu}(\mathbf{X} - \mathbf{x}_q, \mathcal{D}_q^{ub}(\mathbf{b}, \mathbf{y})) d\mathbf{x}_q, \end{aligned} \quad (4.19)$$

where the first and the second integrals in Eq. (4.18) correspond to the first and the second terms in the right-hand side of Eq. (4.17), and $\varphi(v_q, \mathbf{x}_q; \mathbf{X}) = 0$ if $\mathbf{x}_q \in v_i^1(\mathbf{X})$.

The macroscopic stresses in the effective constitutive law are

$$\langle \boldsymbol{\sigma} \rangle(\mathbf{x}) = \langle \mathcal{L}^{\sigma(0)}(\mathbf{u}) \rangle(\mathbf{x}) + \langle \boldsymbol{\tau} \rangle(\mathbf{x}) \quad (4.20)$$

where the first item on the right-hand side is simplified for the linear matrix (see Eq. (3.43)) and depends on the statistical averages $\langle \mathbf{u} \rangle(\mathbf{x})$ ($\mathbf{x} \in \mathbb{R}^d$) (4.19). For an estimation of an average $\langle \boldsymbol{\tau} \rangle(\mathbf{x})$, we consider, at first, the fixed inclusion v_q with the center \mathbf{x}_q . This inclusion produces value $\mathcal{L}_1^\sigma(\mathbf{x} - \mathbf{x}_q, \mathbf{u}) = \mathcal{L}^\sigma(\tilde{\boldsymbol{\tau}})$ estimated by Eq. (2.17) with replacement $\tilde{\mathbf{f}}^{(0)} \rightarrow \tilde{\mathbf{f}}_1$ as in Eq. (3.26). Then a statistical average of the local polarization tensor $\langle \boldsymbol{\tau} \rangle(\mathbf{X})$ is also obtained by averaging over the domain v_i^1

$$\langle \boldsymbol{\tau} \rangle(\mathbf{X}) = \int_{v_i^1(\mathbf{X})} n^{(1)} \mathcal{L}^\sigma(\mathbf{C}_1 \boldsymbol{\eta}^D)(\mathbf{y} - \mathbf{X}) d\mathbf{y}, \quad (4.21)$$

$$\begin{aligned} \boldsymbol{\eta}^D(\mathbf{x}, \mathbf{y}) = & \left[\mathcal{D}_i^{ub}(\mathbf{b}, \mathbf{x}) + \mathcal{L}_i^{uu}(\mathbf{x} - \mathbf{x}_i, \mathcal{D}_i^{ub}(\mathbf{b}, \mathbf{x})) \right. \\ & \left. - \mathcal{D}_i^{ub}(\mathbf{b}, \mathbf{y}) - \mathcal{L}_i^{uu}(\mathbf{y} - \mathbf{x}_i, \mathcal{D}_i^{ub}(\mathbf{b}, \mathbf{y})) \right], \end{aligned} \quad (4.22)$$

where $v_q^1(\mathbf{x})$ is defined by (2.37) and one used the representation for the statistical average of the displacement field in the inclusion $\mathbf{x} \in v_q$: $\langle \mathbf{u} \rangle_q(\mathbf{x})$ (4.18). Estimation of effective micro-modulus [369] (nonlocal parameter) through averaging of the strain energy of peridynamic CM (corresponding to the homogeneous boundary conditions) is questionable.

The new nonlocal effective constitutive law (4.22) looks very similar to the nonlocal effective constitutive law

$$\langle \boldsymbol{\sigma} \rangle(\mathbf{x}) = {}^L \mathbf{L}^{(0)} \langle \boldsymbol{\varepsilon} \rangle(\mathbf{x}) + \langle {}^L \boldsymbol{\tau} \rangle(\mathbf{y}), \quad {}^L \boldsymbol{\tau}(\mathbf{y}) := {}^L \mathbf{L}_1(\mathbf{y}) \boldsymbol{\varepsilon}(\mathbf{y}), \quad (4.23)$$

corresponding to locally elastic constitutive law (2.2) at the microlevel. But, the first term ${}^L \mathbf{L}^{(0)} \langle \boldsymbol{\varepsilon} \rangle(\mathbf{x})$ in the right-hand side of Eq. (4.23) corresponds to the arbitrary inhomogeneous $\langle \boldsymbol{\varepsilon} \rangle(\mathbf{x}) \not\equiv \text{const.}$ whereas $\langle \mathcal{L}^{\sigma(0)}(\mathbf{u}) \rangle(\mathbf{x})$ (4.23) is reduced to $\mathbf{L}^{(0)} \langle \boldsymbol{\varepsilon} \rangle(\mathbf{x})$ only for homogeneous $\langle \boldsymbol{\varepsilon} \rangle(\mathbf{x}) \equiv \text{const.}$

Numerical analysis was performed for 1D case [67], [68] for self-equilibrated and vanished outside some loading region body force: $\mathbf{b}(\mathbf{x}) = 0$ for $|\mathbf{x}| > a^b$. The engineering approach using the scale separation hypothesis (2.28) can be described in the following scheme: estimation of \mathbf{L}^* (4.18) at the homogeneous VBC (2.29), and evaluation of $\langle \mathbf{u}^{\text{EA}} \rangle(\mathbf{x})$ by Eq. (2.1)-(2.2) with replacement $\mathbf{L} \rightarrow \mathbf{L}^*$. It leads to monotonical $\langle \mathbf{u}^{\text{EA}} \rangle(\mathbf{x})$ whereas $\langle \mathbf{u} \rangle(\mathbf{x})$ (6.6) (simultaneous consideration of peridynamic constitutive equation (2.5) and inhomogeneity of $\mathbf{b}(\mathbf{x})$) is strongly nonmonotonical differing from $\langle \mathbf{u}^{\text{EA}} \rangle(\mathbf{x})$ by a factor 9.

For the linear bond-based model of constituents, Eqs. (4.22)-(4.22) are reduced to the corresponding equations in [67], [68]. The representations (4.23) and (4.22) can be generalized to the nonlinear inclusion properties analogous to Eqs. (4.6). A nonlocal effective operator

similar to (4.22) was also obtained from Eq. (4.16) for the linear bond-based model in [67]; generalization to the linear state-based model is obvious.

Comment 4.1. It is interesting that to the best authors' knowledge, there are no academic publications considering the mentioned effective deformations of locally elastic composites produced by prescribed inhomogeneous body forces although the practical importance of this problem is well known, e.g., for laser heating of CMs widely used in both the additive manufacturing [368] and military applications [168]. So, laser pulse heating of surfaces results in the rapid rise of temperature in the region irradiated by the laser beam. This produces a high-temperature gradient with high thermal stress levels in this region. A classical approach is based on the estimation of thermal stresses in a homogeneous half-space subjected to laser heating (see, e.g., [372]). In so doing, the implementation of the additive technologies of laser heating can produce the local fields of both the temperature and thermal stresses with a scale comparable to the material scale of particles in CMs [368] that indicates the need to analyze the nonlocal effects (as in Eqs. (4.16) and (4.19)).

4.3 Estimation of a set of surrogate operators

The loading by inhomogeneous body force $\mathbf{b}(\mathbf{x})$ can also be exploited as a very prospective tool for data-driven learning of the surrogate nonlocal constitutive laws of CMs rather than just a particular parameter of loading. This perspective direction initiated by Silling [315], [374], [376] for periodic systems can be generalized to the random structure CM in the following way. So, two datasets are defined

$$\mathcal{D} = \{ \langle \boldsymbol{\sigma}_k \rangle(\mathbf{b}_k, \mathbf{x}), \langle \mathbf{u}_k \rangle(\mathbf{b}_k, \mathbf{x}), \langle \mathbf{u}_{ik} \rangle(\mathbf{b}_k, \mathbf{x}), \mathbf{b}_k(\mathbf{x}) \}_{k=1}^N, \quad (4.24)$$

$$\tilde{\mathcal{D}} = \{ \tilde{\boldsymbol{\sigma}}_k(\mathbf{b}_k, \mathbf{x}), \tilde{\mathbf{u}}_k(\mathbf{b}_k, \mathbf{x}), \tilde{\mathbf{u}}_{ik}(\mathbf{b}_k, \mathbf{x}), \mathbf{b}_k(\mathbf{x}) \}_{k=1}^N, \quad (4.25)$$

where each effective parameters $\langle \boldsymbol{\sigma}_k \rangle(\mathbf{x})$, $\langle \mathbf{u}_k \rangle(\mathbf{x})$ and $\langle \mathbf{u}_{ik} \rangle(\mathbf{x}) := \langle \mathbf{u}_k \rangle_i(\mathbf{x})$ (4.24) are estimated for each \mathbf{b}_k in the offline stage in k -th realization; the surrogate dataset $\tilde{\mathcal{D}}$ is close to the dataset \mathcal{D} of the effective field parameters presenting, in fact, a combination of both the generation and compression stages; dataset \mathcal{D} is called field PM dataset. Dataset \mathcal{D} defined by statistical averages in the micromechanical problem is approximated by a surrogate model

$$\begin{aligned} \mathcal{L}_\gamma[\langle \mathbf{u}_k \rangle](\mathbf{x}) &= \boldsymbol{\Gamma}(\mathbf{x}), \\ \mathcal{L}_\gamma[\langle \mathbf{u}_k \rangle](\mathbf{x}) &= \int \mathbf{K}_\gamma(|\mathbf{x} - \mathbf{y}|) (\langle \mathbf{u}_k \rangle(\mathbf{y}) - \langle \mathbf{u}_k \rangle(\mathbf{x})) d\mathbf{y}, \end{aligned} \quad (4.26)$$

where $\gamma := b, u_i, \sigma$ and $\boldsymbol{\Gamma}(\mathbf{x}) := -\mathbf{b}(\mathbf{x}), \langle \mathbf{u} \rangle_i(\mathbf{x}), \langle \boldsymbol{\sigma} \rangle(\mathbf{x})$, respectively, correspond to three surrogate operators \mathcal{L}_γ . Obtaining an optimal *surrogate* model for the kernel functions \mathbf{K}_γ^* corresponding to the surrogate dataset $\tilde{\mathcal{D}}$ is achieved by solving three optimization problems

$$\mathbf{K}_\gamma^* = \operatorname{argmin}_{\mathbf{K}_\gamma} \sum_{k=1}^N \| \mathcal{L}_\gamma[\langle \mathbf{u}_k(\mathbf{b}_k) \rangle](\mathbf{x}) - \boldsymbol{\Gamma}_k(\mathbf{x}) \|_{l_2}^2 + \mathcal{R}(\mathbf{K}_\gamma), \quad (4.27)$$

by the use, e.g., Adam optimizer [192] after each step of gradient descent, see for details [374] (see also [132], [377], [375], and [376]) where the kernel \mathbf{K} is presented as a linear combination of Bernstein-based polynomials. Here, the l_2 norm is taken over $\mathbf{x} \in w$, and $\mathcal{R}(\mathbf{K}_\gamma)$ is a regularization term on the coefficients that improves the conditioning of the optimization problem (e.g., Tikhonov regularization).

It should be mentioned that Eqs. (4.16) and (4.19) obtained for general nonlinear cases of either the state-based (2.8) or bond-based (e.g. (2.15)) PM are reduced to their linear counterparts of bond-based PM [67], [68]. However, construction of the surrogate model (4.26) was considered in [67] only for the linear bond-based model.

Of course, the scheme (4.24)-(4.26) can be generalized to the periodic media in the spirit of Eq. (3.53). A parallel transition of the grid \mathbf{x}_α is considered over the vector $\boldsymbol{\chi}$ with uniform random distribution on Ω_{00} . Then for each $\boldsymbol{\chi} \in \Omega_{00}$ and fixed \mathbf{b}^k , estimation of the statistical averages can be obtained

$$\begin{aligned} \langle \boldsymbol{\sigma} \rangle(\mathbf{b}_k, \mathbf{x}) &= \frac{1}{|\Omega_{00}|} \int_{\Omega_{00}} \boldsymbol{\sigma}(\mathbf{b}_k, \mathbf{x}, \boldsymbol{\chi}) d\boldsymbol{\chi}, & \langle \mathbf{u} \rangle(\mathbf{b}_k, \mathbf{x}) &= \frac{1}{|\Omega_{00}|} \int_{\Omega_{00}} \mathbf{u}(\mathbf{b}_k, \mathbf{x}, \boldsymbol{\chi}) d\boldsymbol{\chi}, \\ \langle \mathbf{u} \rangle_i(\mathbf{b}_k, \mathbf{x}) &= \frac{1}{|\Omega_{00}|} \int_{\Omega_{00}} \mathbf{u}_i(\mathbf{b}_k, \mathbf{x}, \boldsymbol{\chi}) d\boldsymbol{\chi}, \end{aligned} \quad (4.28)$$

where $\boldsymbol{\sigma}(\mathbf{b}_k, \mathbf{x}, \boldsymbol{\chi})$, $\mathbf{u}(\mathbf{b}_k, \mathbf{x}, \boldsymbol{\chi})$ and $\mathbf{u}_i(\mathbf{b}_k, \mathbf{x}, \boldsymbol{\chi})$ are the DNS solutions obtained for each $\mathbf{b}_k(\mathbf{x}), \boldsymbol{\chi}$. The fields (4.28) are used for generation of dataset \mathcal{D} (4.24). The rest Eqs. (4.26) and (4.27) are not altered. It should be mentioned that the authors [365] (see also [366]) and [377] used the averaged displacement field $\langle \tilde{\mathbf{u}} \rangle_i^\Omega(\mathbf{x}) = |\Omega_i|^{-1} \int_{\Omega_i} \tilde{\mathbf{u}}(\boldsymbol{\chi}) d\boldsymbol{\chi}$ for the fixed grid \mathbf{x}_i that leads to obtaining a discrete kernel $\mathbf{K}(|\mathbf{x}|)$ as opposite to the continuous ones obtained by averaging over the ‘‘moving averaging’’ cell (4.28) (see for details p. 895 in [64]).

So, the offline dataset \mathcal{D} (4.24) (and (4.24) with (4.28)) are formed offline from the statistical averages $\langle \mathbf{u}_k \rangle(\mathbf{x})$, $\langle \mathbf{u}_{ik} \rangle(\mathbf{x}) := \langle \mathbf{u}_k \rangle_i(\mathbf{x})$ and $\langle \boldsymbol{\sigma}_k \rangle(\mathbf{x})$ (4.28) presenting, in fact, a combination of both the generation and compression stages. Loading by dynamic body force $\mathbf{b}(\mathbf{x}, t)$ is necessary for a surrogate model with nonlocal dynamics properties (see, e.g., [13]): $\rho \ddot{\tilde{\mathbf{u}}}(\mathbf{x}) - l_d^2 \nabla^2 \tilde{\mathbf{u}}(\mathbf{x}) = \mathcal{L}_b(\tilde{\mathbf{u}})(\mathbf{x}) + \mathbf{b}(\mathbf{x})$, where ρ is the mass density, whereas l_d denotes an internal dynamic scale parameter. In so doing the approach [374] and [376] is based on the datasets $\mathcal{D}^{\text{DNS}} = \{\mathbf{u}_k(\mathbf{b}_k, \mathbf{x}), \mathbf{b}_k(\mathbf{x})\}_{k=1}^N$ generated without compression that is the dissimilarity from the approach (4.24)-(4.27). Some sort of compression stage is proposed in a coarse-grained, homogenized continuum model by [375], [373] and [318] presenting a learning framework to extract, from MD data, an optimal Linear Peridynamic Solid (LPS) model as a surrogate for MD displacements. The coarse-graining method allows the dependence of bond force on bond length to be determined, including the horizon and allows substantial reductions in computational cost compared with MD. In the original method proposed in [315], [374], the dataset \mathcal{D}^{DNS} makes it possible to estimate the kernel \mathbf{K}_b^* by the solution of optimization problem (4.27). However, it does not provide reason enough to assume that the kernel \mathbf{K}_b^*

can be used for the estimation of statistical average stresses $\langle \boldsymbol{\sigma} \rangle(\mathbf{x})$ (as a micromodulus was exploited for the estimation of stresses $\boldsymbol{\sigma}(\mathbf{x})$). Then, any information about the statistical averages of displacements inside inclusions $\langle \mathbf{u} \rangle_i(\mathbf{x})$ ($\mathbf{x} \in v_i$) is lost for the online stage in the case of dataset \mathcal{D}^{DNS} , although it is precisely the operator $\mathbf{K}_{u_i}^*$ (rather than \mathbf{K}_b^*) is potentially used for any nonlinear problem (e.g., fracture and plasticity).

Moreover, the surrogate operators (4.26) are constructed for the infinite random (or periodic) media eliminating the edge effects and inconsistencies (see [66]) produced by popular approaches modeling the infinite inclusion fields by a finite set of inclusions (as in [374], [377], [375], [318]). Inconsistencies related with the replacement of PBC by the homogeneous boundary BC are well known in LM (see, e.g., p. 508 in [47]); the same difficulties are expected in PM at the modeling of infinite (e.g. periodic) media by a finite sample (see, e.g., [3], [10], [11], [12], [99] [178], [371], [387], [396]). The use of body force with compact support (like (3.32)) as a training parameter enables the edge effects to be eliminated. It was qualitatively demonstrated for 1D random structures (with different scale ratios $a/a^b/l_\delta$) in the framework of the analytical micromechanics (without DNS, see Fig. 1 and Subsection 4.2) [67] with estimation of $\langle \mathbf{u} \rangle(\mathbf{x})$ ($\mathbf{x} \in R^1$). Owing to nonlocal effects, the domain of the long-range action is limited not only by $|\mathbf{x}| \leq a^b$ but by a domain $|\mathbf{x}| \leq a^{1-r}$ ($a^{1-r} \approx 3a^b$) i.e. the problem domain $\mathbf{x} \in R^1$ is reduced to a finite size domain without inconsistencies mentioned before [66].

In the framework of computational micromechanics for 2D particular realizations of random structures, one [319] proposed a coarse-graining model of the upscaled mechanical properties of CMs with particular Monte-Carlo simulated structures in a finite-size box (corresponding to the domain of the long-range action [67]). the upscaled peridynamic model can have a much coarser discretization than the original small-scale model (exploiting DNS, see Fig. 1), allowing larger-scale simulations to be performed efficiently [estimations of $\langle \mathbf{u} \rangle_i(\mathbf{x})$, $\mathbf{x} \in v_i$, and $\langle \mathbf{u} \rangle(\mathbf{x})$, $\mathbf{x} \in R^1$, are beyond the scope of the study].

A new integral neural operator architecture called the Peridynamic Neural Operator (PNO) [174] provides a surrogate operator \mathcal{G} ($\mathcal{G}(\langle \mathbf{u} \rangle)(\mathbf{x}) \approx -\mathbf{b}(\mathbf{x})$) for physically consistent predictions of the overall behavior of highly nonlinear, anisotropic, and heterogeneous materials and achieves improved accuracy and efficiency compared to baseline models that use prior expert-constructed knowledge of predefined constitutive laws (as, e.g., in Eq. (4.26)). The heterogeneous PNO (HeteroPNO) approach is proposed in [175] for data-driven constitutive modeling of heterogeneous fiber orientation field in anisotropic materials. Physics-informed neural networks (PINN, see [286] and [191]) have attracted considerable attention because of their low data dependence and physical outputs. In particular, PD governing equation is enforced in the PINN's residual-based loss function for analyses of the displacement fields of homogeneous and especially heterogeneous elastic plates [264]; PD theory with PINN is presented in [129] to predict quasi-static damage and crack propagation in brittle materials.

Of course nonlinear micromechanical model (4.15)-(4.22) can be easily incorporated into PNO (and PINN) by replacement of \mathcal{D}^{DNS} (one dataset of full-field, spatial measurements of

displacement and loading) used in PNO by \mathcal{D} (4.24) (a few field PM datasets of compressed sets of statistical average fields) exploited in (4.15)-(4.22). As before, it leads to the elimination of both the edge and size effects. However, the mentioned edge effect (appearing in [174], [175], and [378]) can also be eliminated by a naive way proposed in the minus-sampling method (see Eq. (5.27) in [64]) which, of course, leads to a large loss of information because only the inner points outside of the boundary layer can be used for estimation of \mathcal{D}^{DNS} .

However, what is even more important is that the use of \mathcal{D} (4.24) allows one to get a nonlocal operator counterpart of a basic concept of the LM such as effective concentration factor (e.g. $\langle \boldsymbol{\varepsilon} \rangle_i(\mathbf{x}) = \mathbf{A}^*(\mathbf{x})\langle \boldsymbol{\varepsilon} \rangle$, $\mathbf{x} \in v_i$); precisely these (“downscale”) operators (rather than “upscale” operator \mathcal{G}) are potentially used for any nonlinear problem (e.g., fracture and plasticity). It should be mentioned that the term compressed applied to the field PM dataset \mathcal{D} (4.24) does not mean that the full-field dataset \mathcal{D}^{DNS} for a big sample should be preliminary estimated. In general, the destiny of micromechanics (both the LM and PM) is providing the required estimations by more cheap, fast, robust, and flexible methods (although it takes additional intellectual complexity to the implementations) than DNS. On the other side, the micromechanic scheme (4.15)-(4.22) is not a single way for estimation of the field PM dataset \mathcal{D} (4.24).

Comment 4.2. It should be mentioned that Eq. (4.14) is reduced by centering to more general Eq. (4.13). However, Eq. (4.14) has a fundamental advantage with respect to Eq. (4.13) because precisely Eq. (4.14) is used for the generation of the dataset \mathcal{D} (4.24) exploited for the construction of machine learning (ML) technique such as either the surrogate operators (4.26) or PNO (or PINN). ML technique, in turn, allows us to obtain a surrogate dataset \mathcal{D} (4.25) for any macroscopic loading (either $\langle \mathbf{u} \rangle(\mathbf{x})$ or $\mathbf{b}(\mathbf{x})$) without solution of the micro-problem as in Eqs. (4.13) and (4.13).

Comment 4.3. Effective energy-based criteria will be obtained in Section 5 for the homogeneous VBC (2.29) and (2.30). Generalization of the inhomogeneous body force is straightforward. Then, the dataset (4.24) can be extended by other effective field parameters with a subsequent estimation of the surrogate operators for the effective energy-based criteria.

Comment 4.4. The scheme for obtaining the set of surrogate models is presented in Fig. 2. Block 1 DNS is used in [132], [174], [374], [377], and [375]. In

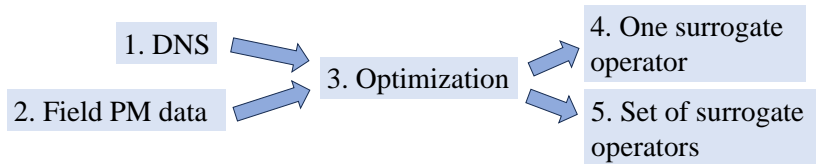


Fig. 2: The scheme of obtaining of surrogate model set

the proposed approach, we consider either the solution of Eq. (4.24) for the random structure CMs or the fields (4.28) for each $\boldsymbol{\chi}$ in the case of periodic structure CMs. Estimations of the

effective fields (4.16), (4.17), and (4.20) (or (4.28)) are estimated in the block 2 Field PM dataset (Compression). Solution of optimization problems (4.27) (Block 3) leads to obtaining either one surrogate operator (e.g. \mathbf{K}_b^* or \mathcal{G} , Bloc 4) or a set of surrogate models (e.g. Eq. (4.24), Block 5). Block 2 Field PM dataset is, in fact, a union of Blocks 1-4 (without Block 5) in the Fig. 2.

4.4 Estimation of effective moduli

Thus, the GIE (3.32) for CM subjected to body force $\mathbf{b}(\mathbf{x})$ with compact support was solved for a general representation of the nonlinear perturbator operator $\mathcal{L}_j^{\theta\zeta}(\mathbf{z}, \bar{\zeta})$ (3.23). Solution (4.7) was obtained in the framework of the closing assumption **H2a** (4.1) with estimation of the statistical averages $\langle \mathbf{u} \rangle_i(\mathbf{x})$ (4.16) and $\langle \mathbf{u} \rangle(\mathbf{x})$ (4.19). A set of effective surrogate operators (4.26) was estimated for the general nonlinear perturbator operator $\mathcal{L}_q^{\theta\zeta}(\mathbf{z}, \bar{\zeta})$ (3.23).

However, for the estimation of effective moduli (requering both the medium statistical homogeneity and homogeneous volumetric boundary conditions (2.29)) from the iteration approach (4.6), some additional assumptions are needed. So, for CM with *linear elastic* properties of the matrix (i.e. ${}^L\mathbf{L}^{(0)}$ and $\mathbf{C}^{(0)}$), Eq. (4.22) is reduced to the representation of the effective elastic modulus similar to their local elastic counterpart

$$\mathbf{L}^* = \mathbf{L}^{(0)} + \mathbf{R}^*, \quad \langle \boldsymbol{\tau} \rangle^l = \mathbf{R}^* \langle \boldsymbol{\varepsilon} \rangle, \quad (4.29)$$

where $\mathbf{L}^{(0)}$ is defined by Eq. (3.41) with no assumption about $\mathbf{C}^{(0)}$ (e.g., either the spherical shape of $\mathcal{H}_{\mathbf{x}}$ or r isotropy of $\mathbf{C}^{(0)}$). Equation (4.29₂) implies linearity of the effective properties (although the limiting representation (3.23) was obtained for generally nonlinear perturbator operators $\mathcal{L}_j^{\theta\zeta}(\mathbf{z}, \bar{\zeta})$). The representation $\langle \boldsymbol{\tau} \rangle_i^l = \langle \boldsymbol{\tau} \rangle_i^{l\omega}$ (4.29₂) can be also expressed through the displacement field at the external interaction interface Γ_i^- of the representative inclusion v_i (see for details [64], [59])

$$\begin{aligned} \langle \boldsymbol{\tau} \rangle_i^{l\omega} &:= (\bar{v}_i^l)^{-1} \int_{\Gamma_i^-} \boldsymbol{\tau}(\mathbf{s}) d\mathbf{s} = \langle [\mathcal{L}^\sigma(\mathbf{u})(\mathbf{s}) \otimes \mathbf{n}(\mathbf{s})] \overset{\mathcal{S}}{\otimes} \mathbf{s} \rangle_i^{l\omega} \\ &- \mathbf{L}^{(0)} \langle \mathbf{u}(\mathbf{s}) \overset{\mathcal{S}}{\otimes} \mathbf{n}(\mathbf{s}) \rangle_i^{l\omega}, \end{aligned} \quad (4.30)$$

where $\mathbf{u}(\mathbf{s})$ ($\mathbf{s} \in \Gamma_i^-$) are evaluated by the use of Eqs. (3.23₂) and (4.7).

Subsequent simplifications of Eqs. (4.6) and (4.12) can be performed in the framework of Hypothesis **H1a** (3.1) for the linear operators $\mathcal{J}_{i,j}^{\theta\zeta}$ (3.28) and $\mathcal{J}_{i,j}^{\theta\zeta\infty}$ (3.31) which can be decomposed and reduced to the tensors at the applying to the constant effective fields (4.1)

$$\mathcal{J}_{i,j}^{I\theta\zeta}(\mathbf{z}, \langle \bar{\zeta}_i \rangle) + \mathcal{J}_{i,j}^{J\theta\zeta}(\mathbf{z}, \langle \bar{\zeta}_j \rangle) = \mathbf{J}_{i,j}^{I\theta\zeta}(\mathbf{z}) \langle \bar{\zeta}_i \rangle(\mathbf{x}_i) + \mathbf{J}_{i,j}^{J\theta\zeta}(\mathbf{z}) \langle \bar{\zeta}_j \rangle(\mathbf{x}_j), \quad (4.31)$$

$$\mathcal{J}_{i,j}^{\theta\zeta\infty}(\mathbf{z}, \langle \bar{\zeta}_j \rangle) = \mathbf{J}_{i,j}^{\theta\zeta\infty}(\mathbf{z}) \langle \bar{\zeta}_j \rangle(\mathbf{x}_j). \quad (4.32)$$

In particular, for the linear operators $\mathcal{L}_i^{\theta\zeta}(\mathbf{z}, \bar{\zeta})$ (3.23) and homogeneous effective strain $\bar{\boldsymbol{\varepsilon}}(\mathbf{x}) = \bar{\boldsymbol{\varepsilon}}_i$ the corresponding operators are reduced to the tensor multiplications

$$\boldsymbol{\vartheta}(\mathbf{z}) - \bar{\boldsymbol{\vartheta}}(\mathbf{z}) = \mathbf{L}_i^{\theta\varepsilon}(\mathbf{z})\bar{\boldsymbol{\varepsilon}}_i, \quad \boldsymbol{\vartheta}(\mathbf{z}) = \mathbf{A}_i^{\theta\varepsilon}(\mathbf{z})\bar{\boldsymbol{\varepsilon}}_i, \quad \boldsymbol{\sigma}(\mathbf{x}) = \mathbf{L}_i^{\sigma\varepsilon}(\mathbf{x})\bar{\boldsymbol{\varepsilon}}_i \quad (4.33)$$

$$\boldsymbol{\tau}(\mathbf{x}) = \mathbf{R}_i(\mathbf{x})\bar{\boldsymbol{\varepsilon}}, \quad (4.34)$$

$$\mathbf{R}_i(\mathbf{x})(\bar{\boldsymbol{\varepsilon}}) = \mathcal{L}^\sigma(\mathbf{C}_1\boldsymbol{\eta})(\mathbf{x}), \quad \boldsymbol{\eta}(\mathbf{z}, \mathbf{y}) = [\mathbf{A}_i^{u\varepsilon}(\mathbf{z} - \mathbf{x}_i) - \mathbf{A}_i^{u\varepsilon}(\mathbf{y} - \mathbf{x}_i)]\bar{\boldsymbol{\varepsilon}}. \quad (4.35)$$

Then, substitutions of Eqs. (4.31) and (4.32) into Eq. (4.4) leads to the linear algebraic equation

$$\begin{aligned} \langle \bar{\boldsymbol{\vartheta}}_i \rangle(\mathbf{z}) &= \langle \boldsymbol{\vartheta} \rangle(\mathbf{z}) + \int \{ [\mathbf{J}_{i,j}^{I\theta\zeta}(\mathbf{z})(\bar{\zeta}_i)(\mathbf{x}_i) + \mathbf{J}_{i,j}^{J\theta\zeta}(\mathbf{z})(\bar{\zeta}_j)(\mathbf{x}_j)] \\ &\quad \times \varphi(v_j, \mathbf{x}_j; v_i, \mathbf{x}_i) - \mathbf{J}_{i,j}^{\theta\zeta\infty}(\mathbf{z})(\bar{\zeta}_j)(\mathbf{x}_j) \} d\mathbf{x}_j. \end{aligned} \quad (4.36)$$

Equations (4.36) and (4.34) can be explicitly solved with the estimation of the effective tensors \mathbf{R}^* (4.29₂) and the effective moduli \mathbf{L}^* (4.29). This scheme was realized for the linear bond-based model of constituents of CM [61], and for the linear state-based thermoelastic model [69], [70]. In particular, the effective field method (EFM) used the closing assumptions **H2b** (4.2) and (4.3)

$$\mathbf{L}^{*\text{EFM}} = \mathbf{L}^{(0)} + c^{l(1)}\mathbf{R}_i^{l\omega}\mathbf{D}^{\text{EFM}}, \quad (4.37)$$

$$(\mathbf{D}^{\text{EFM}})^{-1} = \mathbf{I} - \int \langle \mathbf{n}(\mathbf{s}) \otimes \mathbf{L}_j^{u\varepsilon}(\mathbf{s} - \mathbf{x}_i) \rangle_i^{l\omega} [\varphi(v_j, \mathbf{x}_j; v_i, \mathbf{x}_i) - n^{(j)}] d\mathbf{x}_j, \quad (4.38)$$

where $\mathbf{R}_i^{l\omega} = \mathbf{R}_i^l$. For the Mori-Tanaka approach (MTA) using the closing assumption

$$\bar{\boldsymbol{\varepsilon}}(\mathbf{x}) = \langle \boldsymbol{\varepsilon} \rangle^{(0)} \quad (4.39)$$

instead of the assumptions (4.2) and (4.3), the representations ($\mathbf{s} \in v_i^l$)

$$\mathbf{L}^{*\text{MTA}} = \mathbf{L}^{(0)} + c^{l(1)}\mathbf{R}_i^{l\omega}\mathbf{D}^{\text{MTA}}, \quad (4.40)$$

$$(\mathbf{D}^{\text{MTA}})^{-1} = c^{l(0)}\mathbf{I} + c^{l(1)}\mathbf{A}_i^{l\omega}, \quad \mathbf{A}_i^{l\omega} := \langle \mathbf{A}_i^{u\varepsilon}(\mathbf{s}) \rangle_i^{l\omega} \quad (4.41)$$

can be obtained. Numerical results for 1D cases are presented in [51], [52], [54], [61]. It was detected a dependence of the effective moduli estimations (4.37) and (4.40) on both the micromodulus profile [e.g. either (2.26₁) or (2.26₂)] and the ratio l_δ/a of the horizon and inclusion size whereas the estimations obtained by the mixture theory (see [84], [141], [243], [356], [357]) do not depend on ratio l_δ/a (i.e. the scale separation hypothesis (3.55) is implicitly used in the mixture theory).

Comment 4.4. For local elasticity, this method (called the second background of micromechanics, or computational analytical micromechanics, CAM) uses the new GIE proposed in

[48], [49] (see for details [64]) and permits to abandonment of the basic concepts of micromechanics: the hypothesis of “ellipsoidal symmetry”, and the effective field hypothesis EFH, **H1a** (3.1). The results of this abandonment for local elasticity was quantitatively estimated for some models, e.g. for CMs reinforced by either aligned continuously inhomogeneous fibers or the inclusions of noncanonical shape. Some new effects (with possible correction of a sign of statistical averages of local field estimations) were discovered that were impossible in the framework of the classical (the first) background of micromechanics. Representations (4.23)-(4.26) (with the corresponding estimations of effective material and field parameters) can be considered as generalizations of the mentioned linear models of LM to their peridynamic counterparts. Furthermore, the LM methods mentioned are linear whereas the PM methods (see Eqs. (3.23)-(3.36), (4.1)-(4.6), and (4.22)) are nonlinear. We used only linearity for the matrix at the obtaining of Eqs. (4.17), (4.17₁), and (4.18). It would be interesting to obtain the nonlinear LM counterparts of the mentioned method in PM. I.e. we have a rare (the second) case when the methods developed in PM initiate the new methods of LM unknown before.

4.5 Damage mechanics and microcracked media

Of special interest is damage mechanics. Damage is a basic concept in engineering design exploited for predictions about the initiation, propagation, and fracture of materials without molecular scale, which can be too complex for engineering analysis (see the pioneering works by Kachanov [180] and Rabotnov [284] as well as [181], [194]). Physically justified damage theory was proposed in peridynamics (see [311], [316]), where damage is introduced by permitting damaged bonds to break irreversibly, i.e., damaging the bond is considered as removing if the bond stretch exceeds a critical stretch for some time. In other words, the damaged medium is considered as a composite material in which some two-point micromodulus functions vanish. The effective moduli of the damaged medium (initially homogeneous) are estimated as the functions of damage, damage functions, and micromodulus profile. In so doing, all mentioned parameters of damage are fixed and assumed to be known, i.e., we don't consider the accumulation of damage and their dependence on the applied loading as well as crack initiation and propagation (see, e.g., [2], [154]).

Following [316], a damage function $\mu(\mathbf{x}, \boldsymbol{\xi})$ and local damage $\varphi(\mathbf{x})$ at a point \mathbf{x} are introduced

$$\mu(\mathbf{x}, \boldsymbol{\xi}) = \begin{cases} 0, & \text{the bond } \boldsymbol{\xi} \text{ is missing,} \\ 1, & \text{the bond } \boldsymbol{\xi} \text{ is acting,} \end{cases} \quad \varphi(\mathbf{x}) = 1 - \frac{\int_{\mathcal{H}_x} \mu(\mathbf{x}, \boldsymbol{\xi}) d\boldsymbol{\xi}}{\int_{\mathcal{H}_x} d\boldsymbol{\xi}}. \quad (4.42)$$

Then for an undamaged (pristine) material $\mathbf{C}(\mathbf{x}, \hat{\mathbf{x}}) \equiv \mathbf{C}^{(0)}(\mathbf{x}, \hat{\mathbf{x}})$ while the micromodulus of damaged medium can be presented in the form $\mathbf{C}(\mathbf{x}, \hat{\mathbf{x}}) = \mu(\mathbf{x}, \hat{\mathbf{x}})\mathbf{C}^{(0)}(\mathbf{x}, \hat{\mathbf{x}})$. This micromodulus is decomposed as $\mathbf{C}(\mathbf{x}, \hat{\mathbf{x}}) = \mathbf{C}^{(0)}(\mathbf{x}, \hat{\mathbf{x}}) + \mathbf{C}_1(\mathbf{x}, \hat{\mathbf{x}})$, where $\mathbf{C}_1(\mathbf{x}, \hat{\mathbf{x}}) = (\mu(\mathbf{x}, \boldsymbol{\xi}) - 1)\mathbf{C}^{(0)}(\mathbf{x}, \hat{\mathbf{x}})$

is a jump of micromodulus with respect to the micromodulus of the matrix (undamaged medium). Thus, we reformulated the damage model in the term of PM, which was solved, e.g., for periodic media (see for details [64]), when $\langle \boldsymbol{\sigma} \rangle^\Omega$, $\langle \boldsymbol{\varepsilon} \rangle^\Omega$, and \mathbf{L}^* are estimated. It was proved that for uniform damage functions $\mu(\mathbf{x}, \boldsymbol{\xi})$, for any profile either (2.26₁) and (2.26₂), and any dimension $d = 1, 2, 3$, \mathbf{L}^* is close to the popular engineering approximation (see, e.g. [181]) $\mathbf{L}^* = [1 - \varphi(\mathbf{x})]\mathbf{L}^{(0)}$.

It should be mentioned that the concept of peridynamic damage (initiated by Silling [311], see also [316]) expressed through the damage function $\mu(\mathbf{x}, \boldsymbol{\xi})$ is universally recognized by the Peridynamic Society and widely used for analyses of the finite-size samples of either initially homogeneous media or CMs. However, the infinite damaged media is of special interest just because of the classical continuum damage (CD) theory (see the books [181], [194]) was at first conceptually introduced for statistically homogeneous media as a state variable affecting the exploitation properties of this infinite media. In other words, so-called the scale separation hypothesis is implicitly assumed to be valid, which means that both the sample scale, and the applied field scale infinitely exceed a damage scale. Moreover, it is also interesting to set up relationships between the CD theories and peridynamic damage.

The popular idea for the incorporation of existing classical CD models into the peridynamic damage theory is an approximation of some peridynamic parameters by a function depending on a single parameter φ , which is commonly the case in some of the most popular damage models used in practice. So, one [336] proposed to describe an influence function of damaged medium to be proportional to the conventional (radial) influence function (for a pristine medium) with the proportionality factor $(1 - \varphi)$ depending on the state of damage between two points defining a bond. Han *et al.* [155] used an approximation for the damaged stiffness tensor (called the effective stiffness in our notation) defined by the micromodulus, which in turn depends on the critical local damage rather than on the damage function. Thus, the known incorporations of the CD concept into peridynamics are performed by the presentations of one or another peridynamic parameters (e.g. either influence function, micropotential, or micromodulus) as the functions of a state of damage (which is commonly the case in some of the most popular damage models used in practice). In the fundamental work by Littlewood *et al.* [213], the damage state (which is conceptually more general than the local damage φ) is introduced in the most general thermodynamic framework with the strain energy density function presented as a dot product of micropotential of undamaged bonds, and the damage state.

Numerical results were obtained for 1D case for the different damage function $\mu(\mathbf{x}, \boldsymbol{\xi})$ and the different micromodulus profiles (2.26₁) and (2.26₂) (see for details [58], [64]). It was demonstrated that for fixed local damage $\varphi = 0.5$, the effective modulus E^* has significantly more sensitive dependence on details of both the damage parameters (such as the damage function $\mu(\mathbf{x}, \boldsymbol{\xi})$) and the peristatic properties (such as micromodulus profile either (2.26₁) and (2.26₂)) rather than on only one parameter of the local damage φ . Only in a limiting case of both the homogeneous distribution of damaged bonds within the horizon and the large

node number n^l , the peridynamic periodic damage model is reduced to the classical CD model $\mathbf{L}^* = [1 - \varphi(\mathbf{x})]\mathbf{L}^{(0)}$ [181]. In some sense, a goal of the proposed approach can be considered as an inversion with respect to the goals of the known approaches (see [155], [336], and the most general version of peridynamic damage theory proposed in [213]). We don't try to incorporate the concept of the CD theory into peridynamics. Rather the opposite, we extracted, in particular, apparently the most popular equation of CD theory $\mathbf{L}^* = [1 - \varphi(\mathbf{x})]\mathbf{L}^{(0)}$ as a particular case of the most simple peridynamic damage theory (4.27). Moreover, in the framework of the functional graded theory (see for details [64]) it was proposed the model for the peristatic generalization of the classical feature of damage localization. The detected strain redistributions in damaged material quantitatively explain a qualitative feature of damage proposed in [12] when the breakage of individual bonds more likely generates its neighbors break, because more load is shifted to their neighbors.

In local micromechanics, the determination of effective stiffness for bodies containing microcracks is one of the fundamental aspects of micromechanical modeling. This subject is usually treated from various theoretical standpoints corresponding to one or another class of methods developed for micromechanics of CMs (3.2) (see the reviews, e.g., [47], [64], [263], [334], [353]). Among the self-consistent group, apparently the effective medium method [195], [160], Mori-Tanaka approach [256], and effective field method [351] (see also [185], [187]) are most popular and used for their subsequent generalizations (see for references, e.g. [116], [64]). So, the self-consistent method (some sort of effective medium method) by [28] consists of the calculation of crack opening displacements (COD) for microcracks embedded in the unknown effective medium. When an infinite number of randomly distributed inhomogeneities are analyzed, the average field in the matrix can be considered as a good approximation of the effective field that was pointed out by Benveniste [29] in a reformulation of the MTM which was also applied to the cracked medium [23]; its popularity is probably based upon the simplicity of its application. The effective field hypothesis (EFH, also called the **H1a** hypothesis, p. 253 in [47], see Section 3) is the most fundamental and most exploited concept of micromechanics. It has been demonstrated [348] that the MT approach reduces to the formula by Willis [351] (see also [281]) in the case of a matrix containing a set of aligned ellipsoidal inclusions, and this, apparently, is considered a virtue. For the flat distribution of cracks, the formulae by Willis [351] and MT approach [23] are identical because the MT procedure implicitly assumes the same distribution for the inclusions as their shape, which corresponds to the general estimate [281] for the case where the distribution and inclusion have the same aspect ratio.

Of course, a microcracked medium can be considered as a composite material where $\mathbf{C}^{(1)}(\mathbf{x}, \hat{\mathbf{x}}) = -\mathbf{C}^{(0)}(\mathbf{x}, \hat{\mathbf{x}})$ (as ${}^L\mathbf{L}^{(1)}(\mathbf{x}) = -{}^L\mathbf{L}^{(0)}$) and all methods of the PM considered in Subsection 4.1-4.4 are applicable for such medium.

4.6 Schematic representation of nonlinear GIE implementation

The scheme of the CAM (3.23), (3.28), (4.6)-(4.8) is presented in the blok structure in Fig. 3. For shortening of notations, the presented scheme corresponds to the iteration solution of Eq. (4.6). The central ingredient contains the Blocks *3 Perturbator* and *4 Micromechanics* placed in a circle. The perturbator $\mathcal{L}_i^{\theta\zeta}(\mathbf{z}, \bar{\zeta})$ (3.28) (and related perturbators) is evaluated in Block 3. A preprocessing *1 Input* to Block 3 contains geometrical microtopology of one inclusion $v_i(\mathbf{x})$ in the infinite homogeneous matrix (or large sample), material properties $\mathbb{C}(\mathbf{x})$ (e.g., micromodulus \mathbf{C}^{bond} (2.21)), and square mesh $\Omega^{\text{sq}} := \{(x_1, \dots, x_d)^\top | x_i = hp_i\}$ ($\mathbf{p} = (p_1, \dots, p_d) \in Z^d$). A preprocessing *2 Input* to Block 4 only contains geometrical information: the same mesh Ω^{sq} and the distribution of inclusions $X^{\partial v}$ (described by the probability densities $\varphi(v_j, \mathbf{x}_j)$ and $\varphi(v_j, \mathbf{x}_j | v_i, \mathbf{x}_i)$ for the random structures). The need to use the same mesh Ω^{sq} in Block 3 and Block 4, is explained by the convenience of matching these Blocks (see the case of LM on p. 428 in [64]). In the cycle [Block 3] \rightleftharpoons [Block 4] (4.6), the input-output of the Block 3 are $\langle \bar{\zeta} \rangle_i(\mathbf{x})$ and $\mathcal{L}_i^{\theta\zeta}(\mathbf{z}, \langle \bar{\zeta} \rangle_i)$, respectively, where $\mathbf{x}, \mathbf{z} \in \Omega^{\text{sq}}$. I.e. the mesh Ω^{sq} is only used for compatibility of Blocks 3 and 4 rather than for a solution of the problem inside Block 3 (see Eqs. (3.23)). Any inside knowledge of Bloc 3 (or 4) is not required in Blok 4 (or 3), respectively. Therefore, Blocks 3 and 4 can be considered as the Black Boxes (visualized in Fig. 3 by black color) to each other.

In Fig. 4, a zoomed Block 3 Perturbator is presented for one step in the circle [Block 3] \rightleftharpoons [Block 4] (see Fig.2). The Input Block in Fig. 3 presents the effective field $\langle \bar{\vartheta} \rangle_i(\mathbf{x})$ (estimated at the previous step in Block 4, see Eq. (4.22)) acting in the vicinity of the inclusion v_i (4.3) replaced by the matrix material. The Output block in Fig. 3 contains the perturbation field $\langle \vartheta \rangle_i(\mathbf{z}) - \langle \bar{\vartheta} \rangle_i(\mathbf{z}) = \mathcal{L}_i^{\theta\zeta}(\mathbf{z}, \langle \bar{\zeta} \rangle_i)$ (4.3) ($\mathbf{z} \in \mathbb{R}^d$) inside and outside the inclusion v_i in the local square mesh $\Omega_{\text{local}}^{\text{sq}}$ assigned to the inclusions v_i . In so doing, the mesh used for the solution of Eq. (4.3) (e.g., FEA mesh, an internal mesh of Block 3, which is not presented in Fig. 3) has no connection with the mesh $\Omega_{\text{local}}^{\text{sq}}$ exploited as an external mesh to Block 3 and utilized only for the interaction of Block 3 and Block 4.

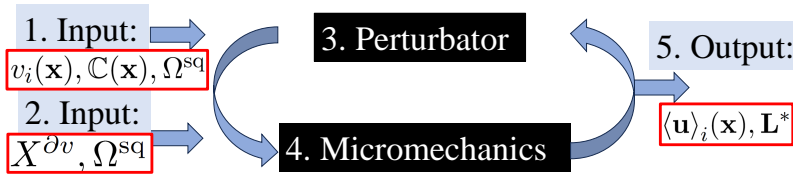


Fig. 3: The iteration scheme of the CAM (4.19)

Zoomed Block 4 is presented in Fig. 5, where the square mesh Ω^{sq} has two meshes. The moving local mesh $\Omega_{\text{local}}^{\text{sq}}$ (solid black grid) is assigned to the moving inclusion v_j (see Eq. (4.19)) with the center \mathbf{x}_j so that $\mathbf{x}_j = \mathbf{0}$ in the system $\Omega_{\text{local}}^{\text{sq}}$.

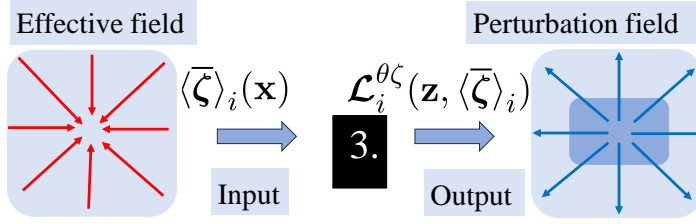


Fig. 4: Zoomed Block 3 (from Fig. 2.) with the input effective field and output perturbation field

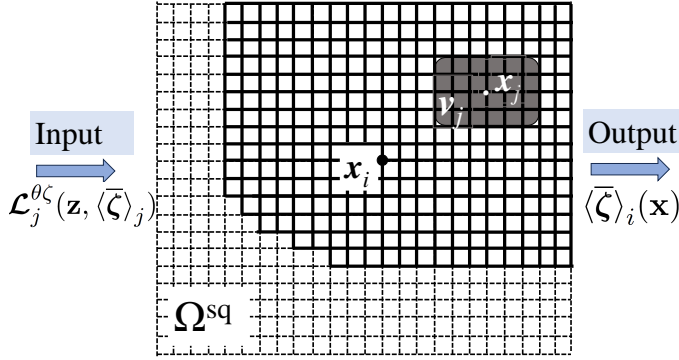


Fig. 5: Zoomed Block 4 (from Fig. 2.) with the input perturbation field and output effective field

The global mesh $\Omega_{\text{global}}^{\text{sq}}$ (dashed black grid) is assigned to the fixed inclusion v_i (see Eq. (4.19)) with the center $\mathbf{x}_i = \mathbf{0}$ in the system $\Omega_{\text{global}}^{\text{sq}}$ and $\mathbf{x}_j \in \Omega_{\text{global}}^{\text{sq}}$ ($j = 1, 2, \dots$). The main reason for the choice of the same square mesh $\Omega_{\text{local}}^{\text{sq}}$ and $\Omega_{\text{global}}^{\text{sq}}$ is explained in [61]. For statistically homogeneous CMs subjected to the homogeneous VBC (2.29) and (2.30), the input perturbation $\mathcal{L}_j^{\theta\zeta}(\mathbf{z}, \langle \bar{\zeta} \rangle_j)$ ($\mathbf{z} \in \mathbb{R}^d$) assigned to the moving inclusion v_j ($j = 1, 2, \dots$) is estimated only one time. The output of the Block 4 is the effective field $\langle \bar{\zeta} \rangle_i(\mathbf{x})$ acting on the fixed inclusion v_i .

Zoomed Block 5 from Fig. 2 is presented in Fig. 6. Here the effective field $\langle \bar{\zeta} \rangle_i(\mathbf{x})$ ($\mathbf{x} \in v_i$) acting on the representative area of the inclusion v_i (replaced by the matrix material) are estimated as output of the Block 4 (see Fig. 2) at the last step in the circle [Block 3] \rightleftharpoons [Block 4]. The field inside the representative inclusion v_i $\langle \vartheta \rangle_i(\mathbf{z}) = \langle \bar{\vartheta} \rangle_j(\mathbf{z}) + \mathcal{L}_i^{\theta\zeta}(\mathbf{z}, \bar{\zeta})$ ($\mathbf{z} \in v_i$) is estimated by the use of the Block 3 (see Fig. 3) at the last step in the circle [Block 3] \rightleftharpoons [Block 4]. At last, the effective constitutive equation (4.23) is evaluated only one time through the substitution of $\langle \vartheta \rangle_j(\mathbf{z})$ into Eqs. (4.21). In the case of the homogeneous VBC (2.29) and (2.30), the effective moduli \mathbf{L}^* (4.29) are expressed (also only one time) through the statistical average displacement field $\langle \mathbf{u}(\mathbf{u}) \rangle_i(\mathbf{s})$ at the external interaction interface ($\mathbf{s} \in \Gamma_i$ marked by

a black color) of the representative heterogeneity v_i ; i.e. the field $\langle \boldsymbol{\vartheta} \rangle_i(\mathbf{z})$ inside the inclusion $\mathbf{z} \in v_i$ is not used at the estimation for estimation of \mathbf{L}^* .

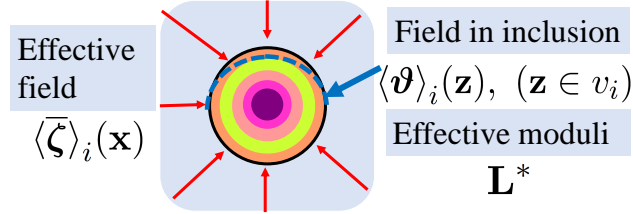


Fig. 6: Zoomed Block 5 (from Fig. 2.) with the field $\langle \boldsymbol{\vartheta} \rangle_i(\mathbf{z})$ (dashed line) inside inclusion v_i

Comment 4.5. It should be mentioned that the LM method’s classification (3.2) is also applicable to the PM counterparts. Model methods Gr1) include the simplified methods such as, e.g. the mixture theory, (see Introduction for details) [10], [11], [12], [162], [163], [243], [356], [357], which have attracted increasing attention for dealing with complex laminated problems [18], [109], [150], [165], [236], [238], [239], [289], [363]). The CAM of peridynamic CM belongs to the area of *Analytical Micromechanics* where the DNS is not used (see Fig. 1). So, Eqs. (4.5)-(4.19) correspond to the LM self-consistent methods Gr4) (3.2), i.e. CAM belongs to the grope Gr4). The term “computational” in CAM is used to emphasize that background hypotheses of analytical micromechanics are abandoned (see Comments 4.4.) which expectedly leads to increasing in the computational complexity of CAM. Perturbation method Gr2) corresponds to the dilute approximation in the PM considered in [62]. The popular method of the effective medium (MEM) belonging to class Gr1) in the LM has a straightforward generalization to the PM as one peridynamic inclusion in the local effective medium. Variational methods (grope Gr3)) were considered in [63]: the theorem of work and energy, Betti’s reciprocal theorem, and the theorem of virtual work were proved. Principles of a minimum of both potential energy and complementary energy were generalized. It was obtained the generalized Hill’s bounds on the effective elastic moduli of peridynamic random structure composites; these bounds depend on both the shape of inclusions and the ratio l_δ/a (in opposite to the Hill’s bound in LM). Of special interest in the LM are Hashin-Shtrilman (H-S) bounds, which were, in particular, obtained from the GIE (3.5), see [353]. However, H-S bounds were also estimated from the GIE (3.7) (see pp. 439-442 in [64]) or CMs with noncanonical inhomogeneous inclusions; the difference between the H-S bounds obtained from Eqs. (3.5) and (3.7) is described by a factor of 2.9. Owing to the formal similarity of GIEs in the LM (3.7), (3.11) and PM (3.34), it would be interesting to generalize the H-S bounds obtained from Eq. (3.7) to their peridynamic counterpart obtained from the GIE (3.34).

Comment 4.6. Just for completeness, it should be also emphasized that the classification of the *Computational Mechanics* used DNS, see Eq. (3.3) and Fig. 1, in the LM is also applicable for the PM counterparts (see Introduction for details). Asymptotic homogenization methods (Block 1 in (3.3) in PM were considered in [7], [123], [121]). The papers

[56], [57],[110], [111], [143], [144], [318] [283], [360], [365] [366] [375] [377] are dedicated to the generalization of classical computational homogenization approaches (Block 2 in(3.3)). At last, there are a lot of problems for one or finite numbers of inclusions (or cracks) in a sample (Block 3 in Fig. 1) [2] [10], [11], [12], [14], [27] , [35], [40], [108], [154], [164], [178], [189], [190], [198], [200], [229], [235], [260], [265], [290] , [296], [341], [347], [371], [387], [399]. It should be mentioned that particular cases of problems indicated in Block 3 in Eq. (3.3) can be considered as a Block 3 Perturbator (see Fig. 2 and 3) for one inclusion (or crack) in a big sample.

Comment 4.7. It should be emphasized that all information about constitutive law (one or another PD model) is incorporated into Block 3 Perturbator (rather than into Block 4 Micromechanics). However, the following problems are beyond the scope of the current review. These are the comparisons between different peridynamic models with some numerical results, analyses of why peridynamic theory is interesting and useful, and descriptions of limitations of the peridynamic models. The methods for the solution of Block 3 Perturbator are also not analyzed (these methods are only briefly mentioned in Introduction). I.e. solution of Block 3 Perturbator is assumed to be known whereas a destiny of the current review is (loosely speaking) descriptions of Block 4 Micromechanics and its adjustment with Block 3 Perturbator (see also the text before Fig. 3).

Comment 4.8. The study [98] demonstrates that the PD community has been growing exponentially in size in recent years. By constructing a network for each year, the authors [98] can analyze the evolution of the collaboration network in time and discuss the implications of this evolution for the PD community. The goal of the current Comment 4.8 is a very approximative and simplified lower estimate (which is largely speculative without any tool like [98]) of the author's number involved in the different groups of methods of PM. It was established in Comments 4.5 and 4.6 that the classification of PM duplicates (in fact) the classification of LM, see Eqs. (3.2) and (3.3).

$$\begin{array}{ccccccc}
 \underline{\text{Gr1}} & \underline{\text{Gr2}} & \underline{\text{Gr3}} & \underline{\text{Gr4}} & \underline{\text{Block1}} & \underline{\text{Block2}} & \underline{\text{Block3}} \\
 & \underbrace{\hspace{1.5cm}} & & & & & \\
 > 100 & & = 1 & & > 8 & > 50 & > 300
 \end{array} \tag{4.43}$$

It is interesting that in LM, background concepts of analytical micromechanics (Gr1-Gr4) (3.2) were proposed 150 years earlier than background concepts of computational micromechanics (Blocks 1 and 2 in (3.3)), see Introduction and Subsection 3.1. In so doing the total numbers of both developers and users involved in the sets either Gr1-Gr4 (3.2) or Block1-Block2 (3.3) are comparable. This author's distribution is drastically changed in PM, see the second line in (4.43) (see for references Introduction and subsequent text). So, the background of the set $\text{Gr2} \cup \text{Gr3} \cup \text{Gr4}$ was proposed in 2014 by Buryachenko [50] and up to now, only one author is involved (as both developer and user) into the set $\text{Gr2} \cup \text{Gr3} \cup \text{Gr4}$ [51], [52], [53], [54], [55], [60], [61], [62], [63], [64], [67], [68], [69], [74], [70], [71], [73], [78] (see Introduction and Sections 3-5), although the contribution of this author to Block2 is also critical (see

Subsection 2.4 and Sections 6 and 7 below); so, the background of Block2 was proposed in 2018 [56], see also [57], [58], [75], [76], [77]. As can be seen in (4.43), the micromechanical models of each block (either Gr1, Block1, Block2, or Block3) are more popular and widely used (at least in the sense of the author's number involved) than the models $\text{Gr2} \cup \text{Gr3} \cup \text{Gr4}$. However, intersection of the sets $\text{Gr1} \cup \text{Block1} \cup \text{Block2} \cup \text{Block3}$ and $\text{Gr2} \cup \text{Gr3} \cup \text{Gr4}$ is empty set. The tools of methods proposed in either Cr1, Block1, or Block2 are absolutely useless for analyses of any problem considered in Gr2-Gr4 (although Block3 is used in Gr2-Gr4, see Comment 4.7) for practically critical cases of real random structure peridynamic CMs (instead of artificial periodic structures in Block1 and Block2 in (4.43)). The author encourages the PD community to eliminate this imbalance in the second line of (4.43).

4.7 Nonlinear incremental Mori-Tanaka approach in PM

In general, within a FEA ABAQUS specifies strain increments, which are taken as the input for the constitutive material law. The stress response and the consistent (algorithmic) tangent tensor of the composite material at the end of the increment have to be evaluated for this strain increment. The following strategy of the incremental Mori-Tanaka approach is used for solving the nonlinear behavior of peridynamic CM (which is a generalization of corresponding approaches in the LM, see, e.g., [112], [120], [186], [278]).

At first, we consider a macroscopic matrix domain w subjected to the remote homogeneous volumetric boundary conditions (2.29) and (2.30) producing a linear displacement field $\mathbf{u}(\mathbf{x}) = \boldsymbol{\varepsilon}^{w\Gamma} \cdot \mathbf{x}$ ($\mathbf{x} \in w$). For nonlinear PD, the tangent moduli $\mathbf{L}_t^{(0)}$ are represented and approximated by a forward difference of the associated stresses

$$\begin{aligned} \Delta \boldsymbol{\sigma} &= \mathbf{L}_t^{(0)} \Delta \boldsymbol{\varepsilon}^{w\Gamma}, \\ \mathbf{L}_t^{(0)} \Delta \boldsymbol{\varepsilon}^{w\Gamma} &= [\mathcal{L}^{\sigma(0)}((\boldsymbol{\varepsilon}^{w\Gamma} + \Delta \boldsymbol{\varepsilon}^{w\Gamma}) \cdot \mathbf{x}) - \mathcal{L}^{\sigma(0)}(\boldsymbol{\varepsilon}^{w\Gamma} \cdot \mathbf{x})] \Delta \boldsymbol{\varepsilon}^{w\Gamma}, \end{aligned} \quad (4.44)$$

where $\mathbf{L}_t^{(0)}$ represents the associated tangent moduli, or the components of the tangent modulus tensor obtained by the perturbation of $\Delta \boldsymbol{\varepsilon}^{w\Gamma}$.

It is assume that up to n th increment $\langle \boldsymbol{\varepsilon} \rangle^{[n]}$ the behavior of CM is linear and can be estimate $\mathbf{L}^{(0)[n]}$ (3.44), $\mathbf{L}^{u\epsilon[n]}$ (4.33₁), $\mathbf{L}^{\sigma\epsilon[n]}$ (4.34₂), $\mathbf{R}_i^{l\omega[n]}$ (4.34₁), $\mathbf{A}_i^{l\omega[n]}$ (4.33₂), $\langle \boldsymbol{\varepsilon} \rangle^{l(0)[n]} \equiv \bar{\boldsymbol{\varepsilon}}^{l(0)[n]}$ (4.39), $\mathbf{L}_i^{*\omega\text{MTA}[n]}$ (4.40). In a backward Euler fully implicit numerical scheme, the value of a given quantity $\boldsymbol{\chi}$ is updated from the previous time step n to the current $n+1$ per $\boldsymbol{\chi}^{[n+1]} = \boldsymbol{\chi}^{[n]} + \Delta \boldsymbol{\chi}^{[n+1]}$. Such an implicit relation is usually solved iteratively, and the current value is updated for each iteration by: $\boldsymbol{\chi}^{[n+1](k+1)} = \boldsymbol{\chi}^{[n+1](k)} + \Delta \boldsymbol{\chi}^{[n+1](k)}$ until $\boldsymbol{\chi}^{[n+1](k+1)}$ has converged. $\mathbf{x}(n+1)(k)$.

Using the Backward Euler framework, equation (4.27) is written in incremental form at time step $n+1$ as

$$\Delta \langle \boldsymbol{\sigma} \rangle^{[n+1]} = \mathbf{L}^{*\omega\text{MTM}[n+1]} \Delta \langle \boldsymbol{\varepsilon} \rangle^{[n+1]}, \quad (4.45)$$

The known global state and instantaneous behavior from the previous increment together with the prescribed strain increment, $\Delta\langle\boldsymbol{\varepsilon}\rangle^{[n+1]}$, are used to calculate a prediction for the new ‘homogenized’ overall state. This predicted new state gives rise to a predicted matrix strain increment $\langle\boldsymbol{\varepsilon}\rangle^{l(0)[n]}$, which is used to solve for matrix perturbators $\mathbf{L}^{u\epsilon[n]}$ (4.33₁) and $\mathbf{L}^{\sigma\epsilon[n]}$ (4.34₂) in an Euler backward scheme on the micro level. In an incremental-iterative form, the prediction step states that the stress during the current loading increment $n + 1$ and at the end of each iteration $k + 1$ is given as

$$\langle\boldsymbol{\sigma}\rangle^{[n+1](k+1)} = \langle\boldsymbol{\sigma}\rangle^{[n]} + \mathbf{L}^{*\omega\text{MTM}[n+1](k+1)}\Delta\langle\boldsymbol{\varepsilon}\rangle^{[n+1]}, \quad (4.46)$$

where $\mathbf{L}^{*\omega\text{MTM}[n+1](1)} = \mathbf{L}^{*\omega\text{MTM}[n]}$ and the initial iteration corresponds to $k = 1$, i.e. $\mathbf{L}^{(0)[n](1)} = \mathbf{L}^{(0)[n]}$ (3.44), $\mathbf{L}^{u\epsilon[n](1)} = \mathbf{L}^{u\epsilon[n]}$ (4.33₁), $\mathbf{L}^{\sigma\epsilon[n](1)} = \mathbf{L}^{\sigma\epsilon[n]}$ (4.34₂), $\langle\boldsymbol{\varepsilon}\rangle^{l(0)[n](1)} = \langle\boldsymbol{\varepsilon}\rangle^{l(0)[n]}$, $\mathbf{R}_i^{l\omega[n](1)} = \mathbf{R}_i^{l\omega[n]}$ (ref4.34₁), $\mathbf{A}_i^{l\omega[n](1)} = \mathbf{A}_i^{l\omega[n]}$ (4.33₂), $\langle\boldsymbol{\varepsilon}\rangle^{l(0)[n](1)} = \langle\boldsymbol{\varepsilon}\rangle^{l(0)[n]}$ (4.39), $\mathbf{L}_i^{*\omega\text{MTM}[n](1)} = \mathbf{L}_i^{*\omega\text{MTM}[n]}$ (4.40).

For the current $\Delta\langle\boldsymbol{\varepsilon}\rangle^{[n+1]}$ we estimate $\langle\boldsymbol{\varepsilon}\rangle^{l(0)[n+1](k)}$ by Eq. (4.40) with $\mathbf{A}_i^{l\omega} = \mathbf{A}_i^{l\omega(k)}$. $\langle\boldsymbol{\varepsilon}\rangle^{l(0)[n+1](k)}$ is substituted to the right-hand side of Eqs. (4.44), (4.33₁) and (4.34₂) with estimations of $\mathbf{L}_i^{(0)(k+1)}$ (4.44), $\mathbf{L}^{u\epsilon[n](k+1)}$ (4.33₁), and $\mathbf{L}^{\sigma\epsilon[n](k+1)}$ (4.34₂) which, in its turn, prove estimations of $\mathbf{R}_i^{l\omega[n](k+1)}$ (4.40), $\mathbf{A}_i^{l\omega[n](k+1)}$ (4.41), and $\mathbf{L}_i^{*\omega\text{MTM}[n](k+1)}$ (4.40). The process is completed when $\|\mathbf{L}_i^{*\omega\text{MTM}[n](k+1)} - \mathbf{L}_i^{*\omega\text{MTM}[n](k)}\| \leq \text{TOL} (\exists k)$ sufficiently close to zero and the iteration loop is closed by again predicting a new state. If the $\langle\boldsymbol{\varepsilon}\rangle^{[n+1](k+1)}$ slowly converges, the increment $\Delta\langle\boldsymbol{\varepsilon}\rangle^{[n+1]}$ (4.45) should be decreased, e.g., $\Delta\langle\boldsymbol{\varepsilon}\rangle^{[n+1]} := \Delta\langle\boldsymbol{\varepsilon}\rangle^{[n+1]}/2$. This way an implicit iterative algorithm is set up to evaluate the stress response to the average strain increment prescribed by Eq. (4.45).

In Subsection 4.7 only one type of nonlinear peridynamics is considered, precisely nonlinear elasticity. However, a more detailed analyses of nonlinear incremental methods for both different physical phenomena (e.g., diffusion, viscosity, thermoelastoplasticity, damage accumulation, debonding, plastic localization, wave propagation) and different random and periodic structures (e.g., polycrystals, fiber networks, hybrid structures, foam materials) are beyond the scope of the current study and deserve further investigations.

5 Estimation of field fluctuations and effective energy-based criteria

In the nonlinear problems of the LM considered, the central deal is an estimation of the second moment of phase fields ($\boldsymbol{\pi} = \boldsymbol{\varepsilon}, \boldsymbol{\sigma}; \mathbf{x} \in v^{(i)}$)

$$\langle\boldsymbol{\pi} \otimes \boldsymbol{\pi}\rangle_i(\mathbf{x}) = \langle\boldsymbol{\pi}\rangle_i(\mathbf{x}) \otimes \langle\boldsymbol{\pi}\rangle_i(\mathbf{x}) + \Delta_i^{\pi^2}(\mathbf{x}). \quad (5.1)$$

where $\Delta_i^{\pi^2}(\mathbf{x})$ is called the dispersion (or the fluctuation field). There are two methods for estimations of $\langle\boldsymbol{\pi} \otimes \boldsymbol{\pi}\rangle_i(\mathbf{x})$: the exact differential method (see pp. 419, 423 in [47], and pp.

252, 253 in [64]), and the method of integral equations (see pp. 427-431 in [47], and pp. 446, 456-475, 532 in [64]). Both methods lead to close numerical results. It was also demonstrated that engineering approach $\langle \boldsymbol{\pi} \otimes \boldsymbol{\pi} \rangle_i(\mathbf{x}) = \langle \boldsymbol{\pi} \rangle_i(\mathbf{x}) \otimes \langle \boldsymbol{\pi} \rangle_i(\mathbf{x})$ can lead to an infinite error at the hydrostatic loading.

However, it is precisely the method of integral equations in LM that enables one to generalize it to the PM. Namely, the following new approximations for the second moment can be obtained by taking only the binary interaction of inclusions into account:

$$\begin{aligned} \langle \bar{\boldsymbol{\vartheta}} \otimes \bar{\boldsymbol{\vartheta}} \rangle_i(\mathbf{x}) &= \langle \bar{\boldsymbol{\vartheta}} \rangle_i(\mathbf{x}) \otimes \langle \bar{\boldsymbol{\vartheta}} \rangle_i(\mathbf{x}) + \int \langle \mathcal{L}_p^{\theta\zeta}(\mathbf{x}, \bar{\boldsymbol{\zeta}}) |; v_i, \mathbf{x}_i \rangle \\ &\otimes \langle \mathcal{L}_p^{\theta\zeta}(\mathbf{x}, \bar{\boldsymbol{\zeta}}) |; v_i, \mathbf{x}_i \rangle \varphi(v_p, \mathbf{x}_p |; v_i, \mathbf{x}_i) d\mathbf{x}_p. \end{aligned} \quad (5.2)$$

Using the known properties of the second statistical moment, we obtain the relations for the average second moments of the fields, $\langle \boldsymbol{\vartheta} \otimes \boldsymbol{\vartheta} \rangle_i(\mathbf{x})$ in the component v_i corresponding to Eqs. (5.2)

$$\begin{aligned} \langle \boldsymbol{\vartheta} \otimes \boldsymbol{\vartheta} \rangle_i(\mathbf{x}) &= \langle \boldsymbol{\vartheta} \rangle_i(\mathbf{x}) \otimes \langle \boldsymbol{\vartheta} \rangle_i(\mathbf{x}) + \int \mathcal{A}_i^{\theta\theta} * \langle \mathcal{L}_p^{\theta\zeta}(\mathbf{x}, \bar{\boldsymbol{\zeta}}) |; v_i, \mathbf{x}_i \rangle \\ &\otimes \mathcal{A}_i^{\theta\theta} * \langle \mathcal{L}_p^{\theta\zeta}(\mathbf{x}, \bar{\boldsymbol{\zeta}}) |; v_i, \mathbf{x}_i \rangle \varphi(v_p, \mathbf{x}_p |; v_i, \mathbf{x}_i) d\mathbf{x}_p. \end{aligned} \quad (5.3)$$

Comment 5.1. New equations (5.2) and (5.3) are obtained for nonlinear problems of PM with nonlinear operators $\mathcal{A}_i^{\theta\theta}$ (3.23₂) and $\mathcal{L}_p^{\theta\zeta}(\mathbf{x}, \bar{\boldsymbol{\zeta}})$ (3.23₁). These equations are reduced to the corresponding equations for the linear bond-based model [74] and linear state-based model [70] as well as to the equations obtained before for the linear LM (in the framework of both the first background [47] and second background [64] of micromechanics). Thus, we have the third (see Comments 3.3.2 and 4.4.) rare case when the methods developed in PM for the field second moments (nonlinear problem) initiate the new methods of LM (a generalization of linear analyses to nonlinear ones) unknown before. In so doing, linearity of matrix properties as in Comment 4.4 is not required. Moreover, Eqs. (5.2) and (5.3) including double-point $\varphi(v_p, \mathbf{x}_p |; v_i, \mathbf{x}_i)$ conditional probability densities can be generalized (analogously to [70]) to the corresponding exact representations containing triple-point $\varphi(v_p, \mathbf{x}_p, v_q, \mathbf{x}_q |; v_i, \mathbf{x}_i)$ densities.

Simplifications of Eq. (5.3) with subsequent applications to obtaining of effective energy-based criteria can be performed for linear operators $\mathcal{A}_i^{\theta\theta}$ (3.23₂) and $\mathcal{L}_p^{\theta\zeta}(\mathbf{x}, \bar{\boldsymbol{\zeta}})$ (3.23₁) in the framework of the EFH **H1a** (4.1):

$$\langle \boldsymbol{\eta} \otimes \boldsymbol{\eta} \rangle_i(\mathbf{z}) = \langle \boldsymbol{\eta} \rangle_i(\mathbf{z}) \otimes \langle \boldsymbol{\eta} \rangle_i(\mathbf{z}) + \Delta_i^{\eta^2}(\mathbf{z}), \quad (5.4)$$

where

$$\begin{aligned} \Delta_i^{\eta^2}(\mathbf{z}) &= \int [\mathbb{A}_{i,j}(\mathbf{z}) \langle \boldsymbol{\varepsilon} \rangle] \otimes [\mathbb{A}_{i,j}(\mathbf{z}) \langle \boldsymbol{\varepsilon} \rangle] \varphi(v_j, \mathbf{x}_j |; v_i, \mathbf{x}_i) d\mathbf{x}_j, \\ \mathbb{A}_{i,j}(\mathbf{z}) &= \mathbf{A}_i^{\eta\varepsilon}(\mathbf{z}) [\mathbf{J}_{i,j}^{I\varepsilon\varepsilon} \mathbf{D}_i^0 + \mathbf{J}_{i,j}^{J\varepsilon\varepsilon}(\mathbf{y}) \mathbf{D}_j^0]. \end{aligned} \quad (5.5)$$

Here $\mathbf{A}_i^{\eta\varepsilon}(\mathbf{z}) = \underline{\mathbf{A}}_i^{u\varepsilon}[\mathbf{x}]\langle\xi\rangle$ ($\xi = \hat{\mathbf{x}} - \mathbf{x}$) whereas \mathbf{D}_i^0 is the effective field concentration factor $\langle\bar{\varepsilon}\rangle_i = \mathbf{D}_i^0\langle\varepsilon\rangle$ (see for details [70]).

Equation (5.4) is a ‘‘elementary block’’ for the construction of many effective energy-based criteria. So, in the energy-based peridynamic approach for fatigue cracking, one [265] estimated the energy release rate for interaction between material points through the micropotentials of the interaction between these points. The state-based version of the effective energy-based criterion is the following ($\xi, \zeta \in \mathcal{H}_{\mathbf{x}} \subset v_i$)

$$\langle \mathbf{U}^\top \mathbb{K} \mathbf{U} \rangle_i(\xi, \zeta) = \langle \mathbf{U}^\top \rangle_i \mathbb{K} \langle \mathbf{U} \rangle_i(\xi, \zeta) + \Delta^{\text{UKU}}(\xi, \zeta), \quad (5.6)$$

$$\Delta^{\text{UKU}}(\xi, \zeta) = \int [\mathbb{A}_{ij}(\xi)\langle\varepsilon\rangle]^\top \mathbb{K}(\xi, \zeta) [\mathbb{A}_{ij}(\zeta)\langle\varepsilon\rangle] \varphi(v_j, \mathbf{x}_j |; v_i, \mathbf{x}_i) d\mathbf{x}_j, \quad (5.7)$$

where the statistical average of the displacement state is defined as $\langle \mathbf{U} \rangle_i[\mathbf{x}]\langle\xi\rangle = \underline{\mathbf{A}}_i^{u\varepsilon*}[\mathbf{x}]\langle\xi\rangle\langle\varepsilon\rangle = \mathbf{A}_i^{\eta\varepsilon*}(\mathbf{z})\langle\xi\rangle\langle\varepsilon\rangle$ (4.17). The energy-based failure model [172] is based on an evaluation of the local strain energy density for bond-based peridynamics at each point. Then the effective criterion for the state-based model can be obtained

$$4\langle \mathcal{W} \rangle_i(\mathbf{x}) = \langle \mathbf{U}^\top \bullet \mathbb{K} \bullet \mathbf{U} \rangle_i(\mathbf{x}) = \langle \mathbf{U}^\top \rangle_i \bullet \mathbb{K} \bullet \langle \mathbf{U} \rangle_i(\mathbf{x}) + \Delta^{\text{UKU}}(\mathbf{x}), \quad (5.8)$$

$$\begin{aligned} \Delta^{\text{UKU}}(\mathbf{x}) &= \int \left\langle [\mathbb{A}_{ij}(\xi)\langle\varepsilon\rangle]^\top \langle \mathbb{K}(\xi, \zeta) [\mathbb{A}_{ij}(\zeta)\langle\varepsilon\rangle] \right\rangle^{\mathcal{H}_{\mathbf{x}}} \Big|_{\mathcal{H}_{\mathbf{x}}}(\mathbf{x}) \\ &\times \varphi(v_j, \mathbf{x}_j |; v_i, \mathbf{x}_i) d\mathbf{x}_j \end{aligned} \quad (5.9)$$

averaging over the horizon region, $\mathcal{H}_{\mathbf{x}} \subset v_i$ ($\mathbf{y} \in v_j$).

Seemingly, a second moment of the force vector state $\mathbf{T} = \mathbb{K} \bullet \mathbf{U}$ (2.19) can be obtained ($\xi, \zeta \in \mathcal{H}_{\mathbf{x}} \subset v_i$)

$$\langle \mathbf{T} \otimes \mathbf{T} \rangle_i^{\mathcal{H}_{\mathbf{x}}}(\mathbf{x}) = \left\langle (\mathbb{K} \bullet \langle \mathbf{U} \rangle_i) \otimes (\mathbb{K} \bullet \langle \mathbf{U} \rangle_i) \right\rangle^{\mathcal{H}_{\mathbf{x}}}(\mathbf{x}) + \Delta^{\text{T2}}(\mathbf{x}), \quad (5.10)$$

$$\begin{aligned} \Delta^{\text{T2}}(\mathbf{x}) &= \int \left\langle \langle \mathbb{K}(\xi, \zeta) [\mathbb{A}_{ij}(\zeta)\langle\varepsilon\rangle] \right\rangle^{\mathcal{H}_{\mathbf{x}}} \otimes \langle \mathbb{K}(\xi, \zeta) \\ &\times [\mathbb{A}_{ij}(\zeta)\langle\varepsilon\rangle] \right\rangle^{\mathcal{H}_{\mathbf{x}}} \Big|_{\mathcal{H}_{\mathbf{x}}}(\mathbf{x}) \varphi(v_j, \mathbf{x}_j |; v_i, \mathbf{x}_i) d\mathbf{x}_j. \end{aligned} \quad (5.11)$$

After that, analogously to Eq. (5.8), we can find from Eq. (5.10) $\langle \mathbf{T} \cdot \mathbf{T} \rangle_i^{\mathcal{H}_{\mathbf{x}}}(\mathbf{x})$ ($\mathbf{x} \in \mathcal{H}_{\mathbf{x}} \subset v_i$). It can also estimate a particular case of the yield function based on the criterium of the co-deviatoric force state: $\psi(\mathbf{x}) = \langle \underline{t}^d[x]\langle\xi\rangle \times \underline{t}^d[x]\langle\xi\rangle \rangle^{\mathcal{H}_{\mathbf{x}}}(\mathbf{x})/2$ (which is equivalent to the second invariant of the deviatoric stress tensor in classical local theory), where $\underline{t}^d[x]\langle\xi\rangle$ is the co-deviatoric part of the scalar force state \underline{t} (see for details [252], [317]).

A failure criterion for breaking the physical bonds between material points based on the energy dissipation $\mathcal{W}_\xi(\mathbf{x})$ (see [140], [327], [328], [342]) is a function of the stress state

$\underline{\mathbf{T}} = \underline{\mathbb{K}} \bullet \underline{\mathbf{U}}$ (2.19) and the displacement state $\underline{\mathbf{U}}$ between two points ($\boldsymbol{\xi} \in \mathcal{H}_{\mathbf{x}} \subset v_i$)

$$\mathcal{W}_{\boldsymbol{\xi}}(\mathbf{x}) = \langle (\underline{\mathbb{K}} \bullet \underline{\mathbf{U}}) \rangle_i \langle \underline{\mathbf{U}} \rangle_i(\mathbf{x}) = (\underline{\mathbb{K}}^{(i)} \bullet \langle \underline{\mathbf{U}} \rangle_i) \langle \underline{\mathbf{U}} \rangle_i(\mathbf{x}) + \Delta^{\text{TU}2}(\boldsymbol{\xi}, \mathbf{x}), \quad (5.12)$$

$$\Delta^{\text{TU}2}(\boldsymbol{\xi}, \mathbf{x}) = \int \langle \underline{\mathbb{K}}(\boldsymbol{\xi}, \boldsymbol{\zeta}) [\mathbb{A}_{ij}(\boldsymbol{\zeta}) \langle \boldsymbol{\varepsilon} \rangle] \rangle^{\mathcal{H}_{\mathbf{x}}} [\mathbb{A}_{ij}(\boldsymbol{\xi}) \langle \boldsymbol{\varepsilon} \rangle](\mathbf{x}) \varphi(v_j, \mathbf{x}_j |; v_i, \mathbf{x}_i) d\mathbf{x}_j. \quad (5.13)$$

Equations (5.6)-(5.13) for the linear operators $\mathcal{A}_i^{\theta\theta}$ (3.23₂) and $\mathcal{L}_p^{\theta\zeta}(\mathbf{x}, \bar{\boldsymbol{\zeta}})$ (3.23₁), are reduced to the corresponding equations for both the linear state-based [70] and linear bond-based model [74] models

Comment 5.2. It is interesting that all effective energy-based criteria considered (5.6)-(5.13) are constructed by the use of the same “elementary block” of the second moment of the relative displacement $\langle \boldsymbol{\eta} \otimes \boldsymbol{\eta} \rangle_i(\mathbf{z})$ (5.4) (or, that is the same, $\langle \underline{\mathbf{U}}[\mathbf{x}] \langle \boldsymbol{\xi} \rangle \otimes \underline{\mathbf{U}}[\mathbf{x}] \langle \boldsymbol{\xi} \rangle \rangle_i(\mathbf{x})$ ($\mathbf{x} \in v_i$, $\boldsymbol{\xi} \in \mathcal{H}_{\mathbf{x}} \subset v_i$)). Moreover, these effective energy-based criteria are defined on either one bond $\boldsymbol{\xi} \in \mathcal{H}_{\mathbf{x}} \subset v_i$, or two bonds $\boldsymbol{\xi}, \boldsymbol{\zeta} \in \mathcal{H}_{\mathbf{x}} \subset v_i$ with the field fluctuations, either $\Delta^{\text{UKU}}(\boldsymbol{\xi}, \boldsymbol{\zeta})$, $\Delta^{\text{UKU}}(\mathbf{x})$, $\Delta^{\text{T}2}(\mathbf{x})$, or $\Delta^{\text{TU}2}(\boldsymbol{\xi}, \mathbf{x})$.

Comment 5.3. The scheme of estimations of different effective energy-based criteria by the use of one “elementary block” $\langle \boldsymbol{\eta} \otimes \boldsymbol{\eta} \rangle_i(\mathbf{z})$ (5.4) is presented in Fig. 7.

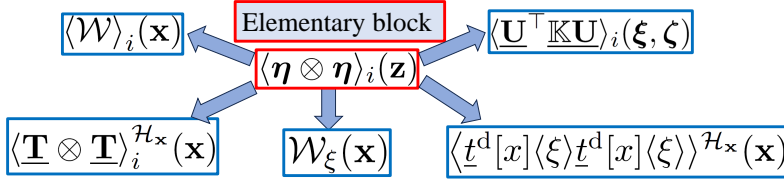


Fig. 7: Estimation of the effective energy-based criteria by the use of the elementary block $\langle \boldsymbol{\eta} \otimes \boldsymbol{\eta} \rangle_i(\mathbf{z})$

6 Fast Fourier transform in peridynamic micromechanics

6.1 Fast Fourier transform

A unit cell $\Omega_{00} = \Pi_{\alpha}[0, l_{\alpha}^{\Omega}]$ ($\alpha = 1, \dots, d$) discretized with the uniform grid of $N_1 \times \dots \times N_d$ nodes is considered

$$\begin{aligned} \mathbf{x}_{\mathbf{N}}^{\mathbf{k}} &= \mathbf{k} \cdot \Delta \mathbf{h} \equiv [k_1 \Delta h_1, \dots, k_d \Delta h_d]^{\top}, \\ \mathbf{k} \in Z_{\mathbf{N}}^d &:= \left\{ \mathbf{m} \in Z^d \mid 0 \leq m_{\alpha} \leq N_{\alpha} - 1 \right\}, \end{aligned} \quad (6.1)$$

hereafter Z^d denotes the set of d -tuples of integers, N_{α} ($\alpha = 1, \dots, d$) are odd, $\mathbf{N} := (N_1, \dots, N_d)^{\top}$, $|\mathbf{N}| = \Pi_{\alpha} N_{\alpha}$, and $\Delta h_{\alpha} = l_{\alpha}^{\Omega} / N_{\alpha}$ are the steps of grid in the direction α with

the unite vector \mathbf{e}_α . In this section, the notation $\Omega_{00} = \Pi_\alpha[0, l_\alpha^\Omega]$ is used which is popular in the DFT (and the corresponding indexation) instead of the notation $\Omega_{00} = \Pi_\alpha[-l_\alpha^\Omega, l_\alpha^\Omega]$ exploited in PM.

The discrete Fourier transform $\widehat{\mathbf{f}} = \mathcal{F}_d(\mathbf{f})$ (DFT) and the inverse DFT (iDFT) $\mathbf{f} = \mathcal{F}_d^{-1}(\widehat{\mathbf{f}})$ for the discrete periodic functions are defined as (see [41], [42], [241])

$$\widehat{\mathbf{f}}_{\mathbf{N}}(\mathbf{k}) = \sum_{\mathbf{n} \in Z_{\mathbf{N}}^d} \mathbf{f}_{\mathbf{N}}(\mathbf{n}) \omega_{\mathbf{N}}^{-\mathbf{k}\mathbf{n}}, \quad \mathbf{f}_{\mathbf{N}}(\mathbf{n}) = \frac{1}{|\mathbf{N}|} \sum_{\mathbf{k} \in Z_{\mathbf{N}}^d} \widehat{\mathbf{f}}_{\mathbf{N}}(\mathbf{k}) \omega_{\mathbf{N}}^{\mathbf{k}\mathbf{n}} \quad (6.2)$$

for \mathbf{N} -point vectors (called also sequences) $\mathbf{k}, \mathbf{n} \in Z_{\mathbf{N}}^d$; hereafter $\mathbf{f}(\mathbf{n})$ and $\widehat{\mathbf{f}}(\mathbf{k})$ are the sequences of \mathbf{N} possibly complex-valued numbers, and $\omega_{\mathbf{N}}^{\mathbf{k}\mathbf{n}} = \exp[2\pi i \sum_{\alpha} (k_{\alpha} n_{\alpha}) / N_{\alpha}]$, where $\alpha = 1, \dots, d$ and $i = \sqrt{-1}$.

The properties of the DFT that are most applied in subsequent presentations are

$$\mathcal{F}_d(\nabla \mathbf{f}) = i\mathbf{k}\widehat{\mathbf{f}}, \quad \mathcal{F}_d(\mathbf{f} \odot \mathbf{g})_{\mathbf{N}}(\mathbf{k}) = \widehat{\mathbf{f}}_{\mathbf{N}}(\mathbf{k}) \cdot \widehat{\mathbf{g}}_{\mathbf{N}}(\mathbf{k}), \quad (6.3)$$

where

$$(\mathbf{f} \odot \mathbf{g})(\mathbf{x}_{\mathbf{N}}^{\mathbf{n}}) := \sum_{\mathbf{j}} \mathbf{f}(\mathbf{x}_{\mathbf{N}}^{\mathbf{n}-\mathbf{j}}) \cdot \mathbf{g}(\mathbf{x}_{\mathbf{N}}^{\mathbf{j}}) \quad (6.4)$$

is a circular (also called periodic) convolution. To obtain a nonperiodic (or noncircular or aperiodic) convolution of two (one length \mathbf{L} and another length \mathbf{M}) sequences using DFT/iDFT approach, the two sequences $\mathbf{f}(\mathbf{x}_{\mathbf{L}}^{\mathbf{n}})$ and $\mathbf{g}(\mathbf{x}_{\mathbf{M}}^{\mathbf{n}})$ have to be extended by adding zeros at the ends such as their length are $\mathbf{N}_e \geq \mathbf{L} + \mathbf{M} - \mathbf{1}$ (This process is called zero padding). So, for L -point sequence in R^1 $\{g(n)\} = \{g_0, g_1, \dots, g_{L-1}\}$, the extended (zero-padded) sequence is $\{g_e(n)\} = \{g_0, g_1, \dots, g_{L-1}, 0, \dots, 0\}$,

$$\{g(n)\} = \{g_0, g_1, \dots, g_{L-1}\} \xrightarrow{\text{ZP}} \{g_e(n)\} = \{g_0, g_1, \dots, g_{L-1}, 0, \dots, 0\}, \quad (6.5)$$

where $\{g_e(n)\} = 0$ at $L \leq n \leq N_e - 1$. Without loss of generality, it is assumed in the current study that the length $\mathbf{N}_e = \mathbf{L} + \mathbf{M}$ is a power of 2 and $\mathbf{L} = \mathbf{M} = \mathbf{N}$. In such a case, e.g., Eqs. (6.2₁) and (6.5) can be recast in the form

$$\widehat{\mathbf{f}}_{\mathbf{eN}}(\mathbf{k}) = \sum_{\mathbf{n} \in Z_{\mathbf{N}_e}^d} \mathbf{f}_{\mathbf{eN}}(\mathbf{n}) \omega_{\mathbf{N}}^{-\mathbf{k}\mathbf{n}}, \quad (\mathbf{f}_e \odot \mathbf{g}_e)(\mathbf{x}_{\mathbf{N}_e}^{\mathbf{n}}) := \sum_{\mathbf{j}} \mathbf{f}_e(\mathbf{x}_{\mathbf{N}_e}^{\mathbf{n}-\mathbf{j}}) \cdot \mathbf{g}_e^{\mathbf{j}}(\mathbf{x}_{\mathbf{N}_e}^{\mathbf{j}}) \quad (6.6)$$

exploiting both the extended sequences $\mathbf{f}_e(\mathbf{n})$ and $\mathbf{g}_e(\mathbf{n})$, and the modified length \mathbf{N}_e depending on the lengths \mathbf{L} and \mathbf{M} of the initial sequences $\mathbf{f}(\mathbf{n})$ and $\mathbf{g}(\mathbf{n})$. In general, the DFT is a very expensive algorithm ($O(N^2)$) requiring N operations for each of the N Fourier components. However, this cost can be significantly reduced to the computational cost of $O(N \log_2 N)$ (where N is usually taken as a power of 2) as in the so-called *Fast Fourier Transformation* (FFT) algorithm [94] (see for references [226]).

6.2 Fast Fourier transform method in peridynamic micromechanics

Expansion of the FFT methods into the LM was initiated by Moulinec and Suquet [258], [259]. They performed the DFT (6.8) of the implicit Lippmann-Schwinger (L-S) equation (6.7) (compare with Eq. (3.4))

$$\boldsymbol{\varepsilon}(\mathbf{x}) = \boldsymbol{\varepsilon}^{w\Gamma} + \mathbf{U}^{(0)} *^L \boldsymbol{\tau}(\mathbf{x}), \quad (6.7)$$

$$\widehat{\boldsymbol{\varepsilon}}(\mathbf{k}) = \widehat{\mathbf{U}}^{(0)}(\mathbf{k})^L \widehat{\boldsymbol{\tau}}(\mathbf{k}) \quad (\mathbf{k} \neq \mathbf{0}), \widehat{\boldsymbol{\varepsilon}}^{w\Gamma}(\mathbf{0}) = \boldsymbol{\varepsilon}^{w\Gamma}, \quad (6.8)$$

where $*$ stands for the convolution operation. The origin FFT based *basic scheme* proposed [258], [259] was solved by the fixed-point iterative method (Picard's iterations).

It is interesting that Eq. (6.7) (with accuracy to notations) looks like linear state-based peridynamic Eq. (2.21) and (2.22). Hence, there is the temptation to use the same method to obtain the DFT of Eq. (2.22) (like, Eq. (6.8)). Unfortunately, there are a few obstacles to the realization of this temptation: O1) a displacement field $\mathbf{u}(\mathbf{x})$ (2.22) is not Ω_{00} -periodic; O2) the kernel $\mathbf{C}(\mathbf{x}, \mathbf{q})$ (2.22) is not a convolution for inhomogeneous media ($\mathbf{C}(\mathbf{x}, \mathbf{q}) \neq \mathbf{C}(\mathbf{x} - \mathbf{q})$), and O3) a convolution (even if it takes place) is not a circular convolution (6.4). We demonstrate how to overcome these obstacles.

Namely, in the so-called decomposition approach based on 'extraction' of a field corresponding to the homogeneous displacement loading, the displacement field is split

$$\mathbf{u}(\mathbf{x}) = \mathbf{u}_0(\mathbf{x}) + \mathbf{u}_1(\mathbf{x}), \quad \mathbf{u}_0(\mathbf{x}) := \boldsymbol{\varepsilon}^{w\Gamma} \mathbf{x}, \quad (6.9)$$

into its fluctuating Ω_{00} -periodic part $\mathbf{u}_1(\mathbf{x})$ with zero average and a linearly growing part $\mathbf{u}_0(\mathbf{x})$ corresponding for the macroscopic strain $\boldsymbol{\varepsilon}^{w\Gamma}(\mathbf{x})$. In additionally to the convolution kernel $\mathbf{C}^{(0)}$ two convolution kernels are introduced

$$\begin{aligned} \mathbf{C}_1^0(\mathbf{x} - \mathbf{q}) &= \mathbf{C}^{(1)}(\mathbf{x} - \mathbf{q}) - \mathbf{C}^{(0)}(\mathbf{x} - \mathbf{q}), \\ \mathbf{C}_{1\epsilon}^0(\mathbf{x} - \mathbf{q}) &= \mathbf{C}_1^0(\mathbf{x} - \mathbf{q}) \boldsymbol{\varepsilon}^{w\Gamma}(\mathbf{q} - \mathbf{x}) \end{aligned} \quad (6.10)$$

with the same horizon l_δ as the horizon of $\mathbf{C}^{(0)}(\mathbf{x} - \mathbf{q})$. It allows us to decompose the equilibrium equation as

$$\mathcal{L}^{(0)}(\mathbf{C}^{(0)}, \mathbf{u}_1)(\mathbf{x}) = \mathcal{L}_1(\mathbf{C}_1, \mathbf{u}_1)(\mathbf{x}) - \mathbf{b}^{w\Gamma}(\mathbf{x}), \quad \mathbf{b}^{w\Gamma}(\mathbf{x}) = \mathcal{L}_1(\mathbf{C}_1, \mathbf{u}_0)(\mathbf{x}), \quad (6.11)$$

which is equivalent to Eqs. (19.37) in [64]. Two terms in the right-hand side of Eq. (6.11₁) can be expressed as (see Eq. (2.31); $v_i^l = v_i + v_i^{\Gamma^-}$)

$$\mathcal{L}_1(\mathbf{C}_1, \mathbf{u}_1)(\mathbf{x}) = \mathcal{L}_1(\mathbf{C}_1^0, V_i \mathbf{u}_1)(\mathbf{x}) + \frac{1}{2} \mathcal{L}_1(\mathbf{C}_1^0, V_i^{\Gamma^-} \mathbf{u}_1)(\mathbf{x}), \quad (6.12)$$

$$\mathcal{L}_1(\mathbf{C}_1, \mathbf{u}_0)(\mathbf{x}) = \mathcal{L}_1(\mathbf{C}_{1\epsilon}^0, V_i)(\mathbf{x}) + \frac{1}{2} \mathcal{L}_1(\mathbf{C}_{1\epsilon}^0, V_i^{\Gamma^-})(\mathbf{x}). \quad (6.13)$$

Thus, instead of the kernel $\mathbf{C}(\mathbf{x}, \boldsymbol{\xi})$ for an inhomogeneous medium (which is neither convolution nor periodic in general), three convolution kernels are introduced: $\mathbf{C}^{(0)}(\boldsymbol{\xi})$, $\mathbf{C}_1^0(\boldsymbol{\xi})$ and $\mathbf{C}_{1\epsilon}^0(\boldsymbol{\xi})$ (i.e., the obstacle O2) is overcome) whereas other variables $\mathbf{u}_1(\mathbf{x})$, $V_i \mathbf{u}_1(\mathbf{x})$ and $V_i^{\Gamma^-} \mathbf{u}_1(\mathbf{x})$ are Ω_{00} -periodic (i.e., the obstacle O1) is overcome). Subsequent zero padding (6.3) (elimination of the obstacle O3)) of both the kernels and integrands ensures the applicability of the convolution theorem (6.3₂) that reduces the integral equation in the real space (6.11) to the multiplication operations in the Fourier space

$$\begin{aligned} \widehat{\mathbf{C}}^{(0)}(\mathbf{k})\widehat{\mathbf{u}}_1(\mathbf{k}) - \mathbf{P}^{(0)}\widehat{\mathbf{u}}_1(\mathbf{k}) &= -\widehat{\mathbf{C}}_1^0(\mathbf{k})\left[\mathcal{F}_d(V_i \mathbf{u}) + \frac{1}{2}\mathcal{F}_d(V_i^{\Gamma^-} \mathbf{u})\right] \\ + \left[\mathcal{F}_d(\mathbf{P}_1^V \mathbf{u}_1) + \frac{1}{2}\mathcal{F}_d(\mathbf{P}_1^{\Gamma^-} \mathbf{u}_1)\right] - \widehat{\mathbf{C}}_{1\epsilon}^0(\mathbf{k})\left[\mathcal{F}_d(V_i) + \frac{1}{2}\mathcal{F}_d(V_i^{\Gamma^-})\right], \end{aligned} \quad (6.14)$$

where

$$\mathbf{P}^{(0)} = \int \mathbf{C}^{(0)}(\mathbf{x}, \hat{\mathbf{x}}) d\hat{\mathbf{x}} = \mathcal{F}_d^{-1}\left(\widehat{\mathbf{C}}^{(0)}(\mathbf{k})\mathbf{1}(\mathbf{k})\right), \quad (6.15)$$

$$\mathbf{P}_1^V(\mathbf{x}) = \int \mathbf{C}_1^0(\mathbf{x}, \hat{\mathbf{x}})V_i(\hat{\mathbf{x}}) d\hat{\mathbf{x}} = \mathcal{F}_d^{-1}\left(\widehat{\mathbf{C}}_1^0(\mathbf{k})\widehat{V}_i(\mathbf{k})\right), \quad (6.16)$$

$$\mathbf{P}_1^{\Gamma^-}(\mathbf{x}) = \int \mathbf{C}_1^0(\mathbf{x}, \hat{\mathbf{x}})V_i^{\Gamma^-}(\hat{\mathbf{x}}) d\hat{\mathbf{x}} = \mathcal{F}_d^{-1}\left(\widehat{\mathbf{C}}_1^0(\mathbf{k})\widehat{V}_i^{\Gamma^-}(\mathbf{k})\right), \quad (6.17)$$

$$\widehat{\mathbf{P}}_1^V(\mathbf{k}) = \widehat{\mathbf{C}}_1^0(\mathbf{k})\widehat{V}_i(\mathbf{k}), \quad \widehat{\mathbf{P}}_1^{\Gamma^-}(\mathbf{k}) = \widehat{\mathbf{C}}_1^0(\mathbf{k})\widehat{V}_i^{\Gamma^-}(\mathbf{k}) \quad (6.18)$$

and the indices \mathbb{N} and $(\cdot)_e$ are omitted for brevity in Eqs. (6.14)-(6.18) as well as in the subsequent representations. It should be mentioned that the authors of [171], [172]) used neither zero padding nor the displacement fluctuation \mathbf{u}_1 (instead of the displacement \mathbf{u}), ensuring a periodicity of the primary unknown variable (avoiding of the obstacles O1).

Applying iDFT to rearranged Eq. (6.14) leads to the implicit analog of the L-S Eq. (6.7) (see for details [76], [77])

$$\mathbf{u}_1(\mathbf{x}) = \mathbf{g}_0^m(\mathbf{x}) + \boldsymbol{\mathcal{K}}^m(\mathbf{u}_1)(\mathbf{x}) \quad (6.19)$$

solved by the iteration method in accompanied with Eq. (6.14) (as in the pair of Eqs. (6.7) and (6.8)). The convergence (algorithm stopping) criteria based on either the compatibility condition or the imposed macroscopic condition were considered [257] for locally elastic problems.

Comment 6.1. The scheme of the FFT method in both the LM and PM is presented in Fig. 8. So, in preprocessing Blocks 1 and 2 (for the LM and PM, respectively) the DFT of the following functions is estimated. According to the properties of the DFT (6.3), in Block 1 (LM), we use either the analytical representations of either integral operator (6.7) (see $\widehat{\mathbf{U}}(\mathbf{k})$ in [261]) or the differential equilibrium operator (2.5). In Block 2 (PM), the following tensors are estimated one time (as in LM) in either the real space ($\mathbf{P}_1^V(\mathbf{x})$ and $\mathbf{P}_1^{\Gamma^-}(\mathbf{x})$) or frequency

domain ($\widehat{\mathbf{C}}^{(0)}(\mathbf{k})$, $\widehat{\mathbf{C}}_1^{(0)}(\mathbf{k})$, $\widehat{\mathbf{C}}_{1\epsilon}^{(0)}(\mathbf{k})$, and $\widehat{V}_i(\mathbf{k})$, $\widehat{V}_i^{\Gamma^-}(\mathbf{k})$) which are also evaluated by the FFT method. Blocks 3 and 4 are involved in the iteration scheme corresponding to either Eqs. (6.7), (6.8) (in the LM) or (6.14), (6.19) (in the PM).

Since Moulinec and Suquet [258] introduced the basic iteration FFT scheme for Eqs. (6.7), (6.8), a family of improved accelerated solvers has been developed to improve the convergence rate for highly-contrasted materials. These methods (*accelerated scheme* [125], [246] and the *augmented Lagrangian scheme* [245]) and others proposed later [255], [257] share the same approach, which is based on the introduction of a dual strain and/or dual stress-based formulation as well as the modification of the polarization term in the L-S equation. It would be interesting to generalize these approaches of the LM to their PM's counterparts.

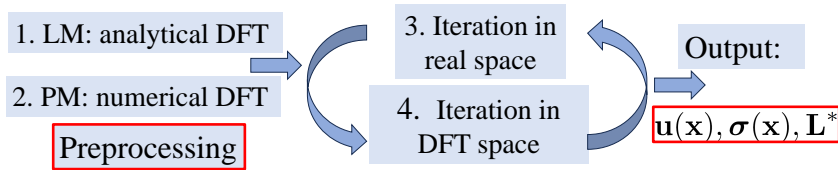


Fig. 8: The scheme FFT methods in the LM and PM

All mentioned FFT schemes (based on the application of DFT (6.3₂) to L-S Eq. (6.7)) have been presented for the strain field as the primary variable. An alternative *displacement-based* FFT approach (based on the application of DFT (6.3₁) to Eq. (2.5) (see [225], [226], [301])) involves solving directly for the displacement field \mathbf{u}_1 , which replaces the strain field as the primary variable. Then, rearrangement of the DFT form of Eq. (2.5) and subsequent application of the iDFT leads to the operator equation (which is not prescribed as a function of a matrix of coefficients) in a real space

$$\mathcal{A}(\mathbf{u}_1) = \mathbf{b}^A, \quad (6.20)$$

where the linear operator \mathcal{A} defines the action on a vector \mathbf{u}_1 . It is interesting that Eq. (6.19) in the PM is, in fact, presented in the form (6.20), where

$$\mathcal{A}(\mathbf{u}_1) = \mathbf{u}_1(\mathbf{x}) - \mathcal{K}^m(\mathbf{u}_1)(\mathbf{x}), \quad \mathbf{b}^A(\mathbf{x}) = \mathbf{g}_0^m(\mathbf{x})$$

and the displacement fluctuation \mathbf{u}_1 is a primary unknown variable in both the LM (2.5) and PM (6.11). Among the numerous methods available for the solution of linear systems (6.20), *Krylov method* (see the Krylov solver available in the PETSc library [31], see also [280]) such as the conjugate gradient (CG) method or the biconjugate gradient method can be efficiently used. According [17] (see also [43]) all we need is to provide the CG method by computing $\mathcal{A}(\mathbf{u}_1)$, where \mathcal{A} is the linear operator (rather than matrix). It was demonstrated [337] that the standard CG algorithm in local micromechanics works well, even though the

linear system is non-symmetric (see also [197]). In the case of the LM, it is also demonstrated in [337], [386] that contrary to the known accelerated FFT methods [125], [245] improving the original basic scheme, the cost of one iteration remains comparable to the basic scheme and the method proposed is insensitive to the choice of the auxiliary reference medium ${}^L\mathbf{L}^{(0)}$ (6.7).

Comment 6.2. The scheme presented in Fig. 7 can be applied to the different methods (e.g. CG method) describing the interactions of Blocks 3 and 4 (rather than only basic scheme [259]) for either LM or PM approaches. The specific feature of the PM is preconditioning Block 2 in Fig. 7 analysing one inclusion (like Block 1 Input in Fig. 2).

6.3 FFT of the nonlinear peridynamic equation

Equation (6.11) with the decomposition of the involved operators $\mathcal{L}_1^{(0)}(\mathbf{C}, \mathbf{u})(\mathbf{x})$ and $\mathcal{L}_1(\mathbf{C}, \mathbf{u}_0)(\mathbf{x})$ can be presented in the following form. So, the left-hand side of Eq. (6.11) is

$$\mathcal{L}^{(0)}(\mathbf{C}^{(0)}, \mathbf{u}_1)(\mathbf{x}) = \int \mathbf{C}^{(0)}(\mathbf{x} - \mathbf{x}')(\boldsymbol{\xi}_{w\Gamma} + \mathbf{u}'_1 - \mathbf{u}_1)^r dV_{\mathbf{x}'}, \quad (6.21)$$

where $\mathbf{u}_1 = \mathbf{u}_1(\mathbf{x})$, $\mathbf{u}'_1 = \mathbf{u}_1(\mathbf{x}')$,

$$\boldsymbol{\xi}_{w\Gamma} = \varepsilon^{w\Gamma} \boldsymbol{\xi} = \varepsilon^{w\Gamma}(\mathbf{x}' - \mathbf{x}). \quad (6.22)$$

By the use of the trinomial expansion

$$(\mathbf{p} + \mathbf{q} + \mathbf{s})^r = \sum_{a+b+c=r} \binom{r}{a,b,c} \mathbf{p}^a \mathbf{q}^b \mathbf{s}^c, \quad \binom{n}{a,b,c} := \frac{n!}{a! b! c!} \quad (6.23)$$

Eq. (6.21) is reduced to

$$\mathcal{L}^{(0)}(\mathbf{C}^{(0)}, \mathbf{u}_1)(\mathbf{x}) = \sum_{a+b+c=r} \binom{r}{a,b,c} (-\mathbf{u}_1)^c \int \mathbf{C}^{(0)}(\mathbf{x} - \mathbf{x}')(\boldsymbol{\xi}_{w\Gamma})^a (\mathbf{u}'_1)^b dV_{\mathbf{x}'}. \quad (6.24)$$

Similarly,

$$\mathcal{L}_1(\mathbf{C}_1^0, \mathbf{u}_1)(\mathbf{x}) = \sum_{a+b+c=r} \binom{r}{a,b,c} (-\mathbf{u}_1)^c \int \mathbf{C}_1^0(\mathbf{x} - \mathbf{x}')(\boldsymbol{\xi}_{w\Gamma})^a (\mathbf{u}'_1)^b V_i^{l\Gamma}(\mathbf{x}') dV_{\mathbf{x}'}. \quad (6.25)$$

Solution of PD Eq. (6.21) with polynomial nonlinearity of the integrand was analyzed in [222], [223], and [224] (see also [91]) by FFT method for the homogeneous matrix $\mathbf{C}_1^0 \equiv \mathbf{0}$. A similar decomposition (6.25) and (6.26) for composite material ($\mathbf{C}_1^0 \neq \mathbf{0}$) are used.

The new convolution kernels are introduced

$$\begin{aligned} \mathbf{C}^{(0)\xi^a}(\mathbf{x} - \mathbf{x}') &= \mathbf{C}^{(0)}(\mathbf{x} - \mathbf{x}')(\boldsymbol{\xi}_{w\Gamma})^a, \\ \mathbf{C}_1^{0\xi^a}(\mathbf{x} - \mathbf{x}') &= \mathbf{C}_1^0(\mathbf{x} - \mathbf{x}')(\boldsymbol{\xi}_{w\Gamma})^a, \end{aligned} \quad (6.26)$$

with initial values

$$\mathbf{C}^{(0)\xi 0}(\mathbf{x} - \mathbf{x}') = \mathbf{C}^{(0)}(\mathbf{x} - \mathbf{x}'), \quad \mathbf{C}_1^{0\xi 0}(\mathbf{x} - \mathbf{x}') = \mathbf{C}_1^0(\mathbf{x} - \mathbf{x}') \quad (6.27)$$

that simplifies Eqs. (6.24) and (6.25)

$$\begin{aligned} & \sum_{a+b+c=r} \binom{r}{a,b,c} (-\mathbf{u}_1)^c \int \mathbf{C}^{(0)\xi a}(\mathbf{x} - \mathbf{x}') (\mathbf{u}'_1)^b dV_{\mathbf{x}'} \\ &= - \sum_{a+b+c=r} \binom{r}{a,b,c} (-\mathbf{u}_1)^c \int \mathbf{C}_1^{0\xi a}(\mathbf{x} - \mathbf{x}') (\mathbf{u}'_1)^b V_i^{l\Gamma}(\mathbf{x}') dV_{\mathbf{x}'} \end{aligned} \quad (6.28)$$

Zero-padding of both the convolution kernels and prime variable in Eq. (6.28) transforms the convolution operations into circular convolutions:

$$\begin{aligned} & \sum_{a+b+c=r} \binom{r}{a,b,c} (-\mathbf{u}_1)^c \mathbf{C}^{(0)\xi a} \odot (\mathbf{u}'_1)^b(\mathbf{x}) \\ &= \sum_{a+b+c=r} \binom{r}{a,b,c} (-\mathbf{u}_1)^c \mathbf{C}_1^{0\xi a} \odot [(\mathbf{u}'_1)^b V_i^{l\Gamma}](\mathbf{x}), \end{aligned} \quad (6.29)$$

hereafter the indices \mathbf{N} and $(\cdot)_e$ (see the notations in Section 4) are omitted for brevity. Thanks to the Convolution Theorem (4.10), the circular convolution in (6.28) can be computed by means of the inverse Fourier transform \mathcal{F}_d^{-1} of the product of Fourier transforms:

$$\mathbf{C}^{(0)\xi a} \odot \mathbf{u}_1^b(\mathbf{x}) = \mathcal{F}_d^{-1} [\mathcal{F}_d(\mathbf{C}^{(0)\xi a})(\mathbf{k}) \mathcal{F}_d(\mathbf{u}_1^b)(\mathbf{k})], \quad (6.30)$$

$$\mathbf{C}_1^{0\xi a} \odot (V_i^{l\Gamma} \mathbf{u}_1^b)(\mathbf{x}) = \mathcal{F}_d^{-1} [\mathcal{F}_d(\mathbf{C}_1^{0\xi a})(\mathbf{k}) \mathcal{F}_d(V_i^{l\Gamma} \mathbf{u}_1^b)(\mathbf{k})]. \quad (6.31)$$

Additionally, according to the Inverse Theorem, it can be obtained

$$\begin{aligned} (\mathbf{u}_1)^c (\mathbf{C}^{(0)\xi a} \odot \mathbf{u}_1^b)(\mathbf{x}) &= \mathcal{F}_d^{-1} \left\{ \mathcal{F}_d(\mathbf{u}_1^c)(\mathbf{k}) \right. \\ &\quad \left. \odot [\mathcal{F}_d(\mathbf{C}^{(0)\xi a})(\mathbf{k}) \mathcal{F}_d((\mathbf{u}'_1)^b)(\mathbf{k})] \right\}, \end{aligned} \quad (6.32)$$

$$\begin{aligned} (\mathbf{u}_1)^c (\mathbf{C}_1^{0\xi a} \odot (V_i^{l\Gamma} \mathbf{u}_1^b)(\mathbf{x})) &= \mathcal{F}_d^{-1} \left\{ \mathcal{F}_d(\mathbf{u}_1^c)(\mathbf{k}) \right. \\ &\quad \left. \odot [\mathcal{F}_d(\mathbf{C}_1^{0\xi a})(\mathbf{k}) \mathcal{F}_d(V_i^{l\Gamma} \mathbf{u}_1^b)(\mathbf{k})] \right\}. \end{aligned} \quad (6.33)$$

In particular, by the DFT/iDFT methods, the terms of Eq. (6.28) corresponding to $b = 0$ can be estimated

$$\mathbf{P}^{(0)\xi a}(\mathbf{x}) := \int \mathbf{C}^{(0)\xi a}(\mathbf{x} - \mathbf{x}') d\mathbf{x}' = \mathcal{F}^{-1} \left(\widehat{\mathbf{C}}^{(0)\xi a}(\mathbf{k}) \widehat{\mathbf{1}}(\mathbf{k}) \right), \quad (6.34)$$

$$\mathbf{P}_1^{V\xi a}(\mathbf{x}) := \int \mathbf{C}_1^{0\xi a}(\mathbf{x} - \mathbf{x}') V_i^{l\Gamma}(\mathbf{x}') d\mathbf{x}' = \mathcal{F}^{-1} \left(\widehat{\mathbf{C}}_1^{0\xi a}(\mathbf{k}) \widehat{V}_i^{l\Gamma}(\mathbf{k}) \right), \quad (6.35)$$

which the generalization of the terms (6.15) and (6.16), respectively. Substitution of Eqs. (6.34)-(6.35) into Eq. (6.29) leads to the representation generalizing Eq. (6.19). However, a more detailed analysis of this approach is beyond the scope of the current study and deserve further investigations.

Comment 6.3. We considered in Section 7 only one type of nonlinear peridynamics, precisely nonlinear elasticity (6.21). In the LM over the past 30 years (after the seminal paper [258]), several high-performance FFT algorithms with improved convergence rates and solution accuracy have been developed to study the non-linear response (such as plasticity, viscoplasticity, damage, fracture, and fatigue, etc.) of microstructures with arbitrary phase contrast subjected to finite deformations (see the comprehensive reviews [90],[148] [149], [226], [301], [303]), which can be computed in desktop computers without the need to use high-performance computational clusters or supercomputers. They have also been exploited to study multi-physics systems involving the coupled mechanical, thermal, electrical, magnetic, and pyroelectric fields; for example, the chemo-thermo-mechanical study of batteries, including phase-field damage, which may rely on different fields coupled by their corresponding PDEs. All mentioned methods and problems are looking forward to their generalizing to the PM.

7 Reduced order models in peridynamic micromechanics

7.1 Clustering discretization method in local micromechanics

In local micromechanics, for the periodic structure CMs, the total fields (displacement, strain, or stress) caused in $v^{(s)}$ by the uniform loading fields either $\boldsymbol{\varepsilon}^{w\Gamma} = \langle \boldsymbol{\varepsilon} \rangle = \text{const.}$ or $\boldsymbol{\sigma}^{w\Gamma} = \langle \boldsymbol{\sigma} \rangle = \text{const.}$ (2.29) and (2.30) (at $l_\delta/a \rightarrow 0$) and the transformation fields (2.2) are represented in the following form ($\mathbf{x} \in v^{(s)}$)

$$\boldsymbol{\vartheta}(\mathbf{z}) = \mathbf{A}_{\theta\zeta}^{(s)}(\mathbf{z})\langle \boldsymbol{\zeta} \rangle + \sum_{r=0}^N \mathbf{D}_{\theta}^{sr}(\mathbf{z})\boldsymbol{\beta}^{(r)}, \quad (7.1)$$

which is a slight modification of [118]. For compactness of representations (7.1), one introduces the substitutions

$$(\mathbf{u}_1, \boldsymbol{\sigma}, \boldsymbol{\eta}) \leftrightarrow \boldsymbol{\vartheta}, \quad (\boldsymbol{\varepsilon}, \boldsymbol{\sigma}) \leftrightarrow \boldsymbol{\zeta}, \quad [\mathbf{x}, (\hat{\mathbf{x}}, \mathbf{x})] \leftrightarrow \mathbf{z}. \quad (7.2)$$

Here, the $\mathbf{A}_{\theta\zeta}(\mathbf{z})$ is the *mechanical influence function* (do not miss with the influence functions in peridynamics, see [308]) whereas the $\mathbf{D}_{\theta}^{sr}(\mathbf{z})$ is the *eigenfield influence functions*.

In the offline stage, the high-fidelity UC is represented by n voxels or elements denoted as ω_m ($m = 1, \dots, n$). K-means clustering gropes data vectors $\mathbf{A}_{\sigma\epsilon m}$ into a predefined number K of clusters $\Omega = \Omega^1 \cup \dots \cup \Omega^K$, based on Euclidean distance as a similarity measure; any points $\mathbf{x} \in \Omega^J$ ($J = 1, \dots, K$) have the same response $\boldsymbol{\sigma}(\mathbf{x})$ close to each other. Owing to a large number of data points, an unsupervised machine learning technique such as k -means

or Self-Organizing Map, SOM, (see [177], [218]) is adopted to perform the decomposition of UC. Combined with the stress concentration tensor, the mathematic definition of k -means clustering is based on optimization of a criterium function for the k sets $\mathbf{S} = (\Omega^1, \dots, \Omega^K)$

$$\mathbf{S} = \underset{\mathbf{S}}{\operatorname{argmin}} \operatorname{SSE}, \quad \operatorname{SSE} := \sum_{J=1}^K \sum_{m \in S^J} \|\mathbf{A}_{\sigma \varepsilon m} - \mathbf{A}_{\sigma \varepsilon}^J\|^2, \quad (7.3)$$

where $\mathbf{A}_{\sigma \varepsilon}^J$ is the average of strain concentration factor in the J th cluster Ω^J $\langle \sigma \rangle_J = \mathbf{A}_{\sigma \varepsilon}^I \varepsilon^{w\Gamma}$ whereas the norm $\|(\cdot)\|$ is defined as e.g., Frobenius norm for matrix.

Averaging of Eq. (7.1) over the domain Ω^J yields

$$\sigma_I = \mathbf{A}_{\sigma \varepsilon}^I \varepsilon^{w\Gamma} + \sum_{J=1}^K \mathbf{D}_{\sigma}^{IJ} \beta^J, \quad (7.4)$$

where the physical meaning of \mathbf{D}_{σ}^{JJ} is the local stress field σ^J in the domain $\mathbf{x} \in \Omega^J$ at $\langle \varepsilon \rangle = \varepsilon^{w\Gamma} \equiv \mathbf{0}$ and the uniform eigenstrain of unit magnitude prescribed in every single domain Ω^J , while all other domains are free of any transformation.

In nonlinear micromechanics, the strains are assumed to be small, but both elastic and inelastic behavior is that at each instant of loading the additive decomposition takes place

$$\sigma_I(\mathbf{x}) = \sigma_I^{\operatorname{lin}}(\mathbf{x}) + \sigma_I^{\operatorname{re}}(\mathbf{x}), \quad \text{or} \quad \varepsilon_I(\mathbf{x}) = \varepsilon_I^{\operatorname{lin}}(\mathbf{x}) + \varepsilon_I^{\operatorname{in}}(\mathbf{x}). \quad (7.5)$$

Here $\sigma_I^{\operatorname{lin}}(\mathbf{x})$ and $\varepsilon_I^{\operatorname{lin}}(\mathbf{x})$ are the linear elastic fields corresponding to the constitutive relations (2.2) and the inelastic fields (analog of the eigenstress $\alpha(\mathbf{x})$ and eigenstrain $\beta(\mathbf{x})$) are linked as

$$\varepsilon_I^{\operatorname{in}}(\mathbf{x}) = -\mathbf{M}^I \sigma_I^{\operatorname{re}}(\mathbf{x}), \quad \sigma_I^{\operatorname{re}}(\mathbf{x}) = -\mathbf{L}^I \varepsilon_I^{\operatorname{in}}(\mathbf{x}). \quad (7.6)$$

It is assumed that clustering is performed and presented for piecewise constant fields ε_I, σ_I and $\varepsilon_I^{\operatorname{in}}$, where $\varepsilon_I^{\operatorname{in}}$ is substituted instead of eigenstrain β^J . Many inelastic constitutive laws relate either $\sigma_J^{\operatorname{re}}$ to ε_J or $\varepsilon_J^{\operatorname{in}}$ to σ_J : $\sigma_J^{\operatorname{re}}(\mathbf{x}) = \mathbf{g}(\varepsilon_J)$, $\varepsilon_J^{\operatorname{in}} = \mathbf{f}(\sigma_J)$. It provides the following systems of governing equations for the evaluation of local fields ($I = 1, \dots, K$)

$$\varepsilon_I = \mathbf{A}_{\varepsilon \varepsilon}^I \varepsilon^{w\Gamma} - \sum_{J=1}^K \mathbf{D}_{\varepsilon}^{IJ} \mathbf{M}^J \mathbf{g}(\varepsilon_J), \quad \sigma_I = \mathbf{A}_{\sigma \varepsilon}^I \varepsilon^{w\Gamma} - \sum_{J=1}^K \mathbf{D}_{\sigma}^{IJ} \mathbf{f}(\sigma_J). \quad (7.7)$$

Numerical solution of Eqs. (7.7) (and their incremental analogs) are usually found by Newton's iteration method (see, e.g., [218]). In so doing, analysis of deformation of each cluster Ω^J ($J = 1, \dots, M$) (possibly multiply connected) is reduced to the analysis of the deformation of *one point*. Speed up of online nonlinear stage for this approach, and their advanced modifications (see, e.g., [218]) over FEA can reach 10^4 .

The expressions of the effective properties and their consistent conditions found in this Subsection are general, *exact*, and obtained for any number and any kind (i.e. the domains Ω^J need not be spatially connected) and shape of domains Ω^J ($J = 1, \dots, K$) with no restriction on the strain-stress field inhomogeneity in Ω^J (e.g. even the field singularity is also possible in Ω^J). A single restriction on mechanical properties is a homogeneity of $\beta(\mathbf{x})$ inside each domain $\mathbf{x} \in \Omega^J$ ($J = 1, \dots, K$).

7.2 Clustering discretization method in peridynamic micromechanics

We perform step-by-step LM representations (4.4)-(4.17) recast to the corresponding counterparts of PM. So, the total relative displacement and stress are presented in the form of additive decomposition ($\mathbf{x} \in \Omega^J$)

$$\boldsymbol{\eta}_J(\boldsymbol{\xi}) = \boldsymbol{\eta}_J^{\text{lin}}(\boldsymbol{\xi}) + \boldsymbol{\eta}_J^{\text{non}}(\boldsymbol{\xi}), \quad \boldsymbol{\sigma}_J(\mathbf{x}) = \boldsymbol{\sigma}_J^{\text{lin}}(\mathbf{x}) + \boldsymbol{\sigma}_J^{\text{non}}(\mathbf{x}). \quad (7.8)$$

Hereafter, $\boldsymbol{\eta}_J^{\text{lin}}(\mathbf{x})$ and $\boldsymbol{\sigma}_J^{\text{lin}}(\mathbf{x})$ are the linear elastic fields related by the constitutive equations (2.21) and (2.27) whereas the inelastic parts $\boldsymbol{\eta}_J^{\text{non}}(\mathbf{x})$ and $\boldsymbol{\sigma}_J^{\text{non}}(\mathbf{x})$ are produced by applied phase stress and strain, respectively (analogous to Eqs. (7.5)). It is assumed homogeneity of the stress $\boldsymbol{\sigma}_J(\mathbf{x})$ as well as the linearity of the relative displacements

$$\boldsymbol{\eta}_J(\boldsymbol{\xi}) = \boldsymbol{\varepsilon}_\eta \cdot \boldsymbol{\xi}, \quad \boldsymbol{\eta}_J^{\text{lin}}(\boldsymbol{\xi}) = \boldsymbol{\varepsilon}_\eta^{\text{lin}} \cdot \boldsymbol{\xi}, \quad \boldsymbol{\eta}_J^{\text{non}}(\boldsymbol{\xi}) = \boldsymbol{\varepsilon}_\eta^{\text{non}} \cdot \boldsymbol{\xi} \quad (7.9)$$

inside the cluster $\mathcal{H}_\mathbf{x} \subset \Omega^J$. For convenience, the linear operator \mathbb{L} returning the coefficients of the linear approximations (7.9) is introduced

$$\mathbb{L}(\boldsymbol{\eta}_J(\boldsymbol{\xi})) = \boldsymbol{\varepsilon}_J, \quad \mathbb{L}(\boldsymbol{\eta}_J^{\text{lin}}(\boldsymbol{\xi})) = \boldsymbol{\varepsilon}_J^{\text{lin}}, \quad \mathbb{L}(\boldsymbol{\eta}_J^{\text{non}}(\boldsymbol{\xi})) = \boldsymbol{\varepsilon}_J^{\text{non}}. \quad (7.10)$$

Equations (2.23) at $\beta^J \equiv \mathbf{0}$ ($J = 1, \dots, K$) is used for estimation of the piecewise linear functions $\boldsymbol{\eta}_J^{\text{lin}}(\mathbf{x})$ of $\mathbf{x} \in \Omega^J$, which is exploited for the evaluation of the piecewise constant functions $\boldsymbol{\sigma}_J^{\text{lin}}(\mathbf{x}) \equiv \text{const.}$ ($\mathbf{x} \in \Omega^J$, $J = 1, \dots, L$) by Eqs. (2.27). The linear parts $\boldsymbol{\eta}_J^{\text{lin}}(\mathbf{x})$, $\boldsymbol{\sigma}_J^{\text{lin}}(\mathbf{x})$ of the fields (7.8) and nonlinear ones $\boldsymbol{\eta}_J^{\text{non}}(\mathbf{x})$, $\boldsymbol{\sigma}_J^{\text{non}}(\mathbf{x})$ are related by the linear constitutive relations

$$\boldsymbol{\sigma}_J^{\text{lin}}(\mathbf{x}) = \mathcal{L}_{\text{lin}}^{\sigma(J)}(\boldsymbol{\eta}_J^{\text{lin}}), \quad \boldsymbol{\eta}_J^{\text{lin}}(\boldsymbol{\xi}) = \mathcal{M}_{\text{lin}}^{\eta(J)}(\boldsymbol{\sigma}_J^{\text{lin}})(\boldsymbol{\xi}), \quad (7.11)$$

$$\boldsymbol{\sigma}_J^{\text{non}}(\mathbf{x}) = -\mathcal{L}_{\text{lin}}^{\sigma(J)}(\boldsymbol{\eta}_J^{\text{non}}), \quad \boldsymbol{\eta}_J^{\text{non}}(\mathbf{x}) = -\mathcal{M}_{\text{lin}}^{\eta(J)}(\boldsymbol{\sigma}_J^{\text{non}})(\mathbf{x}), \quad (7.12)$$

where the linear operator $\mathcal{M}_{\text{lin}}^{\eta(J)} := [\mathcal{L}_{\text{lin}}^{\sigma(J)}]^{-1}$ (defining the linear functions of \mathbf{x} in (7.11₁)) can be found as a solution of Eq. (7.11₁). The operators $\mathcal{L}_{\text{lin}}^{\sigma(J)}$ and $\mathcal{M}_{\text{lin}}^{\eta(J)}$ are defined on the extended cluster $\Omega^{Jl} := \Omega^J \oplus \mathcal{H}_0$ whereas $\boldsymbol{\eta}_J(\boldsymbol{\xi})$ and $\boldsymbol{\sigma}_J(\mathbf{x})$ ($\mathbf{x} \in \Omega^{Jl} \setminus \Omega^J$) is prolonged as a linear function and a constant of $\boldsymbol{\eta}_J(\boldsymbol{\xi})$ and $\boldsymbol{\sigma}_J(\mathbf{y})$, respectively, defined on $\mathbf{y} \in \Omega^J$. For the prescribed structures of the linear $\boldsymbol{\eta}_J(\boldsymbol{\xi})$ and constant $\boldsymbol{\sigma}_J(\mathbf{y})$ fields, the action of the

operators $\mathcal{L}_{\text{lin}}^{\sigma(J)}$ and $\mathcal{M}_{\text{lin}}^{\eta(J)}$, respectively, are reduced to the tensor multiplication (analogous to the tensors ${}^L\mathbf{L}^I$ and ${}^L\mathbf{M}^I$ (2.2)), which can be found only one time at the offline stage.

Nonlinear parts of phase relative displacement $\boldsymbol{\eta}_J^{\text{non}}$ can be expressed through the inverse stress operator $\mathcal{M}^{\eta(J)} := (\mathcal{L}^{\sigma(J)})^{-1}$ (2.18), (2.17) and the linearized inverse stress operator $\mathcal{M}_{\text{lin}}^{\eta(J)}$ (2.18), (2.21)

$$\boldsymbol{\eta}_J^{\text{non}} = \mathcal{M}^{\eta(J)}(\boldsymbol{\sigma}_J)(\boldsymbol{\xi}) - \mathcal{M}_{\text{lin}}^{(J)}(\boldsymbol{\sigma}_J)(\boldsymbol{\xi}). \quad (7.13)$$

presenting peridynamic counterpart of $\boldsymbol{\varepsilon}_J^{\text{in}} = \mathbf{f}(\boldsymbol{\sigma}_J)$ (7.7). The action of the operator \mathbb{L} on both sides of Eq. (7.13) leads to the peridynamic analog of Eq. (7.7)

$$\boldsymbol{\varepsilon}_J^{\text{non}} = \mathbb{L}[\mathcal{M}^{\eta(J)}(\boldsymbol{\sigma}_J)(\boldsymbol{\xi})] - \mathbb{L}[\mathcal{M}_{\text{lin}}^{(J)}(\boldsymbol{\sigma}_J)(\boldsymbol{\xi})]. \quad (7.14)$$

Substitution of Eq. (7.14) into Eq. (7.4) provides the following ROM system of governing equations for evaluation of the local stresses ($I = 1, \dots, K$)

$$\boldsymbol{\sigma}_I = \mathbf{A}_{\sigma\varepsilon}^I \boldsymbol{\varepsilon}^{w\Gamma} + \sum_{J=1}^K \mathbf{D}_{\sigma}^{IJ}(\mathbf{x}) \boldsymbol{\eta}_J^{\text{non}}, \quad (7.15)$$

which is similar to Eq. (7.7₂) for the local micromechanics. For the PM, the estimations of $\mathbf{A}_{\sigma\varepsilon}^I$ and $\mathbf{D}_{\sigma}^{IJ}(\mathbf{x})$ are presented in [75]. The nonlinear equations (7.15) are recast in residual form in each cluster Ω^I ($I = 1, \dots, K$), which can be solved by the Newton-Raphson method with a return-mapping technique [323] (see for details [75]). Averaging of the found $\boldsymbol{\sigma}_I$ ($I = 1, \dots, K$) as the functions of $\boldsymbol{\varepsilon}^{w\Gamma}$ leads to the definition of the overall stiffness (locally elastic) \mathbf{L}^* : $\langle \boldsymbol{\sigma} \rangle = \mathbf{L}^* \boldsymbol{\varepsilon}^{w\Gamma}$, which differs from the linear approximation $\mathbf{L}^* = \sum_{r=0}^N c^{(r)} \mathbf{A}_{\sigma\varepsilon}^r$.

The nonlinear deformation problem for a multiphase CM is reduced to the evaluation of the mechanical and transformation factor tensors (7.4) and (7.15) only one time for the linear offline stage problem (see for details [64]), and integration of the ROM system (7.14) for any nonlinear loading in an online stage. The nonlinear problem at each i -the iteration is reduced to the estimation of actions of the operators $\mathcal{M}^{\eta(J)}$, $\mathcal{M}_{\text{lin}}^{\eta(J)}$ and $\mathcal{L}_{\text{lin}}^{\sigma(J)}$ on the constant and linear functions, respectively, in each cluster $\Omega^{(J)}$. In so doing, the actions of the linear operators $\mathcal{L}_{\text{lin}}^{\sigma(J)}$ and $\mathcal{M}_{\text{lin}}^{\eta(J)}$ can be estimated only one time at the offline stage. Only one micro nonlinear problem for the operator $\mathcal{M}^{\eta(I)}$ (for each $I = 1, \dots, K$) is solved in the point $\mathbf{x} \in \Omega^I$ (2.6) which is a center of the horizon's $\mathcal{H}_{\mathbf{x}}$. I.e. the cluster Ω^I is reduced to *one family* instead of *one point* in the LM. The cluster $\mathbf{x} \in \Omega^I \subset \mathbb{R}^d$ is replaced by a full space \mathbb{R}^d with prescribed linear function $\boldsymbol{\eta}(\mathbf{x})$, and its response is assigned to all points of the cluster Ω^I . Since the number of clusters K is much smaller than the number of elements n ($K \ll n$) of fine-scale, computational efficiency is greatly improved.

7.3 Data-driven modeling and machine learning based on CDM

The presented ROM contains a few stages. The offline stage of material modeling consists of three steps: a) data collection, b) unsupervised learning (i.e., clustering), and c) preprocessing (e.g., estimation of cluster interactions). Since the numbers of clusters are much smaller than the number of fine data points, computational efficiency is greatly increased, and, in such a way that CDM fulfills the role of data compression. The central ingredient of the nonlinear online stage, a material subroutine (7.13) is reduced to only K uncoupled integrals (inversed to (2.17) and (2.18)) on constant functions $\sigma(\mathbf{x})$ over $\mathcal{H}_{\mathbf{x}}$. The computational complexity of estimations of these integrals is comparable with the computational complexity of evaluations of K nonlinear equations of locally elastic counterparts (7.7).

The next step of multi-stage design is usually addressed to the methods of machine learning (ML) and neural networks (see for reference and details [153],[203], [300]) for providing real-time prediction of materials' properties and multi-stage design de novo materials. Neural network techniques are based, loosely speaking, on a generalization of linear regression analysis. So, in the simplest feedforward neural networks (FFNNs, see, e.g., [45]; see also construction of peridynamic surrogate model characterizing failure of materials within the data-driven neural network [339]) each layer consisting of a few neurons computes the output to the next layer l based on the input from the previous $(l - 1)$ th layer. The neurons in the same layer are not connected whereas every pair of neurons in neighboring layers are assigned by network parameters such as a weight \mathbf{w}^l and a bias \mathbf{b}^l so that each layer creates data for the next layer through the following nested transformations:

$$\mathbf{z}^l = \mathcal{A}^l(\mathbf{w}^l \cdot \mathbf{z}^{l-1} + \mathbf{b}^l), \quad l = 1, \dots, L, \quad (7.16)$$

where \mathbf{z}^0 and \mathbf{z}^L are the input and output of the model. The functions \mathcal{A}^l are called activation functions and make the network nonlinear to the inputs. The weights of parameters used for calculation for each neuron are optimized to minimize the loss function. Linear regression supports also other ML approaches such as convolutional neural networks (CNNs) [152] and recurrent neural networks (RNNs) which are generally used for supervised learning.

Running ROMs (such as, e.g., CDM) for RVEs can still be time-consuming in design optimization. To avoid this difficulty, one usually replaces the ROMs with neural networks (such as, e.g., FFNNs, CNNs, etc., see for references [87]) trained on the RVE responses computed with SCA for micro and macro fields. The training procedure is formulated as an optimization problem with the definition of the loss function as Mean Square Error (MSE) among the estimated fields in both the ML approach (7.16) and CDM. These schemes were realized by WK Liu and others for a wide class of nonlinear problems (nonlinear elasticity, [203], [368]; elasto-plastic [167], elasto-viscoplasticity, [380]; damage analysis, [157]) of local micromechanics.

Comment 7.1. The differences and similarities between using CDM in the LM and PM are described by the example of Fig. 9. So, the goal of the linear Offline stage (Block 1) is

estimations of the concentration factors (4.13) for the LM and PM (although the clusters and cluster interactions in the LM and PM are different simply because DNS in the LM and PM are different). The linear solution of the Offline stage (Block 1) is used for the subsequent solution of a nonlinear system of algebraic equations (nonlinear Online stage, Block 2) corresponding to K pairs of points $(\boldsymbol{\varepsilon}_I, \boldsymbol{\sigma}_I)$ ($I = 1, \dots, K$) in the LM, whereas a nonlinear PM counterparts $(\mathcal{L}^{\sigma^{(J)}}, \mathcal{M}^{\eta^{(J)}})$ are defined at K families. Block 3 (Machine learning, see Eq. (7.16)) is identical for both the LM and PM (this is a reason why PM's application in Block 3 is not discussed in more detail).

Comment 7.2. We considered in Section 8 only one type of nonlinear peridynamics, precisely nonlinear elasticity. However, the discovered formal similarity of DSA and CDM opens wide opportunities for a straightforward generalization of well-developed LM theory of data-driven ML approaches [64], [156], [157], [183], [203], [220], [368], [380] (interested readers are referred to these references to achieve a deeper understanding of these topics) to their peridynamic counterparts including different physical phenomena (e.g., state-based models, diffusion, viscosity, thermoelastoplasticity, damage accumulation, debonding, plastic localization, wave propagation) for CMs with different periodic structures (e.g., polycrystals, fiber networks, hybrid structures, foam materials). Consideration of these problems in more detail is beyond the scope of the current presentation.

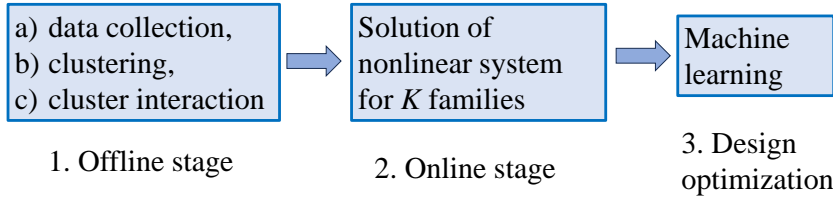


Fig. 9: The scheme of application of CDM in PM

7.4 Proper Orthogonal Decomposition in PM

The Most suitable POD application in PD for reformulation in the framework of the current review is presented in [113] (see also [25]) which is shortly reproduced below. So, to solve the difficulty caused by the nonlocal boundary conditions in the process of ROM construction, a boundary layer separation approach is presented, and the global equilibrium equations are symbolically reorganized in a block form (compare with Eq. (3.16))

$$\begin{bmatrix} \mathbb{K}_{bb} & \mathbb{K}_{bi} \\ \mathbb{K}_{ib} & \mathbb{K}_{ii} \end{bmatrix} \begin{bmatrix} \mathbb{U}_b \\ \mathbb{U}_i \end{bmatrix} = \begin{bmatrix} \mathbb{B}_b \\ \mathbb{B}_i \end{bmatrix}, \quad (7.17)$$

where \mathbb{U}_b and \mathbb{U}_i are the displacement vectors of the boundary layer points w_Γ and internal points w , respectively. Similarly the PD stiffness matrix $\mathbb{K}_{\alpha\beta}$ ($\alpha\beta = b, i$) and the loading vectors \mathbb{B}_b , \mathbb{B}_i are defined. DNS displacement solutions under various loading conditions \mathbb{U}_{ij} ($j = 1, \dots, m$) are collected to a training database called snapshot $\mathbf{S} = \{\mathbb{U}_{ij}\}_{j=1}^m$, $\mathbf{S} \in$

$\mathbb{R}^{N_i \times m}$, $\mathbb{U}_{ij} \in \mathbb{R}^{N_i \times 1}$, where N_i is the total number of DoFs of internal points. The covariance matrix \mathbf{P} is defined as $\mathbf{P} = \mathbf{S}^\top \mathbf{S}$ ($\mathbf{P} \in \mathbb{R}^{m \times m}$). A set of basis vectors ϕ_j is generated by solving an eigenvalue problem $\mathbf{P}\phi_j = \lambda_j\phi_j$ ($\phi_j \in \mathbb{R}^{m \times 1}$, $j = 1, \dots, k$, $\lambda_1 \geq \dots \geq \lambda_k > 0$) where ϕ_j is the eigenvector of \mathbf{P} , λ_j is the eigenvalue of \mathbf{P} , k is the number of nonzero eigenvalues. The POD orthogonal basis functions are expressed as $\Phi_j = \sqrt{\lambda_j}^{-1} \mathbf{S}\phi_j$, where $\Phi_j \Phi_l = \delta_{jl}$. To simplify the system, only $n_i \gg N_i$ basis vectors Φ_j ($j = 1, \dots, n_i$) containing the majority of the information of the snapshot are selected. Finally, the displacement field can be reconstructed by using the Galerkin projection method:

$$\mathbb{U}_i = \overline{\Phi} \mathbf{a}_i, \quad (7.18)$$

where $\overline{\Phi} = [\Phi_1, \dots, \Phi_{n_i}] \in \mathbb{R}^{N_i \times n_i}$ and $\mathbf{a}_i = [\mathbf{a}_{ij}, \dots, \mathbf{a}_{ij}]^\top \in \mathbb{R}^{n_i \times 1}$ are the POD basis and the corresponding coefficient vector, respectively, of the reduced DoFs of internal points, n_i . Substitution of Eq. (7.18) into Eq. (7.17) leads to the reduced PD equations

$$\begin{bmatrix} \mathbb{K}_{bb} & \mathbb{K}_{bi} \overline{\Phi} \\ \overline{\Phi}^\top \mathbb{K}_{ib} & \overline{\Phi}^\top \mathbb{K}_{ii} \overline{\Phi} \end{bmatrix} \begin{bmatrix} \mathbb{U}_b \\ \mathbf{a}_i \end{bmatrix} = \begin{bmatrix} \mathbb{B}_b \\ \overline{\Phi}^\top \mathbb{B}_i \end{bmatrix}. \quad (7.19)$$

\mathbb{U}_b and \mathbf{a}_i can be found from Eq. (7.19), and the displacement field of the internal computational domain \mathbb{U}_i can be reproduced by using Eq. (7.18). In this way, the boundary conditions are accurately reproduced, and the number of DoFs of the PD model dramatically decreases from $N = N_i + N_b$ to $N_b + n_i$.

We now turn our attention to the schematic representation of possible reformulation of the known POD method (7.17)-(7.19). So, the VBC (2.29) and (2.30) are intrinsically incorporated into the first line of Eq. (7.17). For the periodic structure CM, we need to replace the VBC (2.29) and (2.30) with the VPBC (2.32) and VBC (2.33). For the periodic counterpart of Eq. (7.17), it leads to both elimination of the first line in Eq. (7.17) (i.e. elimination of \mathbb{K}_{bb} , \mathbb{K}_{bi} , and \mathbb{K}_{ib}) and correction of the rigidity matrix \mathbb{K}_{ii} (see for details Chapter 19 in [64]) which also depends on the the properties of both the matrix and inclusions in the unit cell w with the numbers $N = N_i$ of DoFs; corrections of Eqs. (7.18) and (7.19) are straightforward.

For statistically homogeneous random structure CMs, estimation of the effective moduli \mathbf{L}^* (4.29) is reduced to a solution of basic problem (3.29) for one inclusion v_i inside the infinite homogeneous matrix subjected to some homogeneous effective field. The truncation method is used for the modeling of the infinite medium by an increased-size sample $\overline{w} = w \cup w_\Gamma$. The scheme (7.17)-(7.19) is not altered whereas Eq. (7.18) is used for estimation of the perturbator $\mathbf{L}_j^{ue}(\mathbf{s} - \mathbf{x}_i)$ ($\mathbf{s} \in v_i^l$) and the concentration factors $\mathbf{R}_i^{l\omega}$ and $\mathbf{A}_i^{l\omega}$ which, in turn, are exploited for estimation of effective moduli \mathbf{L}^* by either the EFM (4.37), (4.38) or the MTA (4.40), (4.41).

Comment 7.3. It is interesting that for random structure CMs subjected to body force with compact support (see Subsection 4.2), Eqs. (7.17)-(7.19) of POD method are simplified. So,

we need to eliminate the first line in Eq. (7.17) (i.e. to eliminate \mathbb{K}_{bb} , \mathbb{K}_{bi} , and \mathbb{K}_{ib}) whereas the rigidity matrix \mathbb{K}_{ii} is not altered and the body force \mathbb{U}_i has compact support. In so doing, Block 3 (Machine learning, see Eq. (7.16) and Fig. 8) are identical for both the LM and PM of both the random and periodic structure peridynamic CM analyzed by POD methods.

8 Peridynamic micromechanics of laminated structure composites

In the subsequent presentation, the inclusions are considered as identical aligned layers $v_i = \{\mathbf{x} = (x^1, x^2, x^3)^\top \mid |x^1| \leq h\}$ with the thickness $2h$ and a statistically homogeneous distribution in the space. For applying the Mori–Tanaka [256] approach, the presence of reference material is required; the layer $v^{(0)}$ is chosen to represent the “matrix” phase. For linear state-based model, Eq. (3.22) is presented in the form

$$\int_{\mathcal{H}_x} \mathbf{C}(\mathbf{x}, \mathbf{q}) [\mathbf{u}(\mathbf{q}) - \mathbf{u}(\mathbf{x}) - \bar{\boldsymbol{\varepsilon}}(\mathbf{q} - \mathbf{x})] d\mathbf{q} = - \int_{\mathcal{H}_x} \mathbf{C}_1(\mathbf{x}, \mathbf{q}) \bar{\boldsymbol{\varepsilon}}(\mathbf{q} - \mathbf{x}) d\mathbf{q}. \quad (8.1)$$

Owing to the form of structure, the displacement field can be obtained one from another by parallel transformation

$$\mathbf{u}(\mathbf{x}) = \mathbf{u}(\mathbf{x}_0) + \bar{\boldsymbol{\varepsilon}}^t(\mathbf{x} - \mathbf{x}_0), \quad \bar{\boldsymbol{\varepsilon}} = \bar{\boldsymbol{\varepsilon}}^n + \bar{\boldsymbol{\varepsilon}}^t, \quad (8.2)$$

where $\mathbf{x} = (x^1, x^2, x^3)^\top$, $\mathbf{x}_0 = (x_0^1, 0, 0)^\top$, and $\bar{\boldsymbol{\varepsilon}}_{ij}$ is an arbitrary symmetric tensor decomposed on the normal $\bar{\boldsymbol{\varepsilon}}^n = \bar{\boldsymbol{\varepsilon}}^n_{ij} = \bar{\boldsymbol{\varepsilon}}_{ij}(\delta_{i1} + \delta_{j1} - \delta_{1i}\delta_{1j})$ and transversal $\bar{\boldsymbol{\varepsilon}}^t = \bar{\boldsymbol{\varepsilon}}^t_{ij} = \bar{\boldsymbol{\varepsilon}}_{ij}(1 - \delta_{i1})(1 - \delta_{j1})$ constituents. A cross-section of the horizon region \mathcal{H}_x ($\mathbf{x} = (x^1, 0, 0)^\top$) is introduced by the plane $q^1 = \text{const.}$ ($x^1 - l_\delta \leq q^1 \leq x^1 + l_\delta$) $\mathcal{S}_{x^1}^{q^1} = \mathcal{H}_x \cap \{\mathbf{q} \mid \mathbf{q} = (q^1, 0, 0)^\top, x^1 - l_\delta \leq q^1 \leq x^1 + l_\delta\}$. Then Eq. (8.1) is reduced to the following equation

$$\int_{\mathcal{H}_{x^1}} \mathbf{C}^1(x^1, q^1) [\mathbf{u}(q^1) - \mathbf{u}(x^1) - \bar{\boldsymbol{\varepsilon}}^n(q^1 - x^1)] dq^1 = \hat{\mathbf{b}}(x^1) \bar{\boldsymbol{\varepsilon}}, \quad (8.3)$$

where

$$\mathbf{C}^1(x^1, q^1) = \int_{\mathcal{S}_{x^1}^{q^1}} \mathbf{C}(\mathbf{x}, \mathbf{q}) dq^2 dq^3, \quad \hat{\mathbf{b}}(x^1) = - \int_{\mathcal{H}_x} \mathbf{C}_1(\mathbf{x}, \mathbf{q}) \otimes (\mathbf{q} - \mathbf{x}) d\mathbf{q} \quad (8.4)$$

and the right-hand side of Eq. (8.3) has a compact support $|x^1| \leq h + l_\delta$. In Fig. 10, a scheme of obtaining the transformed micromodulus $\mathbf{C}^1(x^1, q^1)$ (8.4₁) is presented by the use of the cross-section $\mathcal{S}_{x^1}^{q^1}$ of the 3D horizon region \mathcal{H}_x by the plane $\{\mathbf{q} \mid \mathbf{q} = (q^1, 0, 0)^\top, x^1 - l_\delta \leq q^1 \leq x^1 + l_\delta\}$. It is interesting that for the constant micromodulus $\mathbf{C}(\mathbf{x}, \mathbf{q}) \equiv \text{const.}$ ($\mathbf{q} \in \mathcal{H}_x$) (horizon region $\mathcal{H}_x \subset R^3$ is colored by one color), the transformed micromodulus $\mathbf{C}^1(x^1, q^1)$ (8.4₁) is an

inhomogeneous function of $q^1 \in \mathcal{H}_{x^1}$ (because of this, the 1D horizon region $\mathcal{H}_x \subset R^1$ in Fig. 10 is colored by the same color of varying intensity).

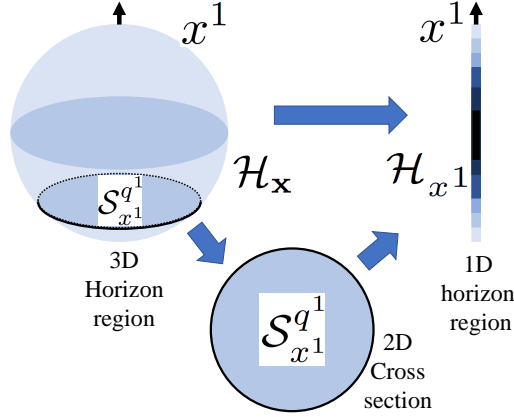


Fig. 10: Schematic transformation of 3D horizon region \mathcal{H}_x into 1D horizon region \mathcal{H}_{x^1}

It should be also mentioned that Eq. (8.3) coincides (with accuracy to notations) with the corresponding 1D equation for one inclusion in the infinite homogeneous bar (we need only to replace the matrix \mathbf{C}^1 and vectors \mathbf{u} , $\bar{\varepsilon}$, $\bar{\varepsilon}^n$ by the corresponding scalar variables):

$$\int_{\mathcal{H}_{x^1}} C(x^1, q^1) [u(q^1) - u(x^1) - \bar{\varepsilon}(q^1 - x^1)] dq^1 = \hat{b}(x^1) \bar{\varepsilon}. \quad (8.5)$$

It means that for Eq. (8.3), the development of generalized methods of the EFM and MTM (and computational homogenization for periodic structures) can be obtained for 1D case (8.3). In particular, the solution of Eq. (8.3) can be presented in the form $(\mathbf{x} = (x^1, 0, 0)^\top \in v_i^j)$ $\mathbf{u}(\mathbf{x}) = \tilde{\mathbf{B}}(\mathbf{x}) \tilde{\varepsilon}$, where $\tilde{\mathbf{B}}(\mathbf{x}) = (\mathbf{B}^n(\mathbf{x}), \mathbf{B}^t(\mathbf{x}))$ and $\tilde{\varepsilon} = (\bar{\varepsilon}^n, \bar{\varepsilon}^t)^\top$ are the decompositions of the corresponding value on the normal and tangential parts. After that, the stresses $\boldsymbol{\sigma}(\mathbf{x})$ (2.27) can be estimated at the interval $l_0^\delta = \{\mathbf{x} | \mathbf{x} = (x^1, 0, 0)^\top, -h - l_\delta \leq x^1 \leq h + l_\delta\}$ and the effective moduli \mathbf{L}^* (3.47) (see for details [64], [71]).

Comment 8.1. The generalization of the present approach (obtained in [71] for the linear bond-based model) to the generalized MTM and EFM for multilayered CM with linearized state-based peridynamic (as in [69]) properties is straightforward. It is expected that the potential exploitation of these methods (MTM, EFM, and periodic homogenization method) for the estimation of effective moduli of peridynamic multilayered CM will lead to different results. It can be considered the prescribed random orientation of the anisotropic layers (with the same normals $\mathbf{n} = (\pm 1, 0, 0)^\top$). The analysis of clustered CMs, where the aligned hierarchical clusters contain some anisotropic layers, is straightforward.

Comment 8.2. It should be mentioned that the fields $\mathbf{u}(\mathbf{x})$ and $\boldsymbol{\sigma}(\mathbf{x})$, see Eq. (4.11) are assumed to be invariant to the parallel transformations along the layers. It means, that

several popular loading (e.g. impact, torsion, deflections, and buckling from both a static and dynamic point of view) can not be reduced from 3D to 1D problems by the method proposed (for both local micromechanics and PD micromechanics). On another side, we did not exploit any additional assumption, such as, e.g. the scale separation hypothesis $l_\delta/2h \rightarrow 0$ or other hypotheses used in [10], [12], [18], [109], [163], [165], [202], [236], [238], [239], [289], [363] which are based on the consideration of PD bounds as the structural elements. Thus, the Mori-Tanaka method (4.39) is reduced to Eq. (8.3) with 1D argument for one (segment) inclusion in the infinite matrix (see Fig. 11). The method proposed can be slightly modified to the periodic infinite field of layers (which, perhaps, are not identical). In such a case the problem for 1D inclusion inside an infinite matrix (see Fig. 11a) should be replaced by the 1D problem at the unit cell $[-l^\Omega, l^\Omega]$ (see Fig. 11b) with the VPBC [56]. Furthermore, in the framework of the hypothesis (8.2), a finite number of layers of deterministic structures ($L^\Omega \leq x^1 \leq L^\Omega$) of the 3D problem is reduced to the 1D problem with the volumetric boundary conditions (see Fig. 11c). In such a case, free edge effect can be easily considered and application of the higher-order homogenization theories, or plate-type homogenization strategies [184] and [358] are not required.

Comment 8.3. The problems for nonlinear peridynamic laminated structure (with the possible imperfect interface model, as in, e.g., Kapitza thermal resistance model [347], [393]) are also affordable. So, a problem linearity was only exploited in the decomposition of the integrand in Eqs. (8.3) for separate integration of the micromodulus in Eq. (8.4₁) over the cross-sections $\mathcal{S}_{x^1}^{q_1}$. For nonlinear model, a bond force density $\mathbf{f}^{\text{bond}}(\boldsymbol{\eta}, \boldsymbol{\xi}, \mathbf{x})$ (2.18) is not decomposed as in Eq. (2.21). But the averages of $\mathbf{f}^{\text{bond}}(\boldsymbol{\eta}, \boldsymbol{\xi}, \mathbf{x})$ can be estimated over the cross-sections $\mathcal{S}_{x^1}^{q_1}$. Owing to Eq. (8.3), we obtain a nonlinear version of Eq. (8.3) with 1D argument x^1 which can be solved, e.g., by the fixed-point iterative method (as in Eq. (3.20)).

9 Conclusion

Basic concepts, methods, their interdependence, and potential generalizations in the LM are straightforwardly generalized to the PM. In the sense of generality of the hypotheses exploited, 70 years of the progress of the EFM in the LM [from Foldy(1945) [138] to [51], [53]) is compressed to a few years of their development in the PM. The proposed universal tool (called CAM) is sufficiently flexible and based on physically clear hypotheses that can be modified and improved if necessary (up to abandonment of these hypotheses that are forced by challenging achievement rather than only by pursuing an abstruse theoretic exercise) in the framework of a unique scheme for analyses of a wide class of micromechanical problems, e.g., statistically homogeneous and inhomogeneous media, inhomogeneous loading (inhomogeneous body force is included), nonlinear and nonlocal constitutive laws of phases, and coupled physical phenomena. Although PM of both the random and periodic structure CMs was historically developed as a generalization of the corresponding methods of the LM, it does not

mean that PM's society manifests itself as a user of the LM methods; we also demonstrated that some methods developed in PM initiate the new methods of LM unknown before (i.e. the methods of both the LM and PM mutually enrich one another). On the other side, for the presentation of PM as a unified theory, PM is described as the formalized schemes of blocked (or modular) structures so that the experts developing one block need not be experts in the underlying another block.

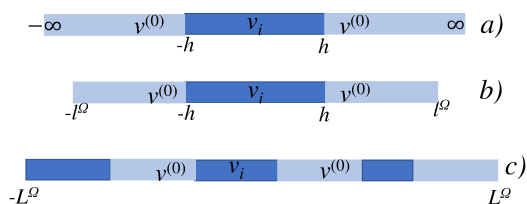


Fig. 11: Schematic representation of the field of layers v_i

The opportunity for the creation of this blocked structure of the PM is supported by a critical generalization of CAM which is extremely flexible, robust, general, physics-based, and data-driven multidisciplinary design and optimization toolkit greatly speeding the rate of technological advance to execute fundamental and applied research in the multi-scale and multi-physics modeling of a wide class of both the random and periodic heterogeneous media. However, these opportunities of CAM can be realized only in the case of joint efforts of both computational mathematics, computational and analytical micromechanics societies as well as material science and physics societies. The modular structure of PM proposed is a good background for effective collaborations of different teams in so many multidisciplinary areas as PM.

Loosely speaking, the review is dedicated to the development of Block 4 Micromechanics and its adjustment with Block 3 Perturbator (see also the text before Fig. 3). The methods for the solution of Block 3 Perturbator are not analyzed (these methods are only briefly mentioned in Introduction and Subsection 3.2) and assumed to be known. Comparisons between different peridynamic models with some numerical results, analyses of why peridynamic theory is interesting and useful, and descriptions of limitations of the peridynamic models are beyond the scope of the current review (see for references Introduction).

Lastly, this review has a dual goal and is intended for the target auditorium, which can be subdivided into two groups. It can be used as guidance for practitioners in the selection of appropriate PM methods based on the characteristics and needs of the problem being considered. On the other side, it can be also exploited by developers in the choice of attack directions in broad prospective problems of the new field of PM.

Acknowledgements:

The author acknowledges Dr. Stewart A. Silling for the fruitful personal discussions, encouragements, helpful comments, and suggestions.

Declarations

Ethical Approval.

(applicable for both human and/ or animal studies. Ethical committees, Internal Review Boards, and guidelines followed must be named. When applicable, additional headings with statements on consent to participate and consent to publish are also required) “not applicable.”

Competing interests.

(always applicable and includes interests of a financial or personal nature) No competing interests.

Authors’ contributions.

(applicable for submissions with multiple authors). “not applicable”. There is only one author.

Funding.

No funding.

References

- [1] Aguiar, A.R., Fosdick, R., 2014. A constitutive model for a linearly elastic peridynamic body *Mathematics and Mechanics of Solids*, **19**: 502–523
- [2] Agwai, A., Guven, I., Madenci, E. (2011) Predicting crack propagation with peridynamics: a comparative study *Int. J. Fracture*, **171**: 65-78
- [3] Ahmadi M, Sadighi M, Hosseini-Toudeshky H. (2022) Microstructure-based deformation and fracture modeling of particulate reinforced composites with ordinary state-based peridynamic theory. *Compos Struct*, **279**:114734.
- [4] Aksoylu B, Parks ML (2011) Variational theory and domain decomposition for nonlocal problems. *Applied Mathematics and Computation*, **217**: 6498–6515
- [5] Alali, B., Albin, N. (2020) Fourier spectral methods for nonlocal models. *J. Peridynamics Nonlocal Modeling*, **2**, 317-335.
- [6] Alali B, Gunzburger M (2015) Peridynamics and material interfaces *J. Elast.*, **120**: 225–248
- [7] Alali B, Lipton R, (2012) Multiscale dynamics of heterogeneous media in the peridynamic formulation. *J. Elast.*, **106**: 71–103
- [8] Arthur, D., Vassilvitskii, S. *k*-means++: the advantages of careful seeding. *Proc. of the 18th Annual ACM-SIAM Symposium on Discrete Algorithms*, 2007; 1027–1035.
- [9] Asgari M, Kouchakzadeh MA (2023) An improved plane strain/plane stress peridynamic formulation of the elastic–plastic constitutive law for von Mises materials. *Engineering with Computers*.
- [10] Askari, E., Xu, J., Silling S.A., 2006. Peridynamic analysis of damage and failure in composites. *44th AIAA Aerospace Sciences Meeting and Exhibition*, **AIAA 2006–88**, Reno, NV, 1–12.
- [11] Askari E, Bobaru F, Lehoucq RB, Parks ML, Silling SA, Weckner O (2009) Peridynamics for multiscale materials modeling. *Journal of Physics: Conference Series*, **125**:012078
- [12] Askari, A., Azdoud, Y., Han, F., Lubineau, G., Silling, S. 2015. Peridynamics for analysis of failure in advanced composite materials *Numerical Modelling of Failure in Advanced Composite Materials*, Woodhead Publishing Series in Composites Science and Engineering, 331–350
- [13] Askes H, Aifantis EC (2011) Gradient elasticity in statics and dynamics: An overview of formulations, length scale identification procedures, finite element implementations and new results. *Int. J. Solids Structures* **48**: 1962–1990

- [14] Azdoud Y, Han F, Lubineau G. (2013) A Morphing framework to couple non-local and local anisotropic continua *Int. J. Solids Struct.*, **50**, 1332–1341
- [15] Babuska I (1976) Homogenization and its application. Mathematical and computational problems. In: Lions, J.-L., Glowinski, R. (Eds.) *Numerical Solution of Partial Differential Equations*. III. Academic Press, New York, pp. 89–116
- [16] Bakhvalov NS, Panasenko GP (1984) *Homogenisation: Averaging Processes in Periodic Media*. Nauka, Moscow (in Russian; English translation: Kluwer, 1989)
- [17] Barrett R, Berry M, Chan TF, Demmel J, Donato J, Dongarra J, Eijkhout V., Pozo R, Romine C, der Vorst HV. (1994) *Templates for the Solution of Linear Systems: Building Blocks for Iterative Methods*, 2nd Edition, SIAM.
- [18] Basoglu MF, Kefal A, Zerín Z, Oterkus E. (2022). Peridynamic modeling of toughening enhancement in unidirectional fiber-reinforced composites with micro-cracks. *Composite Structures*, **297**: 115950
- [19] Bažant, Z, Nguyen N.H., Dönmez, A.A. (2022) Critical Comparison of Phase-Field, Peridynamics, and Crack Band Model M7 in Light of Gap Test and Classical Fracture Tests *J. Appl. Mech.*, **89**: 061008 (26 pages)
- [20] Beckmann R, Mella R, Wenman MR (2013) Mesh and timestep sensitivity of fracture from thermal strains using peridynamics implemented in Abaqus. *Comput. Methods Appl. Mech. Engrg.*, **263**: 71–80
- [21] Benaimche MA, Yvonnet J, Bary B, He Q-C (2022) A k-means clustering machine learning-based multiscale method for inelastic heterogeneous structures with internal variables. *Int J Numer Methods Eng.* **123**: 2012–2041
- [22] Benner P, Grivet-Talocia S., Quarteroni A, Rozza G, Schilders W, Silveira LM. (Eds) (2020) *Model Order Reduction. V.2: Snapshot-Based Methods and Algorithms*. Walter de Gruyter GmbH, Milano
- [23] Benveniste Y. (1986) On the Mori-Tanaka’s method in cracked bodies *Mech. Res. Commun.*, **13**, 193-201
- [24] . Bessa MA, Foster JT, Belytschko T, Liu WK. (2014) A meshfree unification: reproducing kernel peridynamics. *Comput. Mech.*, **53**, 1251–1264.
- [25] Bialecki RA, Kassab AJ, Fic A. (2005) Proper orthogonal decomposition and modal analysis for acceleration of transient FEM thermal analysis *Int. J. Numer. Meth. Engng*, **62**:774–797
- [26] Bie Y, Ren H, Rabczuk T, Bui TQ, Wei Y. (2024) The fully coupled thermo-mechanical dual-horizon peridynamic correspondence damage model for homogeneous and heterogeneous materials *Comput. Meth. Appl. Mech. Engrg*, **420**: 116730
- [27] Birner M, Diehl P, Lipton R, Schweitzer MA. (2023) A fracture multiscale model for peridynamic enrichment within the partition of unity method. *Adv. Engineering Software*, **176** 103360.
- [28] Budiansky B, O’Connell RJ (1976) Elastic moduli of cracked solids. *Int J Solids Struct*, **12**, 81–91
- [29] Benveniste Y (1987) A new approach to application of Mori-Tanaka’s theory in composite materials. *Mech. Mater.* **6**: 147–157
- [30] Bergander H (1995) Finite plastic constitutive laws for finite deformations. *Acta Mechan*, **109**: 79–99
- [31] Balay, S., Abhyankar, S., Adams, M., Brown, J., Brune, P. *et al.* (2016) *PETSc users manual 3.7 Technical Report*, Argonne National Lab. (ANL), Argonne, IL.
- [32] Berveiller, M., and Zaoui, A. (1979). An extension of the self-consistent scheme to plastically-flowing polycrystals. *J. Mech. Phys. Solids*, **26**: 325–344
- [33] Berkooz, G, Holmes, P, Lumley, JL. The proper orthogonal decomposition in the analysis of turbulent flows. *Annu Rev Fluid Mech*, 1993; **25**: 539–575
- [34] Bobaru, F., Foster, J., Geubelle, P., Silling, S., (Editors) 2016. *Handbook of Peridynamic Modeling*, CRC Press, Boca Raton, FL.
- [35] Bobaru, F., Ha, Y.D., 2011. Adaptive refinement and multiscale modeling in 2D peridynamics. *Int. J. Multiscale Comput. Eng.*, **9**, 635–659
- [36] Bobaru, F., Yang, M., Alves, L.F., Silling, S.A., Askari, A., Xu, J., 2009. Convergence, adaptive refinement, and scaling in 1d peridynamics. *Int. J. Numerical Methods Engng*, **77**, 852–877

- [37] Bode T, Weißenfels C, Wriggers P. (2022) Peridynamic Galerkin method: an attractive alternative to finite elements. *Computational Mechanics*. **70**: 723–743.
- [38] Bornert M, Stolz C, Zaoui A (1996) Morphologically representative pattern-based bounding in elasticity. *J Mech Phys Solids*, **44**: 307–331
- [39] Boyaval, S. Reduced-basis approach for homogenization beyond the periodic setting, *Multiscale Modeling & Simulation* 2008; **7**: 466–494.
- [40] Breitenfeld MS, Geubelle PH, Weckner O, Silling SA. (2014) Non-ordinary state-based peridynamic analysis of stationary crack problems *Comput. Meth. Appl. Mech. Engng*, **272**, 233–250
- [41] Briggs, WL, Henson, VE. (1995) *The DFT: An Owner's Manual for the Discrete Fourier Transform*. SIAM, Philadelphia,
- [42] Brigham, EO. (1988) *The Fast Fourier Transform and Its Applications*. Prentice-Hall, NJ,
- [43] Brisard S., Dormieux L (2010) FFT-based methods for the mechanics of composites: a general variational framework. *Comput. Mater. Sci.* **49**, 663–71
- [44] Brisard S., Dormieux L. (2012) Combining Galerkin approximation techniques with the principle of Hashin and Shtrikman to derive a new FFT-based numerical method for the homogenization of composites. *Comput. Methods Appl. Mech. Eng.* **217–220**, 197–212
- [45] Brunton SL, Kutz JN (2022) *Data-driven science and engineering: Machine learning, dynamical systems, and control*. Cambridge University Press, Cambridge, UK
- [46] Bueno-Orovio, A., Kay, D., Burrage, K. (2014) Fourier spectral methods for fractional-in-space reaction-diffusion equations. *BIT Numerical mathematics*, **54**, 937–954.
- [47] Buryachenko VA (2007) *Micromechanics of Heterogeneous Materials*. Springer, NY.
- [48] Buryachenko VA (2010) On the thermo-elastostatics of heterogeneous materials. I. General integral equation. *Acta Mechanica*, 213: 359–374
- [49] Buryachenko VA (2010) On the thermo-elastostatics of heterogeneous materials. II. Analyze and generalization of some basic hypotheses and propositions. *Acta Mech.*, 213: 375–398.
- [50] Buryachenko V A (2014) Some general representations in thermoperidynamics of random structure composites. *Int. J. Multiscale Comput. Enging*, 12: 331—350.
- [51] Buryachenko V (2014) Solution of general integral equations of micromechanics of heterogeneous materials. *Int. J. Solids and Structures*, 51: 3823—3843
- [52] Buryachenko V (2014) Effective elastic modulus of heterogeneous peristatic bar of random structure. *J. Solids and Structures*, **51**: 2940–2948
- [53] Buryachenko V (2015) General integral equations of micromechanics of heterogeneous materials. *J. Multiscale Comput. Enging.*, 13: 11–53
- [54] Buryachenko VA (2015) Effective thermoelastic properties of heterogeneous thermoperi- static bar of random structure. *Int. J. Multiscale Comput. Enging.*, **13**: 55–71
- [55] Buryachenko VA (2017) Effective properties of thermoperidynamic random structure composites: some background principles. *Math. Mech. of Solids.*, **22**: 366–1386
- [56] Buryachenko VA (2018) Computational homogenization in linear elasticity of peridynamic periodic structure composites. *Math. Mech. of Solids*, 23: 2497–2525
- [57] Buryachenko V (2018) Effective elastic modulus of heterogeneous peristatic bar of periodic structure. *Computers & Structures*, **202**:129–139
- [58] Buryachenko V (2018) Effective elastic modulus of damaged peristatic bar of periodic structure. *J. Multiscale Comput. Enging*, **16**:101–118
- [59] Buryachenko VA (2019) Interface integral technique for the thermoelasticity of random structure matrix composites. *Math. Mech. of Solids*, 24: 2785–2813
- [60] Buryachenko VA (2019) Modeling of one inclusion in the infinite peridynamic matrix subjected to homogeneous remote loading *J. Peridynamics and Nonlocal Modeling*, 1: 75–87

- [61] Buryachenko V (2020a) Generalized effective field method in peridynamic micromechanics of random structure composites. *Int. J. Solid Structure*, **202**: 765-786
- [62] Buryachenko V (2020b) Generalized Mori-Tanaka approach in micromechanics of peristatic random structure composites. *J. Peridynamics and Nonlocal Modeling*, **2**: 26-49
- [63] Buryachenko V. (2020c) Variational principals and generalized Hill's bounds in micromechanics of peristatic random structure composites. *Math. Mech. of Solids*, **25**: 682-704
- [64] Buryachenko VA (2022) *Local and Nonlocal Micromechanics of Heterogeneous Materials*. Springer, NY.
- [65] Buryachenko V. A. (2022) Multiscale and multiphysics modelling of advanced heterogeneous materials. *International Association of Advanced Materials Award Lecture*, see 20min Fellow of IAAM video presentation <https://lnkd.in/gYp3SJmy>; Vid. Proc. Adv. Mater., Volume 3, DOI: 10.5185/vpoam.2022.08325)
- [66] Buryachenko, V. (2022) Critical analysis of generalized Maxwell homogenization schemes and related prospective problems. *Mechanics of Materials*, **165**, 104181
- [67] Buryachenko VA (2023a) Effective nonlocal behavior of peridynamic random structure composites subjected to body forces with compact support and related prospective problems. *Math. Mech. of Solids*, **28**: 1401-1436
- [68] Buryachenko V (2023b) Effective displacements of peridynamic heterogeneous bar loaded by body force with compact support. *J. Multiscale Comput. Enging*, **21**: 27-42
- [69] Buryachenko V. A. (2023c). Linearized ordinary state-based peridynamic micromechanics of composites. *J. Materials and Structures*, **18**, 445-477
- [70] Buryachenko V. A. (2023d). Second moment of displacement state and effective energy-based criteria in peridynamic micromechanics of random structure composites *J. Peridynamics and Nonlocal Modeling* **5**, Published: 23 September 2023
- [71] Buryachenko V. A. (2024e) Generalized Mori-Tanaka approach in peridynamic micromechanics of multilayered composites of random structure. *J. Peridynamics and Nonlocal Modeling* **6**, Published: 12 February 2024
- [72] Buryachenko V. A. (2023f) Transformation field analysis as a background of clustering discretization methods in micromechanics of composites. *Math. Mech. of Solids*, **28** 2677-2703
- [73] Buryachenko V. (2023g) Effective nonlocal behavior of peridynamic random structure composites subjected to body forces with compact support. *Math. Mech. of Solids*, **28**: 1401-1436
- [74] Buryachenko VA (2024) Estimations of energy-based criteria in nonlinear phenomena in peridynamic micromechanics of random structure composites. *J. Peridynamics and Nonlocal Modeling*, **6**: 250-269
- [75] Buryachenko V. A. (2024) Transformation field analysis and clustering discretization method in pyridynamic micromechanics of composites. *J. Peridynamics and Nonlocal Modeling* **6**: Published: 22 February 2024
- [76] Buryachenko V. A. (2024) Fast Fourier transform method for peridynamic bar of periodic structure. *J. Multiscale Comput. Enging*, **22**: 1-17
- [77] Buryachenko V. A. (2024) Fast Fourier transform in peridynamic micromechanics of composites *Math. Mech. of Solids*, **29**, <https://doi.org/10.1177/10812865241236878>
- [78] Buryachenko V., (2024) Nonlinear general integral equations in micromechanics of random structure composites. *Math. Mech. of Solids*, **29**
- [79] Buryachenko V. (2024) Local and nonlocal micromechanics of composites. *26th Int. Congress of Theor. Appl. Mech. (ICTAM 2024)*, August 25-30, 2024, Daegu, Korea
- [80] Castrogiovanni A, Marfia S, Auricchio F, Sacco E (2021) TFA and HS-based homogenization techniques for nonlinear composites *Int. J. Solids Structures*, **225**: 111050
- [81] Celebi, ME, Kingravi, HA, Vela, PA. A comparative study of efficient initialization methods for the k-means clustering algorithm *Expert systems with applications*, 2013; **40**: 200-210.
- [82] Chatzigeorgiou G (2022) Study of multilayered composites through periodic homogenization and Mori-Tanaka methods. *Mechanics of Materials*, 164: 10411

- [83] Chen, X., Gunzburger, M. (2011) Continuous and discontinuous finite element methods for a peridynamics model of mechanics. *Computer Methods in Applied Mechanics and Engineering*, **200**, 1237-1250.
- [84] Chen Z, Jafarzadeh S, Zhao J, Bobaru F. (2021) A coupled mechano-chemical peridynamic model for pit-to-crack transition in stress-corrosion cracking, *J. Mechanics Physics Solids* **146**: 104203.
- [85] Cheng, G, Li, X, Nie, Y, Li, H. (2019) FEM-Cluster-based reduction method for efficient numerical prediction of effective properties of heterogeneous material in nonlinear range. *Comput Methods Appl Mech Eng*, **348**: 157–184.
- [86] Cheng H, Torquato S (1997) Electric-field fluctuations in random dielectric composites *Physical Review*, B 56: 8060-8070
- [87] Cheng Z-Q, Liu H, Tan W. (2024) Advanced computational modelling of composite materials. *Engng Fract. Mechanics*, **305**: 110120
- [88] Chinesta F, Huerta A, Rozza G, Willcox K. (2004) Model Order Reduction. *Encyclopedia of Computational Mechanics*. Eds. E. Stein, R. Borst, TJR Hughes. John Wiley & Sons, Ltd.
- [89] Chiu, S.N., Stoyan, D., Kendall, W.S., Mecke, J. (2013) *Stochastic Geometry and its Applications*. Third Edition. J. Wiley & Sons, Chichester, NY.
- [90] Cocke C, Mirmohammad H, Zecevic M, Phung BR, Lebensohn RA, Kingstedt OT, Spear A. (2023) Implementation and experimental validation of nonlocal damage in a large-strain elasto-viscoplastic FFT-based framework for predicting ductile fracture in 3D polycrystalline materials, *Int. J. Plasticity* **162**, 103508
- [91] Coclite GM, Dipierro S, Maddalena F, Valdinoci E (2022a) Wellposedness of a nonlinear peridynamic model. *Nonlinearity*, **32**(1), *arXiv:1804.00273v1*
- [92] Coclite GM, Dipierro S, Fanizza G, Maddalena F, Valdinoci E (2022b) Dispersive effects in a scalar nonlocal wave equation inspired by peridynamics *Nonlinearity*, **35**(11), *arXiv:2105.01558v2*
- [93] Coclite, GM., Fanizzi, A., Lopez, L., Maddalena, F., Pellegrino, SF. (2020) Numerical methods for the nonlocal wave equation of the peridynamics. *Applied Numerical Mathematics*, **155**, 119-139.
- [94] Cooley JW, Tukey JW. (1965) An algorithm for the machine calculation of complex Fourier series. *Math. Comput.*, **19**, 297–301
- [95] Covezzi F, Miranda S, Marfia S, Sacco E (2017) Homogenization of elastic–viscoplastic composites by the Mixed TFA. *Comput. Meth. Appl. Mech. Engng.* 318: 701–723
- [96] Covezzi F., Miranda S, Fritzen F, Marfia S, Sacco E (2018) Comparison of reduced order homogenization techniques: pRBMOR, NUTFA and MxTFA *Meccanica*, 53: 1291–1312
- [97] de Geus T W J, Vondřejc J, Zeman J, Peerlings RHJ, Geers MGD (2017) Finite strain FFT-based non-linear solvers made simple. *Comput. Methods Appl. Mech. Eng.* **318**, 412–30
- [98] Dahal B, Seleson P, Trageser J. (2023) The Evolution of the Peridynamics Co Authorship Network *J.Peridynamics Nonlocal Modeling*, **5**: 311–355
- [99] Decklever J, Spanos P. Nanocomposite material properties estimation and fracture analysis via peridynamics and Monte Carlo simulation. (2016) *Probab Eng Mech*, tenbf 44(SI):77–88
- [100] D’Elia M, Du Q, Glusa C, Gunzburger M, Tian X, Zhou Z (2020) Numerical methods for nonlocal and fractional models. *Acta Numerica*, **29**, 1 - 124
- [101] D’Elia M, Du Q, Gunzburger M. (2017) Recent progress in mathematical and computational aspects of peridynamics *Handbook of Nonlocal Continuum Mechanics for Materials and Structures*. Springer International Publishing.
- [102] D’Elia, M., Xingjie Li, X., Seleson, P., Tian, X., Yu, Y. (2022) A review of Local-to-Nonlocal coupling methods in nonlocal diffusion and nonlocal mechanics. *Journal of Peridynamics and Nonlocal Modeling*, **4**, 1–50
- [103] Diana V. (2023) Anisotropic continuum molecular models: a unified framework based on pair potentials for elasticity, fracture and diffusion type problems. *Archives Comput. Methods in Engng*, **30**:1305–1344
- [104] Diana V, Bacigalupo A, Lepidi M, Gambarotta L. (2022). Anisotropic peridynamics for homogenized microstructured materials. *Comput. Meth. Applied Mech. Engng*, **392**: 114704.

- [105] Diehl P, Lipton R, Wick T, Tyagi M. (2022) A comparative review of peridynamics and phase-field models for engineering fracture mechanics *Computational Mechanics*, **69**, 1259–1293
- [106] Diehl P, Prudhomme S, Levesque M. (2019) A review of benchmark experiments for the validation of peridynamics models. *J. Perid. Nonlocal Modeling*, **1**: 14–35.
- [107] Dimola N, Coclite A, Fanizza G, Politi T (2022) Bond-based peridynamics, a survey prospecting nonlocal theories of fluid-dynamics. *Advances in Continuous and Discrete Models*, 2022:60 (27pp.)
- [108] Dipasquale D, Sarego G, Prapamonthon P, Yooyen S, Shojaei A. (2022) A stress tensor-based failure criterion for ordinary state-based peridynamic models. *J. Appl. Computat. Mechanics*, **8**, 617–628
- [109] Diyaroglu C, Oterkus E, Madenci E, Rabczuk T, Siddiq A (2016) Peridynamic modeling of composite laminates under explosive loading. *Composite Structures*, **144**: 14–23
- [110] Diyaroglu C, Madenci E, Phan N (2019a) Peridynamic homogenization of microstructures with orthotropic constituents in a finite element framework. *Composite Structures*, **227**:111334
- [111] Diyaroglu C, Madenci E, Stewart RJ, Zobi SS (2019b) Combined peridynamic and finite element analyses for failure prediction in periodic and partially periodic perforated structures *Composite Structures*, **227**:111481
- [112] Doghri I, Adam L, Bilger N. (2010) Mean-field homogenization of elasto-viscoplastic composites based on a general incrementally affine linearization method *Int.l J. Plasticity*, **26**: 219–238.
- [113] Dong H, Wang H, Jiang G, Cai Z, Wang W, Liu Y. (2023) An adaptive partitioned reduced order model of peridynamics for efficient static fracture simulation *Engng Analysis Boundary Elements*, **157**, 191–206
- [114] Dorduncu M, Ren H, Zhuang X, Silling S, Madenci E, Rabczuk T. (2024) A review of peridynamic theory and nonlocal operators along with their computer implementations. *Computers and Structures*, **299**: 107395
- [115] Drugan, WJ, and Willis, JR. (1996) A micromechanics-based nonlocal constitutive equation and estimates of representative volume elements for elastic composites. *J Mech Phys Solids*, **44**: 497–524
- [116] Dvorak, G.J. *Micromechanics of Composite Materials*. Dordrecht: Springer, 2013.
- [117] Dvorak, G. Transformation field analysis of inelastic composite materials. *Proc R Soc Lond A*. 1992; **437**, 311–327.
- [118] Dvorak, G J, Benveniste, Y. On transformation strains and uniform fields in heterogeneous media. *Proceedings of the Royal Society London A*, 1992; **437**: 291–310.
- [119] Dvorak, G, Bahei-El-Din, Y, Wafa, A. The modeling of inelastic composite materials with the transformation field analysis. *Modelling Simul. Mater. Sci. Eng*, 1994; **2**: 571–586
- [120] Du C, Liu P, Oeser M. (2023) Homogenization of the elastic viscoplastic damage behavior of asphalt mixtures based on the mesomechanical Mori–Tanaka method *Engineering with Computers*, **39**: 2277–2293.
- [121] Du Q, Engquist B, Tian X. (2020) Multiscale modeling, homogenization and nonlocal effects: Mathematical and computational issues. *Contemporary mathematics*, **754**, 115–140.
- [122] Du Q, Gunzburger M, Lehoucq RB, Zhou, K (2013) Analysis of the volume-constrained peridynamic Navier equation of linear elasticity. *J. Elast.*, **113**: 193–217.
- [123] Du Q, Lipton R, Mengesha T. (2016) Multiscale analysis of linear evolution equations with applications to nonlocal models for heterogeneous media. *ESAIM: Mathematical Modelling and Numerical Analysis*, **50**, 1425–1455.
- [124] Du, Q., Yang, J. (2017) Fast and accurate implementation of Fourier spectral approximations of nonlocal diffusion operators and its applications. *J. Computational Physics*, **332**, 118–134.
- [125] Eyre, D.J, Milton, G.W., (1999) A fast numerical scheme for computing the response of composites using grid refinement. *Eur. Phys. J.: Appl. Phys.*, **6**, 41–47
- [126] Emmrich, E., Weckner, O., 2006. The peridynamic equation of motion in non-local elasticity theory. In: C. A. Mota Soares *et al.* (eds.), *III European Conference on Computational Mechanics. Solids, Structures, and Coupled Problems in Engineering*. Springer, Dordrecht

- [127] Emmrich, E., Weckner, O., 2007a. Analysis and numerical approximation of an integro-differential equation modeling non-local effects in linear elasticity. *Math. Mech. Solids*, **12**, 363–384.
- [128] Emmrich, E., Weckner, O., 2007b. On the well-posedness of the linear peridynamic model and its convergence towards the Navier equation of linear elasticity. *Commun. Math. Sci.* **5**, 851–864.
- [129] Eghbalpoor R, Sheidaei A. (2024) A peridynamic-informed deep learning model for brittle damage prediction *Theoret. Appl. Fracture Mech.*, **131**: 104457
- [130] Eriksson, K, and Stenström, C. Homogenization of the 1D peri-static/dynamic bar with triangular micromodulus. *Journal of Peridynamics and Nonlocal Modeling*, 2021; **3**: 85–112.
- [131] Eshelby, J.D., 1957. The determination of the elastic field of an ellipsoidal inclusion, and related problems. *Proc. Roy. Soc. Lond.*, **A 241**, 376–396.
- [132] Fan Y, D’Elia M, Yu Y, Najm HN, Silling S. (2023) Bayesian nonlocal operator regression: A datadriven learning framework of nonlocal models with uncertainty quantification. *J. Engig Mech.*, **149**, 04023049.
- [133] Fan Y, Tian X, Yang X, Li C, Webster C, Yu Y. (2022) An asymptotically compatible probabilistic collocation method for randomly heterogeneous nonlocal problems. *J. Comput. Physics*, **465**: 111376
- [134] Fan Y, You H, Tian X, Yang X, Li C, Prakash N. (2022) A meshfree peridynamic model for brittle fracture in randomly heterogeneous materials *Comput. Meth. Appl. Mech. and Engng*, **399**: 115340
- [135] Ferreira BP, Pires FM, Bessa MA (2021) Adaptive clustering-based reduced-order modeling framework: fast and accurate modeling of localized history-dependent phenomena *arXiv preprint arXiv*, 2109.11897
- [136] Fish J (2014) *Practical Multiscaleing*. Chichester: John Wiley & Sons.
- [137] Fish J, Chen W (2001) Higher-order homogenization of initial/boundary-value problem. *J. Eng. Mech.*, **127**: 1223–1230
- [138] Foldy LO. (1945) The multiple scattering of waves. *Phys. Rev.* **67**, 107–119
- [139] Forgy, E. Cluster analysis of multivariate data: efficiency vs. interpretability of classification. *Biometrics*, 1965; **21**: 768.
- [140] Foster JT, Silling SA, Chen W. (2011) An energy-based failure criterion for use with peridynamic states. *Int. J. Multiscale Comput. Engng*, **9**: 675–687
- [141] Frank X, Lampoh K, Delenne J-Y. (2023) From stress concentrations between inclusions to probability of breakage: A two-dimensional peridynamic study of particle-embedded materials *Physics Review*, **E108**: 034903
- [142] Galadima Y, Oterkus E, Oterkus S (2019) Two-dimensional implementation of the coarsening method for linear peridynamics. *AIMS Mater Sci* **6**: 252–275
- [143] Galadima YK, Xia W, Oterkus E, Oterkus S (2023) A computational homogenization framework for non-ordinary state-based peridynamics *Engineering with Computers* **39**: 461–487
- [144] Galadima YK, Xia W, Oterkus E, Oterkus S (2023) Peridynamic computational homogenization theory for materials with evolving microstructure and damage. *Engineering with Computers* **39:39**: 2945–2957
- [145] Galadima Y K, Oterkus S, Oterkus E, Amin I, El-Aassar AH, Shawky H. (2023) A nonlocal method to compute effective properties of viscoelastic composite materials based on peridynamic computational homogenization theory *Composite Structures*, **319**, 117147.
- [146] Galadima YK, Oterkus S, Oterkus E, Amin I, El-Aassar A-H, Shawky H. (2024) Effect of phase contrast and inclusion shape on the effective response of viscoelastic composites using peridynamic computational homogenization theory. *Much. Advanced Mater. Structures*. tenbd **31**, 155–163
- [147] Geers, MGD, Kouznetsova, VG, Brekelmans, WAM. (2010) Multi-scale computational homogenization: Trends and challenges. *J. Comput. Applied Mathematics*; **234**: 2175-2182.
- [148] Gélébart, L., Mondon-Cancel, R. (2013) Non-linear extension of FFT-based methods accelerated by conjugate gradients to evaluate the mechanical behavior of composite materials. *Comput. Mater. Sci.* **77**, 430–439.
- [149] Gierden, C., Kochmann, J., Waimann, J., Svendsen, B., Reese, S. (2022) A review of FE FFT-based two-scale methods for computational modeling of microstructure evolution and macroscopic material behavior. *Archives of Computational Methods in Engineering*, **29**, 4115–4135

- [150] Ghajari M, Iannucci L, Curtis P (2014) A peridynamic material model for the analysis of dynamic crack propagation in orthotropic media. *Comput Meth Appl Mech Engrg*, 276: 431–452
- [151] Ghosh, S. *Micromechanical Analysis and Multi-Scale Modeling Using the Voronoi Cell Finite Element Method (Computational Mechanics and Applied Analysis)*. Boca Raton: CRC Press, 2011.
- [152] Goodfellow I, Bengio Y, Courville A (2016) *Deep learning*. MIT Press, Cambridge, MA
- [153] Guo K, Yang Z, Yu C-H, Buehler MJ (2021) Artificial intelligence and machine learning in design of mechanical materials *Mater. Horiz.*, 8: 1153–1172
- [154] Ha, Y.D., Bobaru, F. (2010) Studies of dynamic crack propagation and crack branching with peridynamics, *Int. J. Fract.* **162**, 229–244
- [155] Han, F., Lubineau, G. and Azdoud, Y., (2016) Adaptive coupling between damage mechanics and peridynamics: a route for objective simulation of material degradation up to complete failure. *J. Mechanics Physics of Solids*, **94**, 453–472
- [156] Han, X, Gao, J, Fleming, M, Chenghai, X, Xie, W, Meng, S, Liu, WK. (2020) Efficient multiscale modeling for woven composites based on self-consistent clustering analysis. *Comput Methods Appl Mech Eng*, **364**: 112929.
- [157] He, C, Gao, J, Li, H, Ge, J, Chen, Y, Liu, J, Fang, D. A (2020) data-driven self-consistent clustering analysis for the progressive damage behavior of 3D braided composites. *Compos Struct* **249**: 112471.
- [158] Hernández, JA, Caicedo, MA, Ferrer, A. (2017) Dimensional hyper-reduction of nonlinear finite element models via empirical cubature, *Computer Methods in Applied Mechanics and Engineering*, **313**: 687–722.
- [159] Hernández, JA, Oliver, J, Huespe, A, Caicedo, M, Cante, J. (2014) High-performance model reduction techniques in computational multiscale homogenization, *Computer Methods in Applied Mechanics and Engineering*, **276**: 149–189.
- [160] Hill, R. (1965) A self-consistent mechanics of composite materials. *J. Mech. Phys. Solids* **13**, 212–222
- [161] Hu, W., Ha, Y.D., Bobaru, F., (2010) *Numerical integration in peridynamics*, Tech. rep., University of Nebraska-Lincoln
- [162] Hu W, Ha YD, Bobaru F (2011) Modeling dynamic fracture and damage in a fiber- reinforced composite lamina with peridynamics. *Int J Multiscale Comput Eng.* 9: 707–726
- [163] Hu, W., Ha, Y.D., Bobaru, F. (2012a) Peridynamic model for dynamic fracture in unidirectional fiber-reinforced composites. *Comput. Methods Appl. Mech. Engrg.*, **217**—**220**, 247—261.
- [164] Hu, W., Ha, Y.D., Bobaru, F., Silling, S.A., (2012b) The formulation and computation of the nonlocal J-integral in bond-based peridynamics. *Int. J. Fract.*, **176**, 195–206.
- [165] Hu Y-L, Yu Y, Wang H (2014) Peridynamic analytical method for progressive damage in notched composite laminates. *Composite Structures*, 108: 801—810
- [166] Hu YL, . Wang JY, Madenci E, Mu Z, Yu Y. (2022) Peridynamic micromechanical model for damage mechanisms in composites. *Composite Structures*, **301**, 116182
- [167] Huang O, Saha S, Guo J, Liu WK. (2023) An introduction to kernel and operator learning methods for homogenization by self-consistent clustering analysis *Computational Mechanics*, **72**, 195–219
- [168] Isakari S, Asakura T, Haraguchi Y, Yano Y, Kakami A. (2017) Performance evaluation and thermography of solid-propellant microthrusters with laser-based throttling. *Aerospace Science Technology*, **71**: 99–108.
- [169] Isiet M, Mišković I, Mišković S. (2021) Review of peridynamic modelling of material failure and damage due to impact. *Int. J. Impact Engrg*, **147**, 103740
- [170] Jafarzadeh S, Hillman M. (2024) An ultra-high-speed reproducing kernel particle method. *arXiv preprint arXiv:2403.19854*
- [171] Jafarzadeh, S., Larios, A., Bobaru, F. (2020) Efficient solutions for nonlocal diffusion problems via boundary-adapted spectral methods. *Journal of Peridynamics and Nonlocal Modeling*, **2**, 85–110.
- [172] Jafarzadeh S, Mousavi M, Larios A, Bobaru F (2022) A general and fast convolution-based method for peridynamics: Applications to elasticity and brittle fracture. *Comp. Meth. Appl. Mech. Enging*, **392**: 114666

- [173] Jafarzadeh S, Mousavi M, Wang L, Bobaru F. (2024) PeriFast/Dynamics: A MATLAB code for explicit fast convolution based peridynamic analysis of deformation and fracture. *Journal of Peridynamics and Nonlocal Modeling*, **6**, 33–61
- [174] Jafarzadeh S, Silling S, Liu N, Zhang Z, Yu Y. (2024) Peridynamic neural operators: a data-driven nonlocal constitutive model for complex material responses. *arXiv preprint arXiv:2401.06070*
- [175] Jafarzadeh S, Silling S, Zhang L, Ross C, Lee CH, Rahman SM, Wang S, Yu Y. (2024) Heterogeneous peridynamic neural operators: discover biotissue constitutive law and microstructure from digital image correlation measurements. *ArXiv preprint arXiv:2403.18597*.
- [176] Javili A, Morasata R, Oterkus E (2019) Peridynamics review. *Mathematics Mechanics of Solids*, **24**: 3714–3739
- [177] Jain AK (2010) Data clustering: 50 years beyond K-means. *Pattern Recognition Letters*, **31**: 651–666
- [178] Jenabidehkordi A, Abadi R, Rabczuk T. (2020) Computational modeling of meso-scale fracture in polymer matrix composites employing peridynamics *Composite Structures*, **253**, 112740
- [179] Kabel M, Böhlke T and Schneider M (2014) Efficient fixed point and Newton–Krylov solvers for FFT-based homogenization of elasticity at large deformations. *Comput. Mech.* **54**, 1497–514
- [180] Kachanov, L.M. (1958) On the time to rupture under creep conditions. *Izv. AN SSSR, Ofd. Tekhn. Nauk.* **8**, 26–31 (in Russian) [Also available in Kachanov, L.M. (1999) Rupture time under creep conditions. *Int. J. Fracture* **97**, 11–18].
- [181] Kachanov L.M. (1986) *Introduction to Continuum Damage Mechanics*. Maritinus Nijhoff Publishers, Springer: Netherlands
- [182] Kachanov M, Sevostianov I (2018) *Micromechanics of materials, with applications*. Springer International. Cham
- [183] Kafka, OL, Yu, C, Shakoor M, Liu, Z, Wagner, GJ, Liu, WK. Data-driven mechanistic modeling of the influence of microstructure on high-cycle fatigue life of nickel-titanium. *JOM*, 2018; 1–5.
- [184] Kalamkarov AL, Kolpakov AG (1997) *Analysis, design and optimization of composite structures*. John Wiley & Sons, Chichester
- [185] Kanaun SK. (1977) Self-consistent field approximation for an elastic composite medium. *Zhurnal Prikladnoi Mekh. i Tehnich Fiziki*, 18(2):160–169 (In Russian. Engl Transl. *J Appl Mech Techn Phys*, **8**, 274–282)
- [186] Kanouté P, Boso DP, Chaboche LJ, Schrefler BA. (2009) Multiscale methods for composites: a review *Archives of Computational Methods in Engineering*, **16**: 31–75.
- [187] Khoroshun, L.P., 1978. Random functions theory in problems on the macroscopic characteristics of microinhomogeneous media. *Priklad Mekh*, **14**(2), pp. 3–17 (In Russian. Engl Transl. *Soviet Appl Mech*, **14**, pp. 113–124)
- [188] Kilic B (2008) *Peridynamic theory for progressive failure prediction in homogeneous and heterogeneous materials*. Ph.D. Thesis, Dep. Mechan. Engng, The University of Arizona, 1–262
- [189] Kilic B, Madenci E (2010) Peridynamic theory for thermomechanical analysis. *IEEE Trans Adv Packag*, **33**: 97–105
- [190] Kilic B, Madenci E. (2010) An adaptive dynamic relaxation method for quasi-static simulations using the peridynamic theory. *Theor. Applied Fract. Mech.* **53**(3), 194–204.
- [191] Kim D, Lee J. (2024) A review of physics informed neural networks for multiscale analysis and inverse problems. *Multiscale Science and Engineering*, **6**: 1–11
- [192] Kingma DP, Ba J (2014) Adam: A method for stochastic optimization. *arXiv:1412.6980*
- [193] Kouznetsova VG, Brekelmans WAM, Baaijens FPT (2001) An approach to micro–macro modeling of heterogeneous materials, *Comput. Mech.* **27**: 37–48
- [194] Krajcinovic D. (1996) *Damage mechanics*. Amsterdam: North Holland.
- [195] Kröner E. (1967) Elasticity theory of materials with long range cohesive forces. *Int. J. Solids Struct.* **3**, 731–742

- [196] Ladevéze P, Passieux JC, Néron D. (2010) The LATIN multiscale computational method and the proper generalized decomposition, *Computer Methods in Applied Mechanics and Engineering*, **199**: 1287-1296.
- [197] Lahellec N, Michel J C, Moulinec H., Suquet P (2003) Analysis of inhomogeneous materials at large strains using fast Fourier transforms. *IUTAM Symposium on Computational Mechanics of Solid Materials at Large Strains* (Berlin: Springer) pp. 247–58
- [198] Laurien M, Javili A, Steinmann P.(2023) Peridynamic modeling of nonlocal degrading interfaces in composites. *Forces in Mechanics*, **10**: 100124.
- [199] Lax M (1952) Multiple scattering of waves II. The effective fields dense systems. *Phys. Rev.* 85: 621–629.
- [200] Le QV, Chan WK, Schwartz J. (2014) A two-dimensional ordinary, state-based peridynamic model for linearly elastic solids. *Int. J. Numerical Methods Engng* **98**, 547–561.
- [201] Lehoucq RB, Silling SA (2008) Force flux and the peridynamic stress tensor. *J. Mech. Phys. Solids*, **56**: 1566—1577.
- [202] Li F, Yang X, Gao W, Liu W. (2023) A single-layer peridynamic model for failure analysis of composite laminates. *Materials Today Communications*, **37**, 106988
- [203] Li, H, Kafka, OL, Gao, J, Yu, C, Nie, Y, Zhang, L, Tajdari, M, Tang, S, Guo, X, *et al.* Clustering discretization methods for generation of material performance databases in machine learning and design optimization. *Comput Mech*, 2019; **64**: 281–305.
- [204] Li, J., Li, S., Lai, X., Liu, L. (2022) Peridynamic stress is the static first Piola–Kirchhoff Virial stress. *Int. J. Solids and Structures*, **241**, 111478.
- [205] Li J, Wang Q, Li X, Ju L, Zhang Y. (2022) Homogenization of periodic microstructure based on representative volume element using improved bond-based peridynamics *Engng Analysis Boundary Elements*, **143**: 152–162
- [206] Li S, Jin Y, Huang X, Zhai L. (2020) An extended bond-based peridynamic approach for analysis on fracture in brittle materials. *Math. Problems Engineering*, ID 9568015, 1–12.
- [207] Li X, Gu X, Xia X, Madenci E, Chen X, Zhang Q. (2022) Effect of water-cement ratio and size on tensile damage in hardened cement paste: Insight from peridynamic simulations. *Construction Building Materials*, **356**: 129256
- [208] Li Z, Huang D, Rabczuk T. (2023) Peridynamic operator method. *Comput. Methods Appl. Mech. Engrg.*, **411**, 116047
- [209] Li Z, Lu Y, Huang D, Rabczuk T. (2024) Nonlocal anisotropic model for deformation and fracture using peridynamic operator method. *Int. J. Mech. Sciences*, **268**: 109023
- [210] Liang X, Wang L, Xu J, Wang J. (2021) The boundary element method of peridynamics *Int. J. Numerical Methods Engng*, **122**, 5558–5593.
- [211] Lindsay P, Parks M, Prakash A. (2016) Enabling fast, stable and accurate peridynamic computations using multi-time-step integration. *Comp. Methods Appl. Mech. Engineering* **306**:382–405.
- [212] Littlewood DJ, Parks ML, Foster JT, Mitchell JA. (2024) The Peridigm meshfree peridynamics code *J. Peridynamics Nonlocal Modeling*, **6**, 118–148
- [213] Littlewood, D.J., Silling, S.A., Mitchell, J.A., Seleson, P.D., Bond, S.D., Parks, M.L., Turner, D.Z., Burnett, D.J., Ostien, J., Gunzburger, M. (2015) *Strong local-nonlocal coupling for integrated fracture modeling*. Technical report SAND2015-7998, Sandia National Laboratories, Albuquerque, NM.
- [214] Liu C, Sun J, Tian H, Don W.C, Ju L. (2024) A high-order multi-time-step scheme for bond-based peridynamics *J. Comput. Appl. Math.*, **449**: 115968
- [215] Liu R, Xue Y, Li S. (2023) A three-dimensional (3D) micro-potential-based peridynamics model for deformation and fracture in solid materials *Engng Fracture Mechanics*, tenbf 282: 109180
- [216] Liu W, Hong J-W. (2012) Discretized peridynamics for brittle and ductile solids. *Int. J. Numer. Meth. Engng*, **89**: 1028–1046
- [217] Liu YL, Mukherjee S, Nishimura N, Schanz M, Ye W, Sutradhar A, Pan E, Dumont NA, Frangi A, Saez A. (2011) Recent advances and emerging applications of the boundary element method. *Applied Mechanics Reviews*, **64**, 031001 (38 pages)

- [218] Liu Z, Bessa MA, Liu WK (2016) Self-consistent clustering analysis: an efficient multi-scale scheme for inelastic heterogeneous materials. *Comput Methods Appl Mech Eng.*, **306**: 319–41.
- [219] Liu Z, Fleming M, Liu WK. (2018) Microstructural material database for self-consistent clustering analysis of elastoplastic strain softening materials. *Comput Methods Appl Mech Eng*, **330**: 547–577.
- [220] Liu Z, Kafka OL, Yu C, Liu WK. (2018) Data-driven self-consistent clustering analysis of heterogeneous materials with crystal plasticity. In: *Advances in Computational Plasticity*, 221–242. Springer
- [221] Lloyd S. (1982) Least squares quantization in PCM. *IEEE Trans. on Information Theory*, **28**: 129–136.
- [222] Lopez L, Pellegrino SF. (2021) A spectral method with volume penalization for a nonlinear peridynamic model. *Int. J. Numer. Methods Eng.* **122**, 707–725
- [223] Lopez L, Pellegrino SF. (2022a) A space-time discretization of a nonlinear peridynamic model on a 2D lamina. *Comput. Math. Appl.* **116**, 161–175
- [224] Lopez L, Pellegrino SF. (2022b) A fast-convolution based space-time Chebyshev spectral method for peridynamic models. *Advances Continuous Discrete Models*, **2020**, 70
- [225] Lucarini S, Segurado J. (2019) DBFFT: a displacement-based FFT approach for non-linear homogenization of the mechanical behavior. *Int. J. Eng. Sci.*, **144**, 103-131
- [226] Lucarini S, Upadhyay MV, Segurado J. (2022) FFT-based approaches in micromechanics: fundamentals, methods, and applications. *Modelling Simul. Mater. Sci. Eng.* **30**, 023002 (97pp.)
- [227] Lu J, Nie Y. (2022) A reduced-order fast reproducing kernel collocation method for nonlocal models with inhomogeneous volume constraints. *Computers & Mathematics Applications.* **121**: 52–61.
- [228] Lu J, Yang M, Nie Y. (2022) Convergence analysis of Jacobi spectral collocation methods for weakly singular nonlocal diffusion equations with volume constraints. *Applied Mathematics Computation.* **431**: 127345.
- [229] Macek RW, Silling SA (2007) Peridynamics via finite element analysis *Finite Elements in Analysis and Design*, **43**: 1169–1178
- [230] MacQueen J. (1967) Some methods for classification and analysis of multivariate observations. *Proc. of the 5th Berkeley Symposium on Mathematical Statistics and Probability*, 281–297.
- [231] Madenci E, Barut A, Futch M. (2016) Peridynamic differential operator and its applications. *Comput. Methods Appl. Mech. Engrg.* **304**, 408–451
- [232] Madenci E, Barut A, Phan ND (2017) Peridynamic unit cell homogenization, 58th *AIAA/ASCE/AHS/ASC Structures, Structural Dynamics, and Materials Conference, AIAA SciTech Forum*, (AIAA 2017-1138)
- [233] Madenci E, Barut A, Phan N. (2018) Peridynamic unit cell homogenization for thermoelastic properties of heterogenous microstructures with defects. *Composite Structures*, **188**: 104-115.
- [234] Madenci E, Dorduncu M, Gu X. (2019) Peridynamic least squares minimization. *Comput. Methods Appl. Mech. Engrg.*, **348**, 846–874.
- [235] Madenci E, Guven I. (2015) *The Finite Element Method and Applications in Engineering Using ANSYS*. Springer, NY
- [236] Madenci E, Oterkus E (2014) *Peridynamic Theory and Its Applications*. Springer, NY
- [237] Madenci E, Oterkus S (2016) Ordinary state-based peridynamics for plastic deformation according to von Mises yield criteria with isotropic hardening. *J. Mech. Phys. Solids*, **86**: 192–219
- [238] Madenci E, Yaghoobi A, Barut A, Phan N (2021) Peridynamic modeling of compression after impact damage in composite laminates. *J Peridyn Nonlocal Model*, **3**: 327–347
- [239] Madenci E, Yaghoobi A, Barut A, Phan N (2023) Peridynamics for failure prediction in variable angle tow composites *Archive of Applied Mechanics*, **93**: 93–107
- [240] Malyarenko A, Ostoja-Starzewski M. (2019) *Tensor-Valued Random Fields for Continuum Physics*, Cambridge University Press, Cambridge, UK
- [241] Marks II R. J. (2009) *Handbook of Fourier Analysis and its Applications*. Oxford University Press, NY

- [242] Matouš K, Geers MGD, Kouznetsova VG, Gillman A (2017) A review of predictive nonlinear theories for multiscale modeling of heterogeneous materials. *J. Comput. Physics*, **330**: 192–220
- [243] Mehrmashhadi J, Chen Z, Zhao J, Bobaru F. (2019) A stochastically homogenized peridynamic model for intraply fracture in fiber-reinforced composites *Composites Science Technology*, **182**: 107770
- [244] Mengesha T, Du Q. (2014) The bond-based peridynamic system with Dirichlet-type volume constraint. *Proc. R. Soc. Edinburgh, A* **144**: 161–186
- [245] Michel J, Moulinec H, Suquet P (2000) A computational method based on augmented Lagrangians and fast Fourier transforms for composites with high contrast. *Comput. Model. Eng. Sci.* **1**: 79–88
- [246] Michel J C, Moulinec H, Suquet P (2001) A computational scheme for linear and non-linear composites with arbitrary phase contrast. *Int. J. Numer. Methods Eng.* **52**, 139–60
- [247] Michel J, Suquet P. (2003) Nonuniform transformation field analysis, *Int. J. Solids Struct.*, **40**, 6937–6955.
- [248] Michel J, Suquet P. (2004) Computational analysis of nonlinear composite structures using the nonuniform transformation field analysis, *Comput. Methods Appl. Mech. Eng.* **193**(48–51): 5477–5502
- [249] Mikata Y (2012) Analytical solutions of peristatic and peridynamic problems for a 1D infinite rod. *Int. J. Solids and Structures*, **49**: 2887–2897
- [250] Mikata Y (2023) Analytical solutions of peristatics and peridynamics for 3D isotropic materials. *Eur J Mech A/Solids*, **101**: 104978
- [251] Miehe C, Koch A (2002) Computational micro-to-macro transition of discretized microstructures undergoing small strain. *Arch. Appl. Mech.* **72**: 300–317
- [252] Mitchell JA (2011) A nonlocal, ordinary, state-based plasticity model for peridynamics. *Sandia National Laboratories*, Albuquerque SAND2011-3166.
- [253] Mitchell JA, Silling SA, Chiu E, Bond SD. (2023) Modeling additively manufactured metallic microstructures for dynamic response. *J. Peridynamics Nonlocal Modeling*, <https://doi.org/10.1007/s42102-022-00093-2>
- [254] Moës N., Belytschko T. (2002) Extended finite element method for cohesive crack growth *Enginng Fracture Mechanics*, **69**: 813–833
- [255] Monchiet V, Bonnet G. (2012) A polarization-based FFT iterative scheme for computing the effective properties of elastic composites with arbitrary contrast. *Int. J. Numer. Methods Eng.*, **89**: 1419–1436
- [256] Mori T, Tanaka K. (1973) Average stress in matrix and average elastic energy of materials with misfitting inclusions. *Acta Metall.* **21**: 571–574
- [257] Moulinec H, Silva F. (2014) Comparison of three accelerated FFT-based schemes for computing the mechanical response of composite materials. *Int. J. Numer. Methods Eng.*, **97**: 960–85
- [258] Moulinec H, Suquet P (1994) Fast numerical method for computing the linear and nonlinear properties of composites. *C. R. Acad. Sci., Paris*, **318**: 1417–23
- [259] Moulinec H, Suquet P. (1998) A numerical method for computing the overall response of nonlinear composites with complex microstructure. *Comput. Methods Appl. Mech. Eng.*, **157**: 69–94
- [260] Mousavi F, Jafarzadeh S, Bobaru F (2021) An ordinary state-based peridynamic elastoplastic 2D model consistent with J2 plasticity. *Int. J. Solids Structures*, **229**, 111146
- [261] Mura T. (1987) *Micromechanics of Defects in Solids (Mechanics of Elastic and Inelastic Solids)* 2nd edn Berlin: Springer
- [262] Nie Y Li Z, Cheng G. (2021) Efficient prediction of the effective nonlinear properties of porous material by FEM-Cluster based Analysis (FCA) *Comput. Methods Appl. Mech. Engrg.*, **383**: 113921
- [263] Nemat-Nasser S, Hori M (1993) *Micromechanics: Overall Properties of Heterogeneous Materials*. Elsevier, North-Holland.
- [264] Ning L, Cai Z, Dong H, Liu Y, Wang W. (2023) A peridynamic-informed neural network for continuum elastic displacement characterization *Comput. Methods Appl. Mech. Engrg.*, **407**: 115909

- [265] Nguyen CT, Oterkus S, Oterkus E (2021) An energy-based peridynamic model for fatigue cracking *Engineering Fracture Mechanics*, **241**: 107373
- [266] Nowak M, Mulewska K, Azarov A, Ustrzycka A, *et al.* (2023) A peridynamic elasto-plastic damage model for ion-irradiated materials. *Int. J. Mechanical Sciences* **237**: 107806.
- [267] O'Brian RW (1979) A method for the calculation of the effective transport properties of suspensions of interacting particles. *J Fluid Mech*, **91**: 17–39
- [268] Öchsner (2021) *Foundations of Classical Laminate Theory*. Springer, NY
- [269] Ojo SO, Budarapu PR, Paggi M. (2017) A nonlocal adaptive discrete empirical interpolation method combined with modified hp-refinement for order reduction of molecular dynamics systems. *Computational Materials Science*, **140**: 189–208
- [270] Ongaro G, Seleson P, Galvanetto U, Ni T, Zaccariotto M. (2021) Overall equilibrium in the coupling of peridynamics and classical continuum mechanics *Comput. Meth. Appl. Mech. Engng*, **381**: 113515
- [271] Ongaro G, Shojaei A, Mossaiby f, Hermann A, Cyron CJ, Trovalusci P. (2023) Multi-adaptive spatial discretization of bond-based peridynamics. *Int J Fract*, **244**: 1–24
- [272] Oterkus R, Oterkus S. (2024) Recent advances in peridynamic theory: A review *AIMS Materials Science*, **11**: 515–546
- [273] Otero JA, Rodríguez-Ramos R, Monsivais G, Pérez-Alvarez R (2005) Dynamical behavior of a layered piezocomposite using the asymptotic homogenization method. *Mech. Mater.*, **37**: 33–44
- [274] Pan Y, Wu P, Fan S, Peng X, Chen Z. (2024) Peridynamic simulation of fatigue crack growth in porous materials. *Engng Fracture Mech.*, **300**: 109984.
- [275] Parks ML, Seleson P, Plimpton SJ, Silling SA, Lehoucq RB. (2011) *Peridynamics with LAMMPS: A user guide v0.3 beta*, *SAND Report 2011-8523*, Sandia National Laboratories, Albuquerque, NM, and Livermore, CA
- [276] Parnell WJ. (2016) The Eshelby, Hill, moment and concentration tensors for ellipsoidal inhomogeneities in the Newtonian potential problem and linear elastostatics *J Elast*, **125**: 231–294.
- [277] Pashazad H, Kharazi M (2019) A peridynamic plastic model based on von Mises criteria with isotropic, kinematic, and mixed hardenings under cyclic loading *Int. J. Mechanical Sciences*, **156**: 182–204
- [278] Pettermann HE, Plankensteiner AF, Böhm HJ, Rammerstorfer FG. (1999) A thermo-elasto-plastic constitutive law for inhomogeneous materials based on an incremental Mori–Tanaka approach. *Computers & Structures*, **71**, 197–214.
- [279] Pirzadeh A, Barba FD, Bobaru F, Sanavia L, Zaccariotto M, Galvanetto U. (2024) Elastoplastic peridynamic formulation for materials with isotropic and kinematic hardening. *Engineering with Computers*, doi.org/10.1007/s00366-024-01943-x
- [280] Plimpton, S., Kohlmeyer, A., Coffman, P., Blood, P. (2018) *fftMPI, a library for performing 2d and 3d FFTs in parallel*. Computer software. Sandia National Lab. (SNL-NM) <https://www.osti.gov/servlets/purl/1457552>. USDOE. 25 Apr. 2018. Web. doi:10.11578/dc.20201001.68.
- [281] Ponte Castañeda P, Willis JR (1995) The effect of spatial distribution on the effective behavior of composite materials and cracked media. *J Mech Phys Solids*, **43**, 1919–1951
- [282] Ponte Castañeda P, Suquet P (1998) Nonlinear composites. *Adv. Appl. Mech.*, **34**: 171–302
- [283] Qi J, Li C, Tie Y, Zheng Y, Cui Z, Duan Y. (2024) A peridynamic-based homogenization method to compute effective properties of periodic microstructure *Computational Particle Mechanics*. <https://doi.org/10.1007/s40571-023-00698-4>
- [284] Rabotnov, Y.N. (1959) A mechanism of a long time failure. In *Creep problems in structural members, AN SSSR*, 5–7 (In Russian)
- [285] Rabczuk T, Ren H, Zhuang X. (2023) *Computational Methods Based on Peridynamics and Nonlocal Operators*. Springer, Cham

- [286] Raissi M, Perdikaris P, Karniadakis GE. (2019) Physics-informed neural networks: A deep learning framework for solving forward and inverse problems involving nonlinear partial differential equations. *J. Comput. Phys.*, **378**: 686–707
- [287] Rayleigh L. (1892) On the influence of obstacles arranged in rectangular order upon the properties of a medium. *Philosophical Magazine*, **34**: 481–502.
- [288] Ren, B., Wu, C., Askari, E. (2017) A 3D discontinuous Galerkin finite element method with the bond-based peridynamics model for dynamic brittle failure analysis. *International Journal of Impact Engineering*, **99**: 14–25
- [289] Ren B, Wu CT, Seleson S, Zeng D, Nishi M, Pasetto M (2022) An FEM-Based Peridynamic Model for Failure Analysis of Unidirectional Fiber-Reinforced Laminates *J. Peridynamics and Nonlocal Modeling*, **4**: 139–158
- [290] Ren H, Zhuang X, Rabczuk T. (2017) Dual-horizon peridynamics: A stable solution to varying horizons *Comput. Methods Appl. Mech. Engrg.*, **318**, 762–782
- [291] Ren Y, Lu G, Chen J. (2024) Physically consistent nonlocal macro–meso-scale damage model for quasi-brittle materials: A unified multiscale perspective *Int. J. Solids Structures*, **293**: 112738
- [292] Ri J-H, Hong H-S, Ri S-G. (2021) Cluster-based nonuniform transformation field analysis: An efficient homogenization for inelastic heterogeneous materials *Int J Numer Methods Eng.* **122**: 4458–4485
- [293] Rice JR (1989) Weight function theory for three-dimensional elastic crack analysis. In: Wei RP, Gangloff RP (eds), *Fracture Mechanics: Perspectives and Directions* (Twentieth Symp). Amer Soc Test Mater, Philadelphia: 29–57
- [294] Sab K, Nedjar B. (2005) Periodization of random media and representative volume element size for linear composites. *C R Mecanique*, **333**: 187–195
- [295] Sahimi M. (2003) *Heterogeneous Materials II Nonlinear and Breakdown Properties*, Springer-Verlag, Berlin
- [296] Sarego G, Le QV, Bobaru F, Zaccariotto M, Galvanetto U. (2016) Linearized state-based peridynamics for 2-D problems *Int. J. Numer. Meth. Engrg.*, **108**: 1174–1197
- [297] Scabbia F, Zaccariotto M, Galvanetto U. (2023) A new surface node method to accurately model the mechanical behavior of the boundary in 3D state-based peridynamics. *J. Peridyn. Nonloc. Modeling*, **5**: 521–555
- [298] Scabbia F, Zaccariotto M, Galvanetto U. (2023) Accurate computation of partial volumes in 3D peridynamics *Engrg with Computers*, **39**: 959–991
- [299] Scabbia F, Zaccariotto M, Galvanetto U. (2024) A general ordinary state-based peridynamic formulation for anisotropic materials. *Comput. Methods Appl. Mech. Engrg.* **427**: 117059
- [300] Schmidhuber J (2015) Deep learning in neural networks: An overview. *Neural Networks*, **61**: 85–117
- [301] Schneider M. (2021) A review of nonlinear FFT-based computational homogenization methods. *Acta Mech*, **232**, 2051–2100
- [302] Scott JM, Mengesha T. (2020) Asymptotic analysis of a coupled system of nonlocal equations with oscillatory coefficients *Multiscale Modeling & Simulation*, **18**: 1137/19M1288085
- [303] Segurado J, Lebensohn R A, Llorca J (2018) Computational homogenization of polycrystals *Advances in Applied Mechanics* **51**, 1–114
- [304] Sejnoha, M, Zeman, J. *Micromechanics in Practice*. Southampton, UK: WIT Press, 2013.
- [305] Seleson P, Du Q, Parks M. (2016) On the consistency between nearest-neighbor peridynamic discretizations and discretized classical elasticity models. *Comp. Meth. Applied Mech. Engrg.*, **11**, 698–722. 2016.
- [306] Seleson P, Gunzburger M, Parks ML (2013) Interface problems in nonlocal diffusion and sharp transitions between local and nonlocal domains. *Comput. Methods Appl. Mech. Engrg.*, **266**: 185–204
- [307] Seleson P, Littlewood DJ. (2016) Convergence studies in mesh-free peridynamic simulations. *Comput. Mathematics with Applications*, **71**: 2432–2448

- [308] Seleson P, Parks ML. (2011) On the role of the influence function in the peridynamic theory. *Int. J. Multiscale Comput. Eng.*, **9**: 689–706
- [309] Seleson P, Pasetto M, John J, Trageser J, Reeve ST. (2024) PDMATLAB2D: A peridynamics MATLAB two dimensional code. *J. Peridyn. Nonl. Modeling*, **6**:149–205
- [310] Shermergor TD. (1977) *The Theory of Elasticity of Microinhomogeneous Media*. Nauka, Moscow (In Russian)
- [311] Silling S. (2000) Reformulation of elasticity theory for discontinuities and long-range forces. *J. Mech. Physics of Solids* **48**: 175–209
- [312] Silling S. (2010) Linearized theory of peridynamic states. *Journal of Elasticity*, **99**: 85–111
- [313] Silling S. (2011) A coarsening method for linear peridynamics. *Int. J. Multiscale Computational Engng*, **9**: 609–622
- [314] Silling, S.A. 2014. Origin and effect of nonlocality in a composite. *J. Mechanics of Materials and Structures*, **9**, 245–258.
- [315] Silling S. (2020) Propagation of a stress pulse in a heterogeneous elastic bar. *Sandia Report SAND2020-8197*, Sandia National Laboratories.
- [316] Silling SA, Askari E. (2005) A meshfree method based on the peridynamic model of solid mechanics. *Comput. Struct.* **83**: 1526–153
- [317] Silling SA, Epton M, Weckner O, Xu J, Askari E (2007) Peridynamic states and constitutive modeling. *J. Elasticity*, **88**: 151–184
- [318] Silling SA, D’Elia M, Yu Y, You H, Fermen-Coker M. (2023) Peridynamic model for single-layer graphene obtained from coarse-grained bond forces. *J Perid. Nonlocal Modeling*, **5**: 183–204.
- [319] Silling SA, Jafarzadeh S, Yu Y. (2024) Peridynamic models for random media found by coarse graining *J. Peridynamics and Nonlocal Modeling*, **6**
- [320] Silling SA, Lehoucq RB. (2008) Convergence of peridynamics to classical elasticity theory, *J. Elasticity*, **93**: 13–37.
- [321] Silling SA, Lehoucq RB. (2010) Peridynamic theory of solid mechanics. *Adv. Appl.Mech.*, **44**: 73–168
- [322] Silling SA, Zimmermann M, Abeyaratne R (2003) Deformation of a peridynamic bar. *J. Elasticity*, **73**: 173–190.
- [323] Simo JC, Taylor RL. (1986) A return mapping algorithm for plane stress elastoplasticity. *Int. J. Numer. Methods Eng.*, **22**: 649–670
- [324] Song Y, Li S, Li Y. (2023) Peridynamic modeling and simulation of thermo mechanical fracture in inhomogeneous ice. *Engineering with Computers*, **39**: 575–606
- [325] Suquet P-M (1985) Local and global aspects in the mathematical theory of plasticity. In: Sawczuk, A., et al. (Eds.), *Plasticity Today*. Elsevier, London, New York, pp. 279–309
- [326] Suquet P (1997). Effective properties of nonlinear composites. In: *Continuum micromechanics* (P. Suquet, ed.). CISM Courses and Lecture Notes No. 377. Springer-Verlag, Wien: 197–264
- [327] Sun W, Fish J (2021) Coupling of non-ordinary state-based peridynamics and finite element method for fracture propagation in saturated porous media. *Int J Numer Anal Methods Geomech.*, **45**: 1260–1281
- [328] Sun W, Fish J, Zhang G (2020) Superposition of non-ordinary state-based peridynamics and finite element method for material failure simulations. *Meccanica*, **55**: 681–699
- [329] Tandon GP, Weng GJ (1988) A theory of particle-reinforced plasticity. *J. Appl. Mech.* **55**: 126–135
- [330] Tang, S, Zhang, L, Liu, WK. From virtual clustering analysis to self-consistent clustering analysis: a mathematical study. *Comput Mech.* 2018; **62**: 1443–1460.
- [331] Terada K, Kikuchi N (2001) A class of general algorithms for multi-scale analyses of heterogeneous media, *Comput. Methods Appl. Mech. Eng.* **190**: 5247–5464

- [332] Theocaris PS (1991) The elliptic paraboloidal failure criterion for cellular solids and brittle forms. *Acta Mechan*, **89**: 93–121
- [333] Tian, X., Du, Q. (2015) Nonconforming discontinuous Galerkin methods for nonlocal variational problems. *SIAM Journal on Numerical Analysis*, **53**, 762–781.
- [334] Torquato, S. 2002. *Random Heterogeneous Materials: Microstructure and Macroscopic Properties*. Springer-Verlag, New York, Berlin.
- [335] van Tuijl RA, Harnish C, Matous K, Remmers JJC, Geers MGD. (2019) Wavelet-based reduced order models for microstructural analyses, *Computational Mechanics*, **63**: 535–554.
- [336] Tupek MR, Rimoli JJ, Radovitzky R. (2013) An approach for incorporating classical continuum damage models in state-based peridynamics. *Comput. Methods Appl. Mechanics and Enging*, **263**: 20–26
- [337] Vondřejc J, Zeman J, Marek I. (2012) Analysis of a fast Fourier transform-based method for modeling of heterogeneous materials. *Large-Scale Scientific Computing*. Eds. I Lirkov, S Margenov, J Waśniewski (Berlin: Springer), 515–22
- [338] Wang H, Wu L, Guo J, Yu C, Li Y, Wu Y. (2024) Three-dimensional modeling and analysis of anisotropic materials with quasi-static deformation and dynamic fracture in non-ordinary state-based peridynamics. *Appl. Math. Model.*, **125**: 625–648
- [339] Wang H, Wu L, Huang D, Chen J, Guo J, Yu C, Li Y, Wu Y. (2024) A machine-learning-based peridynamic surrogate model for characterizing deformation and failure of materials and structures *Engineering with Computers*, <https://doi.org/10.1007/s00366-024-02014-x>
- [340] Wang L, Xu J, Wang J, Karihaloo BL. (2020) Nonlocal thermo-elastic constitutive relation of fibre-reinforced composites. *Acta Mechanica Sinica*, **36**: 176–187
- [341] Wang Y, Zhou X, Wang Y, Shou Y. (2018) A 3-D conjugated bond-pair-based peridynamic formulation for initiation and propagation of cracks in brittle solids *Int. J. Solids Structures*, **134**: 89–115
- [342] Wang Y, Wu W. (2023) A bond-level energy-based peridynamics for mixed-mode fracture in rocks. *Comput. Methods Appl. Mech. Engrg.*, **414**: 116169
- [343] Weckner O, Abeyaratne R (2005) The effect of long-range forces on the dynamics of a bar. *J. Mech. Physics of Solids* **53**: 705–728
- [344] Weckner O, Brunk G, Epton MA, Silling SA, Askari E. (2009) Green's functions in nonlocal three-dimensional linear elasticity. *Proc. R. Soc., A* **465**: 3463–3487
- [345] Weckner O, Emmrich E. 2005 Numerical simulation of the dynamics of a nonlocal, inhomogeneous, infinite bar. *J. Comp. Appl. Mech.*, **6**, 311–319
- [346] Weiss JA. (2019) Tutorial on the Proper Orthogonal Decomposition. In: *2019 AIAA Aviation Forum*. 17–21 June 2019, Dallas, Texas, United States.
- [347] Wen Z, Hou C, Zhao M, Wan X. (2023) A peridynamic model for non-Fourier heat transfer in orthotropic plate with uninsulated cracks. *Applied Mathematical Modelling*, **115**: 706–723
- [348] Weng GJ (1992) Explicit evaluation of Willis' bounds with ellipsoidal inclusions *Int. J. Engng Science*, **30**: 83–92
- [349] Wicht D, Schneider M., Böhlke T (2021) Anderson-accelerated polarization schemes for FFT-based computational homogenization. *Int. J. Numer. Methods Eng.*, **122**: 2287–311
- [350] Wildman R, Gazonas G. (2015) A dynamic electro-thermo-mechanical model of dielectric breakdown in solids using peridynamics *J. Mech. Mater. Structures*, **10**: 613–630
- [351] Willis JR (1977) Variational and related methods for the overall properties and selfconsistent estimates for the overall properties. *J Mech Phys Solids*, **25**, 85–202
- [352] Willis JR. (1980) A polarization approach to the scattering of elastic waves – I. Scattering by a single inclusion. II. Multiple scattering from inclusions. *J. Mech. Physics of Solids*, **28**, 287–327.
- [353] Willis JR. (1981) Variational and related methods for the overall properties of composites. *Advances in Applied Mechanics*, **21**: 1–78

- [354] Wildman RA, O'Grady JT, Gazonas GA. (2017) A hybrid multiscale finite element/peridynamics method. *Int J Fract*, (2017) 207:41–53
- [355] Witman DR, Gunzburger M, Peterson J. (2017) Reduced-order modeling for nonlocal diffusion problems. *Int J Numer Methods Fluids*, **83**: 307–327
- [356] Wu P, Chen Z. (2023) Peridynamic electromechanical modeling of damaging and cracking in conductive composites: A stochastically homogenized approach. *Composite Structures*, **305**: 116528
- [357] Wu P, Yang F, Chen Z, Bobaru F. (2021) Stochastically homogenized peridynamic model for dynamic fracture analysis of concrete. *Eng Fract Mech*, 107863.
- [358] Xia Z, Zhang Y, Ellyin F (2003) A unified periodical boundary conditions for representative volume elements of composites and applications. *Int. J. Solids Struct.* **40**: 1907–1921
- [359] Xia, W., Galadima, Y.K., Oterkus, E. and Oterkus, S., 2019, Representative volume element homogenization of a composite material by using bond-based peridynamics **J. Compos. Biodegradable Polymers**, **7**: 51-56.
- [360] Xia W, Oterkus E, Oterkus S. (2020) Peridynamic modeling of periodic microstructured materials. *Procedia Structural Integrity*, **28**: 820–828
- [361] Xia W, Oterkus E, Oterkus S. (2021) 3-dimensional bond-based peridynamic representative volume element homogenization. *Physical Mesomechanics*, **24**: 45-51.
- [362] Xia W, Oterkus E, Oterkus S. (2021) Ordinary state-based peridynamic homogenization of periodic micro-structured materials *Theoret. Applied Fract. Mech.*, **113**, 102960.
- [363] Xu J, Askari A, Weckner O, Silling SA (2008) Peridynamic analysis of impact damage in composite laminates. *J. Aerospace Engineering*, **21**: 187–194
- [364] Xu J, Yang Z, Wang Z, Wang X, Li Y, Zhang J. (2024) Peridynamic simulation for the damage patterns of glass considering the influence of rate-dependence and pre-defects. *Engng Fracture Mechanics*, **291**: 109539
- [365] Xu X, D'Elia M, Foster JT (2021) A machine-learning framework for peridynamic material models with physical constraints. *Computer Meth Appl. Mech. Engng* **386**: 114062
- [366] Xu X, Foster JT. (2020) Deriving peridynamic influence functions for one-dimensional elastic materials with periodic microstructure. *J. Peridyn. Nonlocal Modeling*, **2**: 337–351
- [367] Yang X, Gao W, Liu W, Zhang X. (2024) Coupling four-parameters bond-based peridynamic and finite elements for damage analysis of composite structures *Theor. Appl. Fracture Mech.*, **129**: 104230
- [368] Yang Y, Ragnvaldsen O, Bai Y, Yi M, Xu BX. (2019) 3D non-isothermal phase-field simulation of microstructure evolution during selective laser sintering. *Npj Comput Mater*, **5**: 81 (12 pages).
- [369] Yang Z, Shen S, Guan X, He X, Cui J. (2024) Multiscale analysis-based peridynamic simulation of fracture in porous media. *Front. Struct. Civ. Eng.* **18**: 1–13
- [370] Yang Z, Zheng S, Han F, Cui, J. (2023) An efficient peridynamics-based statistical multiscale method for fracture in composite structures. *Int. J. Mech. Sciences*, **259**: 108611
- [371] Yang Z, Zheng S, Han F, Guand X, Zhange J. (2023) An adaptive coupling approach of local and non-local micromechanics *J. Comput. Physics*, **489**, 112277
- [372] Yilbas, B.S. (2013) *Laser Drilling-Practical Applications*. Springer: Heidelberg, Germany.
- [373] You H, Xu X, Yu Y, Silling S, D'Elia M, Foster J. (2023) Towards a unified nonlocal, peridynamics framework for the coarse-graining of molecular dynamics data with fractures. *Applied Mathematics Mechanics*, **44**: 1125–1150.
- [374] You H, Yu Y, Silling S, D'Elia M (2020) Data-driven learning of nonlocal models: from high-fidelity simulations to constitutive laws. *arXiv:2012.04157*
- [375] You H, Yu Y, Silling S, D'Elia M. (2022) A data-driven peridynamic continuum model for upscaling molecular dynamics. *Comput. Meth. Appl. Mechanics Engng.*, **389**: 114400.
- [376] You H, Yu Y, Silling S, D'Elia M. (2024) Nonlocal operator learning for homogenized models: from high-fidelity simulations to constitutive laws. *J. Peridynamics Nonlocal Modeling*, <https://doi.org/10.1007/s42102-024-00119-x>

- [377] You H, Yu Y, Trask N, Gulian M, D’Elia M (2021) Data-driven learning of robust nonlocal physics from high-fidelity synthetic data. *Computer Methods Applied Mech. Engineering*, **374**: 113553
- [378] You H, Zhang Q, Ross C, Lee C-H, Hsu M-C, Yu Y. (2022) A physics-guided neural operator learning approach to model biological tissues from digital image correlation measurements. *J. Biomechanical Engng*, **144**, 121012
- [379] Yvonnet J, He QC (2007) The reduced model multiscale method (R3M) for the non-linear homogenization of hyperelastic media at finite strains. *J Comput Phys*, **223**: 341–368
- [380] Yu C, Kafka OL, Liu WK. (2019) Self-consistent clustering analysis for multiscale modeling at finite strains. *Comput Methods Appl Mech Eng.*, **349**: 339–359
- [381] Yu Q, Fish J (2002) Multiscale asymptotic homogenization for multiphysics problems with multiple spatial and temporal scales: a coupled thermo-viscoelastic example problem. *Int. J. Solids Struct.*, **39**: 6429–6452
- [382] Yu X-L, Zhou X-P. (2024) A nonlocal energy-informed neural network for peridynamic correspondence material models. *Engng Anal. Boundary Elements*, **160**, 273–297
- [383] Yu Y, Bargas FF, You H, Parks ML, Bittencourt ML, Karniadakis GE. (2018) A partitioned coupling framework for peridynamics and classical theory: analysis and simulations. *Comput. Meth. Appl. Mech. Engineering*, **340**: 905–931
- [384] Zaccariotto M, Mudric T, Tomasi D, Shojaei A, Galvanetto U. (2018) Coupling of FEM meshes with peridynamic grids. *Comput. Meth. Applied Mech. Engineering*, **330**: 471–497.
- [385] Zeman J, de Geus TWJ, Vondřejc J, Peerlings RHJ, Geers MGD. (2017) A finite element perspective on nonlinear FFT-based micromechanical simulations. *Int. J. Numer. Methods Eng.* **111**: 903–26
- [386] Zeman J, Vondřejc J, Novák J, Marek I. (2010) Accelerating an FFT-based solver for numerical homogenization of periodic media by conjugate gradients. *J. Comput. Phys.* **229**: 8065–71
- [387] Zhan JM, Yao XH, Zhang XQ. (2021) Study on predicting the mechanical properties and fracturing behaviors of particle reinforced metal matrix composites by non-local approach. *Mech. Materials*, **155**: 103790
- [388] Zhang H, Yang M, Wei J, Nie Y. (2024) Stability and error analysis of reduced-order methods based on POD with finite element solutions for nonlocal diffusion problems. *Digital Engineering Digital Twin*, **2**: 49-77
- [389] Zhang J, Han F, Yang Z, Cui J. (2023) Coupling of an atomistic model and bond-based peridynamic model using an extended Arlequin framework. *Comput. Meth. Appl. Mech. Engineering*, **403**: 115663.
- [390] Zhang, L, Tang, S, Yu, C, Zhu, X, Liu, WK. Fast calculation of interaction tensors in clustering-based homogenization. *Comput Mech*, 2019; **64**: 351–364.
- [391] Zhang SY, Nie YF. (2020) A POD-based fast algorithm for the nonlocal unsteady problems. *Int J Numer Anal Model*, **17**: 858–871
- [392] Zhang S, Nie Y. (2023) Localized Chebyshev and MLS collocation methods for solving 2D steady state nonlocal diffusion and peridynamic equations. *Math. Computers in Simulation*. **206**: 264–285
- [393] Zhang W, Zhao Y, Ma X, Tian X. (2023) Thermoelastic response of laminated plates considering interfacial conditions and cracks based on peridynamics *Acta Mechanica*, **234**: 2179–2203
- [394] Zhang X, Gunzburger M, Ju L. (2016a) Nodal-type collocation methods for hypersingular integral equations and nonlocal diffusion problems. *Comput. Meth. Appl. Mech. Engrg.*, **299**: 401–420
- [395] Zhang X, Gunzburger M, Ju L. (2016b) Quadrature rules for finite element approximations of 1D nonlocal problems. *J. Comp. Phys.*, **310**: 213–236.
- [396] Zhang Y, Qiao P. (2021) A fully-discrete peridynamic modeling approach for tensile fracture of fiber-reinforced cementitious composites. *Eng Fract Mech*, **242**: 107454
- [397] Zhao T, Shen Y. (2023) A reduced-order peridynamic model for predicting nonlocal heat conduction in nanocomposites *Composite Structures*, **323**: 117477
- [398] Zhou K, Hoh HJ, Wang X, Keer LM, Pang JHL, Song B, Wang QJ. (2013) A review of recent works on inclusions *Mechanics of Materials*, **60**: 144–158.

- [399] Zhou XP, Wang YT. (2021) State-of-the-art review on the progressive failure characteristics of geomaterials in peridynamic theory. *J. Eng. Mech.*, **147**: 03120001
- [400] Zohdi TI, Wriggers P. (2008) *Introduction to Computational Micromechanics*. Berlin: Springer.